

Review

Open Access



Heterogeneous nanoporous organic frameworks-based catalysts for electrochemical CO₂ reduction reaction

Yajuan Ma^{1,2,*}, Guangjin Zhang^{1,3}, Qiuhan Yu^{1,2}, Shuai Lyu^{4,*}, Xiaoguang Duan⁵, Shiming Zhang^{6,*}

¹School of Chemical & Environmental Engineering, Pingdingshan University, Pingdingshan 467000, Henan, China.

²Yaoshan Laboratory, Pingdingshan University, Pingdingshan 467000, Henan, China.

³School of Innovation and Entrepreneurship, Pingdingshan University, Pingdingshan 467000, Henan, China.

⁴Hubei Key Laboratory of Biomass Fibers and Eco-Dyeing & Finishing, College of Chemistry and Chemical Engineering, Wuhan Textile University, Wuhan 430200, Hubei, China.

⁵School of Chemical Engineering and Advanced Materials, The University of Adelaide, Adelaide, SA 5005, Australia.

⁶Institute for Sustainable Energy/College of Sciences, Shanghai University, Shanghai 200444, China.

***Correspondence to:** Dr. Yajuan Ma, School of Chemical & Environmental Engineering, Pingdingshan University, Weilai Road, Xincheng District, Pingdingshan 467000, Henan, China. E-mail: 27103@pdsu.edu.cn; Dr. Shuai Lyu, Hubei Key Laboratory of Biomass Fibers and Eco-Dyeing & Finishing, College of Chemistry and Chemical Engineering, Wuhan Textile University, 1 Yangguang Avenue, Jiangxia District, Wuhan 430200, Hubei, China. E-mail: shuailyu@wtu.edu.cn; Dr. Shiming Zhang, Institute for Sustainable Energy/College of Sciences, Shanghai University, 99 Shangda Road, Baoshan District, Shanghai 200444, China. E-mail: smzhang@shu.edu.cn

How to cite this article: Ma, Y.; Zhang, G.; Yu, Q.; Lyu, S.; Duan, X.; Zhang, S. Heterogeneous nanoporous organic frameworks-based catalysts for electrochemical CO₂ reduction reaction. *Energy Mater.* **2025**, 5, 500053. <https://dx.doi.org/10.20517/energymater.2024.215>

Received: 16 Oct 2024 **First Decision:** 12 Nov 2024 **Revised:** 25 Nov 2024 **Accepted:** 2 Dec 2024 **Published:** 25 Feb 2025

Academic Editors: Ho Won Jang, Yuhui Chen **Copy Editor:** Fangling Lan **Production Editor:** Fangling Lan

Abstract

Converting captured carbon dioxide (CO₂) into valuable chemicals and fuels through electrocatalysis and realizing the anthropogenic closed-carbon cycle can provide new solutions to environmental and energy problems. Nanoporous organic frameworks, including metal-organic frameworks (MOFs) and porous organic polymers (POPs), as a class of potential electrocatalysts, have made great progress in CO₂ reduction reaction due to their high porosity, large specific surface area, and structural/functionalization diversity. In this review, the recent developments in pristine MOFs/POPs, MOFs/POPs composite, and MOFs-/POPs-derived catalysts are discussed from aspects of catalyst design, synthesis strategy, test techniques, performance validation, active sites, and basic mechanism. We further summarize the challenges and prospects of MOFs/POPs-based materials in practical applications for CO₂ reduction reactions and point out the potential paths of future research. This review can



© The Author(s) 2025. **Open Access** This article is licensed under a Creative Commons Attribution 4.0 International License (<https://creativecommons.org/licenses/by/4.0/>), which permits unrestricted use, sharing, adaptation, distribution and reproduction in any medium or format, for any purpose, even commercially, as long as you give appropriate credit to the original author(s) and the source, provide a link to the Creative Commons license, and indicate if changes were made.



provide a comprehensive reference for the advanced design and systematic cognition of efficient nanoporous organic framework catalysts for electrocatalytic CO₂ reduction.

Keywords: Metal organic frameworks, porous organic polymers, electrochemical CO₂ reduction reaction, high porosity, structural/functionalization diversity

INTRODUCTION

The rapid development of global industries and human activities has led to a substantial increase in greenhouse gas emissions, causing continued damage to our ecological environment^[1]. The idea of the conversion of carbon dioxide (CO₂), the primary representative component of greenhouse gases, into hydrocarbon fuel has gained traction around the world^[2]. So far, several strategies have been reported for CO₂ conversion, such as chemical transformation^[3], mineralization^[4], enzymatic catalysis^[5], photochemical catalysis^[6], electrochemical catalysis^[7,8], and so on. Electrochemical CO₂ reduction reaction (CO₂RR) serves as an effective method to realize chemical energy storage with (excess) renewable electricity energy resources; this process can be conducted at room temperature and standard pressure, and can realize an artificial closed carbon cycle^[9]. However, the C=O bond in CO₂ has a high bond energy (750 kJ mol⁻¹), creating an urgent need for efficient and stable electrocatalysts to activate and convert it into value-added products^[10]. Therefore, through ideal design and tailored synthesis of highly efficient catalysts, combined with the understanding of catalytic mechanisms, the industrial application of electrocatalytic CO₂RR technology and its expected challenges have gained increasing interest^[11].

It is worth noting that electrocatalytic CO₂RR is a relatively complex process with slow reaction kinetics. Different reaction conditions, i.e., electrode materials, reduction potential, electrolytes, pH, and so on, can lead to diverse reduction products, including compounds of single carbon [C₁: carbon monoxide (CO), formic acid (HCOOH), methanol (CH₃OH), and methane (CH₄)], double carbon [C₂: ethylene (C₂H₄), ethanol (C₂H₅OH), ethylene glycol (C₂H₆O₂), acetic acid (CH₃COOH), and oxalic acid (COOH)₂], and triple carbon [C₃: propylene (C₃H₆), n-propanol (C₃H₇OH), propionaldehyde (C₃H₆O), and acetone (CH₃COCH₃)]; these can be produced by CO₂ acquiring 2, 4, 6, 8, or 12 electrons^[12]. Bushuyev *et al.* identified that CO, HCOOH (or HCOO⁻), C₂H₄, and CH₃CH₂OH are the most commercially promising target products based on a comprehensive analysis of the Faradic efficiency (FE) and current density^[13]. At present, the FE of electrocatalytic CO₂RR to produce CO and HCOOH has reached > 95%; in contrast, for C₂H₄ and CH₃CH₂OH, it is generally not more than 60%^[14], attributing to the formation of C₂ products involving C-C coupling process which is a second-order reaction requiring higher energy barrier^[15]. However, in practical electrocatalytic CO₂RR, the competitive hydrogen evolution reaction (HER) adversely affects the selectivity of target products^[16,17]. Due to factors such as low catalytic activity, poor catalyst stability/durability, and insufficient understanding of the mechanism, electrocatalytic CO₂RR remains extremely challenging to implement in practice^[18].

High overpotential, poor catalyst stability and low product selectivity are the main problems for electrocatalytic CO₂RR^[19]. The exploration of efficient electrocatalysts is a critical factor in improving the activity and selectivity of CO₂RR^[20,21]. At present, studies have explored a series of catalysts for electrochemical CO₂RR, including transition-metal-based catalysts (metals^[22], alloys^[23], metal oxides^[24,25], metal sulfides^[26], *etc.*), non-metallic catalysts (heteroatom-doped carbon nanomaterials^[27] and polymers^[28]), and their composites^[29]. Based on the structural design, porous materials tend to exhibit superior electrocatalytic performance^[30,31]. For example, metal-organic frameworks (MOFs) and porous organic polymers (POPs) have tunable properties, and their structural diversity makes them ideal candidates for catalyst optimization^[32-34]. The high microporosity of MOFs and POPs not only allows good CO₂ adsorption

capacity under low-pressure conditions, inducing high local CO₂ concentration at the electrode under liquid electrolyte conditions, but also promotes the transport of reactants to active sites and reduces mass transfer limitations. Moreover, their large specific surface area (SSA) can ensure the participation of more active sites during catalysis. However, due to their structural limitations, their catalytic activity remains insufficient to meet the requirements for industrial usage. Their structures can be modified to further improve the electrocatalytic activity through the following processes: (1) to prevent the loss of catalytic sites, strong covalent bonds can be used to tightly anchor them on the porous material; (2) to improve conductivity, electron-conducting molecules can be inserted into the porous materials; (3) electroactive components can be implanted into the porous materials through methods such as coating and hybridization to generate an intermediate product which further promotes the conversion to a specific product; (4) porous materials can be compounded with conductive carbon materials, mono-/bimetallic electrodes, and metal oxides, to synergistically promote the electron and mass transfer; and (5) using MOFs or POPs as sacrificial precursors, pyrolysis can produce heteroatom-doped carbon materials and single-atom catalysts (SACs).

In this work, we will discuss the recent developments of MOFs- and POPs-based nanoporous organic framework materials (pristine, hybrids, and derivatives) as catalysts for electrochemical CO₂RR [Figure 1]. Apart from using the original MOFs and POPs as catalysts, we explore the following improvement strategies: (1) modification with metals; (2) encapsulation of guests (metal-based molecular catalysts or conductive molecules); (3) combination with functional groups to form composite materials; and (4) inclusion of derivatives (monatomic catalysts of MOFs or POPs). All these steps can enhance electron conductivity, CO₂ adsorption capacity, and active site exposure, further improving activity and stability of catalysts. Finally, we identified the current challenges and offered solutions to enable the commercial application of electrocatalytic CO₂ reduction technologies.

FUNDAMENTALS OF ELECTROCATALYTIC CO₂RR

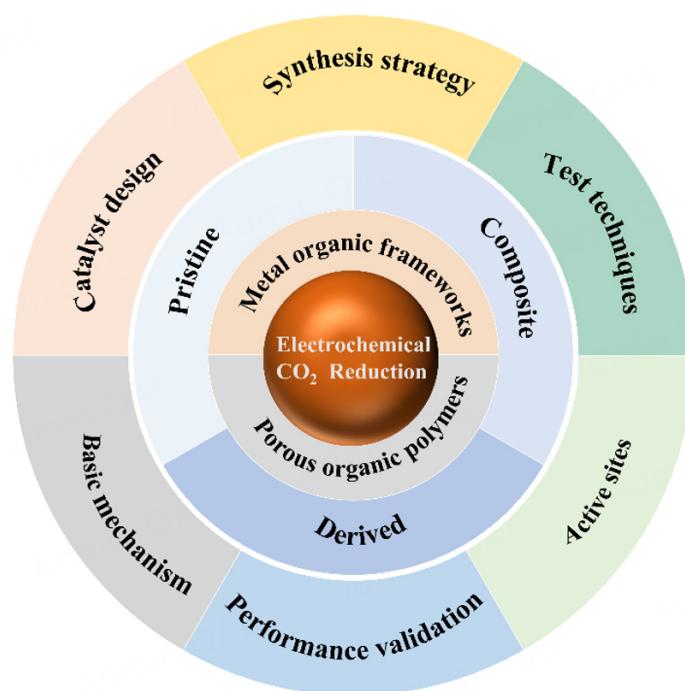
Principle

CO₂ is an inert, linear molecule highly stable at room temperature and standard pressure. Hence, electrocatalytic CO₂RR can occur only under a highly negative potential. The reaction occurs at the interface of electrode and electrolyte, where the electrode is a solid electrocatalyst and the electrolyte is generally a CO₂-saturated potassium bicarbonate (KHCO₃) aqueous solution^[35,36]. This heterogeneous electrocatalytic process includes three main steps: (1) chemisorption of CO₂ on the catalyst surface; (2) transfer of electrons and protons to the catalyst surface to destroy the C-O bond and form the C-H bond; and (3) reconstitution of the product, desorption from the electrode surface, and diffusion into the electrolyte.

From a thermodynamic perspective, a CO₂ molecule adsorbs onto the working electrode to gain an electron; this process requires high energy to activate the CO₂ molecule, enabling it to rearrange from its original linear structure into a curved free radical anion (i.e., intermediate CO₂^{•-}), which can then drive the subsequent reaction. The generation of this intermediate state slows down the kinetics of CO₂RR, generating a super-potential during the reaction process, and is often considered as a rate-determining step (RDS) for the whole reaction. The complicated process can trigger a series of chemical reactions^[37]. The relevant reactions occurring during CO₂RR are mentioned in Table 1. Different products involve varying electron/proton transfer and coupling processes of reaction intermediates, and the formation of surface species such as *COOH, *OCHO, *CO, *CHO and *OCCOH (* indicates the adsorption state) produced during the CO₂RR process is usually revealed by *in-situ* Raman spectroscopy, *in-situ* infrared spectroscopy and isotope labeling. Transition metals Au, Ag, Zn and Pd are easy to adsorb *COOH, so the main product of CO₂RR is CO. Pb, In, Sn and Bi are easy to adsorb *OCHO, which promote the formation of HCOOH. Cu has suitable adsorption energy for *CO, which is beneficial to the dimerization of *CO and the further

Table 1. Possible pathways of electrochemical CO₂RR

Reaction equations	Electrode potentials E^0 (V vs. SHE)
$\text{CO}_2(\text{g}) + 2\text{H}^+ + 2\text{e}^- \rightleftharpoons \text{HCOOH}(\text{l})$	-0.25
$\text{CO}_2(\text{g}) + \text{H}_2\text{O}(\text{l}) + 2\text{e}^- \rightleftharpoons \text{HCOO}^-(\text{aq}) + \text{OH}^-$	-1.08
$\text{CO}_2(\text{g}) + 2\text{H}^+ + 2\text{e}^- \rightleftharpoons \text{CO}(\text{g}) + \text{H}_2\text{O}(\text{l})$	-0.11
$\text{CO}_2(\text{g}) + \text{H}_2\text{O}(\text{l}) + 2\text{e}^- \rightleftharpoons \text{CO}(\text{g}) + 2\text{OH}^-$	-0.93
$\text{CO}_2(\text{g}) + 4\text{H}^+ + 4\text{e}^- \rightleftharpoons \text{CH}_2\text{O}(\text{l}) + \text{H}_2\text{O}(\text{l})$	-0.07
$\text{CO}_2(\text{g}) + 3\text{H}_2\text{O}(\text{l}) + 4\text{e}^- \rightleftharpoons \text{CH}_2\text{O}(\text{g}) + 4\text{OH}^-$	-0.90
$\text{CO}_2(\text{g}) + 6\text{H}^+ + 6\text{e}^- \rightleftharpoons \text{CH}_3\text{OH}(\text{l}) + \text{H}_2\text{O}(\text{l})$	+0.02
$\text{CO}_2(\text{g}) + 5\text{H}_2\text{O}(\text{l}) + 6\text{e}^- \rightleftharpoons \text{CH}_3\text{OH}(\text{l}) + 6\text{OH}^-$	-0.81
$\text{CO}_2(\text{g}) + 8\text{H}^+ + 8\text{e}^- \rightleftharpoons \text{CH}_4(\text{g}) + 2\text{H}_2\text{O}(\text{l})$	+0.17
$\text{CO}_2(\text{g}) + 6\text{H}_2\text{O}(\text{l}) + 8\text{e}^- \rightleftharpoons \text{CH}_4(\text{g}) + 8\text{OH}^-$	-0.66
$2\text{CO}_2(\text{g}) + 2\text{H}^+ + 2\text{e}^- \rightleftharpoons \text{H}_2\text{C}_2\text{O}_4(\text{aq})$	-0.50
$2\text{CO}_2(\text{g}) + 2\text{e}^- \rightleftharpoons \text{C}_2\text{O}_4^{2-}(\text{aq})$	-0.59
$2\text{CO}_2(\text{g}) + 12\text{H}^+ + 12\text{e}^- \rightleftharpoons \text{C}_2\text{H}_4(\text{g}) + 4\text{H}_2\text{O}(\text{l})$	+0.06
$2\text{CO}_2(\text{g}) + 12\text{H}^+ + 12\text{e}^- \rightleftharpoons \text{CH}_3\text{CH}_2\text{OH}(\text{aq}) + 3\text{H}_2\text{O}(\text{l})$	+0.08
$2\text{CO}_2(\text{g}) + 8\text{H}^+ + 8\text{e}^- \rightleftharpoons \text{CH}_3\text{COOH}(\text{aq}) + 2\text{H}_2\text{O}(\text{l})$	+0.12
$2\text{CO}_2(\text{g}) + 14\text{H}^+ + 14\text{e}^- \rightleftharpoons \text{C}_2\text{H}_6(\text{g}) + 4\text{H}_2\text{O}(\text{l})$	+0.14
$3\text{CO}_2(\text{g}) + 18\text{H}^+ + 18\text{e}^- \rightleftharpoons \text{C}_3\text{H}_7\text{OH}(\text{aq}) + 5\text{H}_2\text{O}(\text{l})$	+0.10

**Figure 1.** Illustration of the MOFs/POPs-based catalysts for electrochemical CO₂RR.

transfer of protons and electrons to generate hydrocarbons. At present, the selectivity of the C₁ and C₂ products of CO₂RR is relatively high, and its reaction path is widely studied. The representative reaction paths of the C₁ and C₂ products are described below in Figure 2.

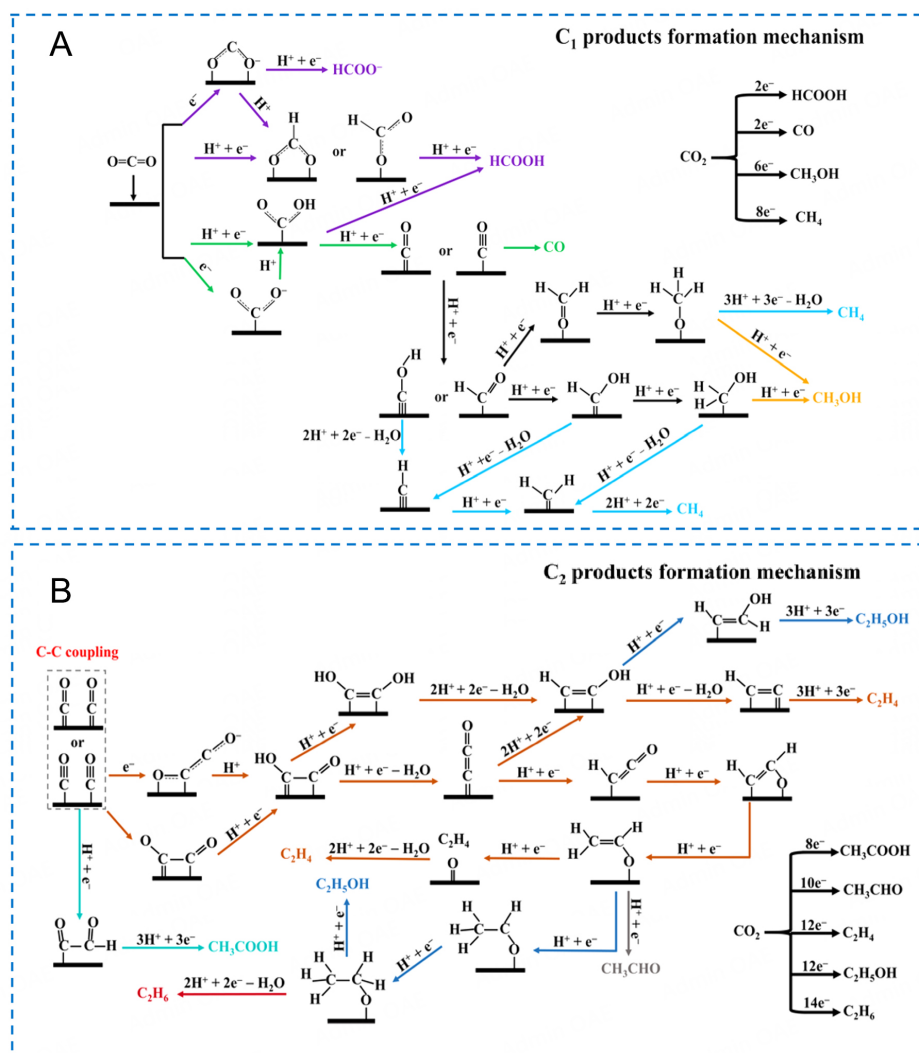


Figure 2. The formation mechanism of various (A) C₁ and (B) C₂ products^[38]. Copyright 2023 Elsevier.

(a) Pathway for electrocatalytic reduction of CO₂ to C₁ products

As shown in Figure 2A, the different adsorption states of reaction intermediates in CO₂RR can lead to the change of the reaction path, resulting in various types of products^[38]. For example, it is generally believed that the carbon adsorption (*COOH) and oxygen adsorption (*OCHO) of the reaction intermediate correspond to the paths to generate the 2e⁻ reduction products CO and HCOOH, respectively^[39]. *COOH undergoes electron/proton transfer and dehydration to produce *CO, which can be hydrogenated to form *CHO/*COH. The *CHOH formed by further hydrogenation of *CHO and *COH can be protonated to form *CH₂OH, which then branches into two paths to form CH₃OH, the 6e⁻ reduction product, and CH₄, the 8e⁻ reduction product^[40]. In addition, *CHO can also be protonated to form CH₂O* and CH₃O*, which are key intermediates for the formation of CH₄ and CH₃OH. However, in the CO₂RR process, the selectivity of CH₃OH is much lower than that of CH₄, due to the high energy barrier in the conversion of *CH₂OH and CH₃O* to CH₃OH, resulting in the kinetic hindrance of CH₃OH generation^[40].

(b) Pathway for electrocatalytic reduction of CO₂ to C₂ products

The different pathways for the formation of various C₂ products are shown in Figure 2B, in which *CO is an essential intermediate for the formation of multi-carbon products by C-C coupling^[38]. The *CO dimers undergo proton and electron transfer to form *COCHO, which is further protonated to form CH₃COOH^[41]. In the C₂ pathway, C-C coupling is considered the RDS for *CO dimerization or COCO* formation^[42]. *CO dimer or negatively charged COCO* can form *COCO⁻H by proton transfer, followed by several proton-electron transfer steps to form the 12e⁻ reduction product C₂H₄. C₂H₅OH is generated by further reduction of CH₃CH₂O*/*CHCOH^[43]. In addition, CH₂CHO* and CH₃CH₂O* undergo a further proton-electron transfer step to give the product CH₃CHO and C₂H₆, respectively^[41]. The formation pathways of different CO₂RR products, including key intermediates and reaction pathways, can provide a theoretical basis for the selective regulation of CO₂RR products.

Performance evaluation

It is crucial to evaluate the performance of electrocatalysts using the following indexes based on the fundamental principle of electrocatalytic CO₂RR^[44]:

1. Initial potential: it is the external voltage to be applied when the current density of the electrocatalyst reaches a certain value.
2. Overpotential: it represents the difference between the actually applied working electrode potential and the standard/equilibrium potential, which reflects the driving force of the catalytic reaction.
3. Faradaic efficiency (FE): this parameter is defined as

$$FE = n\alpha F/Q$$

where Q represents the charge in the catalytic process, n is the mole number of the product, α denotes the number of electrons transferred, and $F = 96,485 \text{ C mol}^{-1}$ is the Faraday constant. FE mainly reflects the selectivity of an electrocatalyst for a specific reduction product. A high FE (> 80%) indicates a good CO₂ reduction electrocatalyst:

4. Current density: The total current density is usually calculated as the current through the electrode during CO₂RR divided by the geometric surface area of the working electrode, and the current density required for commercial applications should be greater than 300 mA cm^{-2} ^[45]. The partial current density is the effective current density for the formation of the target product and can be calculated by multiplying the total current density by the FE of the target product.
5. Stability: It means that the activity of the catalyst, the selectivity of the product and the reaction rate remain stable for a long time. In the process of the experiments, the stability of the FE of the target product and the stability of the running current/potential under potentiostatic/galvanostatic electrolysis conditions are usually evaluated. Currently, the longest running time reported is hundreds of hours, which can not reach the goal of thousands of hours of stable operation required by industrial applications^[46]. The factors affecting the stability of the CO₂RR mainly include the deactivation of the catalyst, the deposition of carbonate on the electrode surface, etc.
6. Turnover frequency (TOF): This parameter denotes the mole number of reduction products produced by each electrocatalysis active site per unit time. However, when the active sites of the catalyst are confused, it

can be very difficult to calculate the TOF value.

7. Energy efficiency (EE): Also known as voltage efficiency, it is closely related to the cell voltage and FE through $EE(\%) = E_{\text{thermo}}/E_{\text{cell}} \times FE$, where E_{thermo} is the thermodynamic potential required for the electrocatalytic CO₂RR to produce a product. E_{cell} is the actually applied potential (including the potential required for the reaction, the potential to overcome the catalytic overpotential, the resistance of the electrolyzer, and the potential to generate by-products, etc.). Improving EE helps reduce the total power input for the CO₂RR. So far, only a few studies have calculated the EE of CO₂RR systems, and there remains much space for improvement from the 70% EE of commercial application target^[47].

Electrolytic cells

The design of CO₂RR electrolytic cells has a great impact on mass transfer; the most common of these reactors are the H-type, continuous flow electrolytic cells and membrane electrode assembly (MEA) cells^[48] [Figure 3].

H-type: The H-type cell is a typical reactor commonly used in laboratories. It comprises three electrodes (working, reference, and counter) and two compartments (cathode and anode). This cell design allows different chemical reactions in the two compartments while maintaining the electrochemical quarantine between them. The main feature of the H-cell is that its structure allows researchers to independently control the reaction conditions in each compartment, thus enabling precise control and optimization of the electrochemical reaction.

Continuous flow: The continuous flow cell is a relatively new type of microfluidic cell applied to electrochemical CO₂RR in recent years^[49]. In this cell, the gas diffusion electrode (GDE) is separated from the flowing liquid electrolyte. An external reference electrode can be used to test the electrode performance. The GDE is designed to improve the control and efficiency of the three-phase boundary in various electrochemical reactions. The gas/liquid products can be kept well separated while performing real-time analyses.

MEA: The core component of the MEA cell is the MEA formed by laminating a GDE, a catalyst layer and an ion exchange membrane in sequence. The MEA cell removes the cathode electrolyte chamber, achieving zero distance transfer of protons and ions, and effectively solving the difficulty of flooding electrodes. Meanwhile, this design reduces the impedance of the system and further accelerates the rate of CO₂ electroreduction.

MOF-BASED ELECTROCATALYSTS

MOFs are a kind of crystal material self-assembled by coordination bonds between metal ions or inorganic clusters as nodes and organic ligands as linkers. They have been gradually adopted into electrocatalysis reactions given their high SSA, adjustable microporosity, confinement effect, and the availability of diverse functional groups^[50,51]. Compared with conventional solid metal electrodes, the ordered porous structure of MOFs allows the permeation of ions and dissolved CO₂ into the membrane to increase CO₂ concentration at the local electrode through the inherent pore confinement. The pore sizes and SSA of MOFs can be adjusted through the coordination of different ligands with metal centers, which can make the active centers more accessible to CO₂ and promote charge and mass transfer. Due to the regulable metal nodes and ligands serving as active centers or electron transfer agents, the number of useable active sites can be maximized by dispersing them with organic ligands, so MOFs can be finely tuned to possess the best performance as electrocatalysts for the CO₂RR. Additionally, different kinds of active sites and reaction conditions can allow

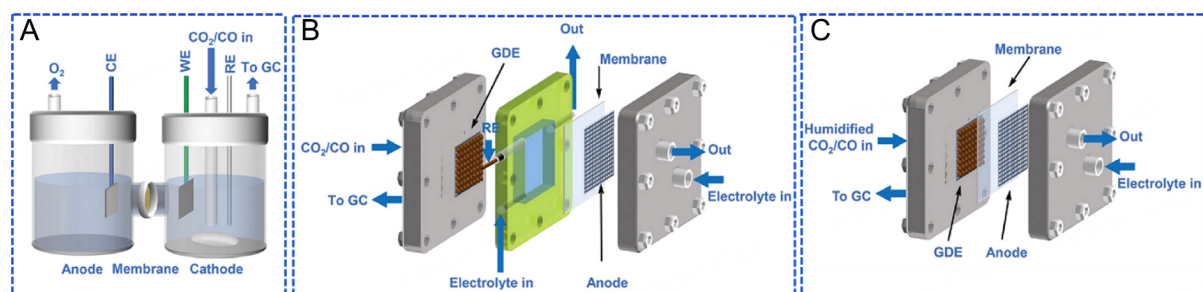


Figure 3. Schematic diagram of different reactors. (A) H-cell. (B) Flow cell. (C) MEA^[48]. Copyright 2021 the Royal Society of Chemistry.

the formation of diverse reaction products by tuning the ligands and active metals. Various MOF-based materials, including their main products and catalytic activities, were summarized in Table 2.

Pristine MOFs

Bulk MOFs

The isolated metal nodes of MOFs can serve as active sites, providing excellent monoatomic dispersity with 100% atomic efficiency. Bismuth (Bi) is considered to be a promising electrocatalytic material that can convert CO₂ into HCOOH^[52]. Therefore, Bi-based MOF (Bi-MOF) catalysts for CO₂RR can be expected to possess high catalytic activity and product selectivity at low overpotential^[53]. A stable Bi-MOF (Bi-BTC-D) was previously prepared by a hydrothermal process using trimesic acid (H₃BTC) and bismuth nitrate pentahydrate [Bi(NO₃)₃·5H₂O] with a high FE of 95.5% for HCOOH at -0.86 V_{RHE}^[54]. For this sample, the FE remained at ~90.0% even after 12 h of continued electrolysis, showing good stability. Moreover, the morphology of Bi-MOFs could be regulated to expose more active sites, thereby improving production efficiency of HCOOH. Inspired by this study, CAU-17 Bi-MOFs with hexagonal prism (CAU-17-hp) and nanofiber (CAU-17-fiber) morphologies have been synthesized by a wet-chemical process^[55]. In particular, the sample CAU-17-fiber with a carbonization temperature of 400 °C (CAU-17-fiber₄₀₀) with a hierarchical structure developed by H₃BTC-mediated morphology reconstruction had a high FE of 96.4% for HCOOH at -0.90 V_{RHE}.

The coordination environment of metal sites plays a significant role in CO₂ activation and stabilization of important intermediates in the electrocatalytic process. A porous zeolitic MOF (Bi-ZMOF) was prepared by introducing carboxylic acid groups (pyrazole-3,5-dicarboxylic acid, PDC) as ligands, which could convert CO₂ to HCOOH with FE of 91% at -1.1 V_{RHE}^[56]. Theoretical calculations showed that the coordination of Bi with the pyrazole-N atom in the MOF facilitated electron mobility from the ligand to Bi sites, which promoted the activation of CO₂, thereby reducing the potential for the generation of OCHO* and ultimately facilitating conversion of CO₂ to HCOOH; Meanwhile, the weak bonding (hydrogen bonding) of COOH to the carboxyl group results in weak adsorption of COOH* on the MOF, ultimately inhibiting CO production. It has been reported that biomass-derived materials can capture Pb²⁺ in wastewater to synthesize Pb-based MOFs, which can not only solve lead (Pb) poisoning but also electrochemically convert CO₂ to HCOOH. The ellagic acid (EA) obtained from pomegranate bark could effectively capture Pb²⁺ in aqueous media to synthesize stable Pb-based MOFs (EA-Pb), which could efficiently convert CO₂ to HCOOH with FE of 95.37% at -1.08 V_{RHE}^[57]. At the same time, the removal rate of Pb²⁺ even at lower concentrations by EA was close to 99%. In the structure of EA-Pb, PbO₆ as a metal node, has a tunable coordination mode (coordination number of 4-9) with the EA linker, which was essential for the reduction of CO₂ to form the key intermediate HCOO*. Since the formation of CO and HCOOH involved the same RDS (*COO→HCOO*), the reaction pathway and product selectivity were revealed by theoretical calculations. Gibbs free energy change values for *HCOOH formation (-0.96 eV) and *HCOOH desorption

Table 2. The performance of different MOF-based electrocatalysts and their related products in CO₂RR

Sample	Main products	Electrolyte	Maximum FE (%)	Electrode potential	Partial current density (mA cm ⁻²)	Refs.
Pristine MOFs						
Bi-BTC-D	HCOOH	0.5 M KHCO ₃	95.5	-0.86 V _{RHE}	11.2	[54]
CAU-17-fiber_400	HCOOH	0.1 M KHCO ₃	96.4	-0.90 V _{RHE}	20.4	[55]
Bi-ZMOF	HCOOH	0.1 M KHCO ₃	91.0	-1.10 V _{RHE}	-15.0 at -1.3 V _{RHE}	[56]
EA-Pb	HCOOH	0.1 M KHCO ₃	95.4	-1.08 V _{RHE}	6.5	[57]
Co-PMOF	CO	0.5 M KHCO ₃	99.0	-0.80 V _{RHE}	18.1	[58]
Cu-MFU-4l	CH ₄	0.5 M KHCO ₃	92.0	-1.20 V _{RHE}	9.8	[59]
Cu-DBC	CH ₄	0.1 M KHCO ₃	56.0	-1.40 V _{RHE}	11.4	[60]
Cu(I)-BTC	C ₂ H ₄	0.1 M KHCO ₃	57.0	-1.60 V _{RHE}	/	[61]
CALF20	CO	0.1 M KHCO ₃	94.5	-0.97 V _{RHE}	32.8	[66]
STPyP-Co	CO	0.5 M KHCO ₃	96.0	-0.62 V _{RHE}	6.5	[81]
Co-PPOLs	CO	0.1 M KHCO ₃	94.2	-0.90 V _{RHE}	/	[83]
Cu ₂ (CuTCCP) nanosheets	HCOOH	1 M H ₂ O /CH ₃ CN solution with 0.5 M EMIMBF ₄	68.4	-1.55 V _{Ag/Ag+}	3.5 at -1.60 V _{Ag/Ag+}	[85]
2D Ni (Im) ₂	CO	0.5 M KHCO ₃	78.8	-0.85 V _{RHE}	7.0 at -0.95 V _{RHE}	[87]
NiPc-NiO ₄	CO	0.5 M KHCO ₃	98.4	-0.85 V _{RHE}	34.5 at -1.2 V _{RHE}	[90]
NiPc-Ni(NH) ₄	CO	0.5 M KHCO ₃	96.4	-0.70 V _{RHE}	24.8 at -1.1 V _{RHE}	[91]
PcCu-Cu-O	C ₂ H ₄	0.1 M KHCO ₃	50.0	-1.20 V _{RHE}	7.3	[93]
Cu ₃ (HHTQ) ₂	CH ₃ OH	0.1 M KHCO ₃	53.6	-0.40 V _{RHE}	/	[94]
HATNA-Cu-MOF	CH ₄	0.1 M KHCO ₃	78.0	-1.50 V _{RHE}	8.2	[95]
2Bn-Cu@UiO-67	CH ₄	1 M KOH	81.0	-1.50 V _{RHE}	420.0	[96]
Cu-DBC	CH ₄	1 M KOH	80.0	-0.90 V _{RHE}	162.4	[97]
Cu-SAs@ Ir-PCN-222-PA	C ₂ H ₄	1 M PBS	70.9	-1.00 V _{RHE}	20.4	[99]
Cu _{0.5} Zn _{0.5} /ZIF-8	CO	0.5 KHCO ₃	88.5	-1.00 V _{RHE}	11.6	[101]
MOFs composites						
Bi-UiO-66-CN	HCOOH	0.1 KHCO ₃	93.0	-0.75 V _{RHE}	1.5	[109]
Cu-SIM NU-1000	HCOOH	0.1 M NaClO ₄	31.0	-0.82 V _{RHE}	1.2	[111]
Cu@ZIF-8 NWs	C _x H _y (CH ₄ , C ₂ H ₄)	0.1 KHCO ₃	57.5	-0.70 V _{RHE}	/	[112]
Bi/UiO-66	HCOOH	1.0 M KOH	73.0	-0.70 V _{RHE}	59.0	[113]
Ag@UiO-66-SH	CO	0.1 M KHCO ₃	74.0	-1.10 V _{RHE}	19.5	[115]
Cu ₂ O@Cu-MOF	CH ₄	0.1 M KHCO ₃	63.2	-1.71 V _{RHE}	8.4	[120]
Cu ₂ O/CPFs	C ₂ H ₄	0.1 M KHCO ₃	61.8	-1.30 V _{RHE}	8.0	[121]
Cu ₂ O@MOF/CF	C ₂ H ₅ OH	0.5 M KHCO ₃	44.3	-0.615 V _{RHE}	9.7	[123]
Bi ₂ O ₃ /MOL	HCOOH	0.5 M KHCO ₃	> 85.0	-0.87-1.17 V _{RHE}	11.8	[118]
CuO/Cu-MOF	C ₂ H ₄	0.1 M KHCO ₃	50.0	-1.10 V _{RHE}	7.0	[119]
CoCp ₂ @MOF-545-Co	CO	0.5 M KHCO ₃	97.0	-0.70 V _{RHE}	25.6 at -0.9 V _{RHE}	[124]
PPy@MOF-545-Co	CO	0.5 M KHCO ₃	98.0	-0.80 V _{RHE}	13.0 at -1.0 V _{RHE}	[125]
ZIF-A-LD	CO	0.1 M KHCO ₃	90.57	-1.10 V _{RHE}	6.83	[126]
MOFs derivatives						
ZIF-CNT-FA-p	CO	0.1 M NaHCO ₃	100.0	-0.86 V _{RHE}	7.7	[132]
MNC-D	CO	0.1 M KHCO ₃	92.0	-0.58 V _{RHE}	6.8	[134]
NPC-1000	CO	0.5 M KHCO ₃	98.4	-0.55 V _{RHE}	3.0	[135]
Cu-MOF _{20/300}	CO	0.5 M KHCO ₃	39.6	-0.56 V _{RHE}	34.97 at -0.64 V _{RHE}	[138]
InCuO-0.92	CO	0.5 M KHCO ₃	92.1	-0.80 V _{RHE}	11.2	[139]
Bi NP@MWCNT	HCOOH	0.5 M KHCO ₃	95.2	-1.50 V _{SCE}	10.7	[146]

Ni-NC_ATPA@C	CO	0.5 M KHCO ₃	94.0	-0.70 V _{RHE}	-6.0	[149]
Ni _{1/150} NCs@NC	CO	0.5 M KHCO ₃	98.7	-0.88 V _{RHE}	40.4	[151]
Co ₁ Cu ₃ @C	CO	0.5 M KHCO ₃	34.0	-0.70 V _{RHE}	11.67	[154]
Sb _{2.5} /Bi@C	HCOOH	0.5 M KHCO ₃	94.8	-0.78 V _{RHE}	4.74	[157]
Ce _{0.05} Bi _{0.95} @C NRs	HCOOH	0.1 M KHCO ₃	96.1	-1.50 V _{RHE}	18.9	[158]
Co/CNTs	CO	0.5 M KHCO ₃	90.0	-0.70 V _{RHE}	20.6	[160]
Bi ₂ O ₃ @C-800	HCOOH	1.0 M KOH	93.0	-1.10 V _{RHE}	208.0	[161]
Sn (101)/SnO ₂ /C-500	HCOOH	0.5 M KHCO ₃	93.3	-0.80 V _{RHE}	8.2	[130]
FeSAs/CNF-900	CO	0.5 M KHCO ₃	86.9	-0.47 V _{RHE}	2.9	[165]
C-AFC@ZIF-8	CO	0.1 M KHCO ₃	91.6	-0.63 V _{RHE}	4.1	[166]
Fe-N-C	CO	0.5 M KHCO ₃	93.5	-0.50 V _{RHE}	-6.0	[167]
C-Zn ₇ Ni ₄ ZIF-8	CO	0.5 M KHCO ₃	98	-0.83 V _{RHE}	22.0	[168]
Ni-N-C	CO	0.1 M KHCO ₃	97	-0.75 V _{RHE}	7.5	[171]
Ni ₁ -N-C	CO	0.5 M KHCO ₃	96.8	-0.80 V _{RHE}	27.0	[172]
Ni-N ₃ -C	CO	0.5 M KHCO ₃	95.6	-0.65 V _{RHE}	6.64	[176]
Co-N ₂	CO	0.5 M KHCO ₃	94	-0.78 V _{RHE}	32.7	[178]
Fe ₁ N ₂ O ₂ /NC	CO	0.1 M KHCO ₃	99.7	-0.50 V _{RHE}	6.5 at -0.7 V _{RHE}	[180]
PA-CUDBC-1	CH ₄	0.5 M KHCO ₃	75.3	-1.10 V _{RHE}	47.8	[181]
Fe ₁ -Ni ₁ -NC	CO	0.5 M KHCO ₃	96.2	-0.50 V _{RHE}	2.4	[183]
L-Co ₁ Mn ₁ -NC	CO	0.5 M KHCO ₃	97.6	-0.47 V _{RHE}	34.7 at -0.97 V _{RHE}	[185]
MoFe-N-C	CO	0.5 M KHCO ₃	95.96	-0.60 V _{RHE}	11.7 ± 0.7	[186]

(-0.59 eV) were more negative than *CO formation from HCOO* decomposition (-0.73 eV) and *CO desorption (-0.48 eV), indicating that the reduction of CO₂ to HCOOH was thermodynamically more favorable. In parallel, the energy barrier of HER (1.99 eV) was much higher than that of CO₂ reduction (1.37 eV), proving that the catalyst inhibited hydrogen evolution, thus showing the advantage of greater HCOOH selectivity.

The generation of any CO₂ reduction product requires a multi-electron transfer process, and the poor conductivity and electron-donating ability have been the primary limiting factors for the exploration of efficient MOFs. Therefore, the integration of electron-rich units, electron mobility, and active components into MOFs may be an efficient method to enhance CO₂RR performance. For example, (i) electron-rich polyoxometalates (POMs) can provide a large number of electrons; and (ii) metal-tetrakis(4-carboxyphenyl) porphyrins (M-TCPPs, where M refers to a metal species) exhibit an intrinsic macrocyclic conjugated π -electron system, which can be highly conducive to electron migration. A range of POM-based MOFs (M-PMOFs) have been synthesized by a one-step process using a POM and M-TCPP^[58]. The direct connection between POM and M-TCPP generated a directional electron transport channel from POM to M-TCPP under the application of an electric field. This helped promote the multi-electron migration during CO₂ reduction and efficiently realize the conversion of CO₂ to CO. The FE_{CO} of the cobalt (Co)-PMOF reached 99% at -0.8 V_{RHE}, with excellent stability of > 36 h of recycling. This study showed that the intramolecular multi-electron transfer in the catalyst can also improve the electrocatalytic CO₂RR performance. Theoretical calculations showed that the formation energy barrier of *COOH was significantly reduced after the assembly of POM and Co-TCPP (0.34 eV), compared with that of POM (0.96 eV), indicating that Co in Co-TCPP was the active site of the reaction rather than POM and there was an effective synergy between Co-TCPP and POM. The Co center in Co-TCPP could be reduced from Co(II) to Co(I) by accepting electrons captured by POM, and then Co(I) interacted with CO₂ to generate Co(II) *COOH, which combined with protons and electrons to form Co(II) *CO, and finally to form CO.

In addition, Zhu *et al.* synthesized a copper (Cu)-based MOF structure (Cu-MFU-4l) with copper triazole (Cu(I)N_3) as an active site to realize the process of CO_2 -to- CH_4 ^[59]. The FE of CH_4 for this catalyst reached 92% at $-1.2 \text{ V}_{\text{RHE}}$. It has been reported that the selectivity of product was greatly affected even by slight differences in coordination environment of metal ions. Liu *et al.* compared two kinds of coordination structures based on catechol ($\text{C}_6\text{H}_6\text{O}_2$)-derived ligands with copper oxide (CuO_4 and CuO_5) nodes to study the impact of metal d-orbital energy levels on the selectivity of electrocatalytic CO_2 RR products^[60]. Compared to the square-planar CuO_4 site, the square-pyramidal CuO_5 site had a higher Cu 3d orbital energy level through coordination with its axial oxygen (O) atom. This enabled the CuO_5 site to form a stronger π -back bond with the intermediate CO, thus facilitating its adsorption and the subsequent multi-step hydrogenation process to form CH_4 .

The high selectivity of C_2 products can be achieved by controlling the valence state of metal nodes in the MOF. Deng *et al.* used methanol as a reducing agent to reduce Cu^{2+} in Cu(II)-Trimesic acid (BTC) framework (Cu(II)-BTC) to Cu^+ which played a key role in the selectivity of C_2 products, realizing the reconstruction of Cu^+ and BTC and the generation of free carboxyl groups^[61]. The electroreduction of CO_2 to C_2H_4 was promoted by the change of the valence state of metal nodes and the generation of free carboxyl groups, and the FE was increased from 22% to 57% at $-1.6 \text{ V}_{\text{RHE}}$. The electrocatalytic performance did not decay after 38 h, indicating good stability. In addition, controlling the crystal face of MOFs with different solvents can also be used to adjust the selectivity of CO_2 reduction. Lu *et al.* prepared Cu(I) 5-mercapto-1-methyltetrazole frameworks (Cu-MMTs) with (100) and (001) crystal faces using water and isopropanol as solvents, respectively^[62]. Cu-MMTs with (001) crystal faces were beneficial to the formation of multi-carbon products with 73.75% FE. The difference was that the Cu-MMT with (100) crystal faces promoted the formation of single carbon with 63.98% FE. Furthermore, the size of MOFs also affects the selectivity of CO_2 reduction. Four different sizes of Cu-MOFs (53, 109, 307, 1,335 nm) were synthesized^[63]. As a result, small-sized MOFs with polycrystalline structures converted CO_2 to ethylene and multi-carbon products with FEs of 55.4% and 81.8%, respectively, which was superior to large-sized single-crystal nanostructures.

Zinc (Zn)-based MOFs (Zn-MOFs) can also be used as electrocatalysts to convert CO_2 to CO^[64,65]. For this type of MOF, due to complete occupation of Zn(II) 3d orbitals, active sites mainly originate from the coordination of the ligands with the Zn(II) centers; i.e., the CO_2 RR performance can be adjusted by regulating the ligands. Al-Attas *et al.* employed 1, 2, 4-triazolate and 2-methylimidazolate as ligands to synthesize two different Zn-MOFs, Calgary framework 20 (CALF20) and zeolitic imidazolate framework-8 (ZIF-8), respectively^[66]. The study indicated that CALF20 had a higher CO_2 adsorption capacity (more than 4.5 times that of ZIF-8). Moreover, the sp^2 C active sites in the 1, 2, 4-triazolate of CALF20 were far more in number than in the 2-methylimidazolate of ZIF-8. With increased CO_2 adsorption performance and multiple binding sites, CALF20 exhibited better performance with a high CO FE of 94.5% at $-0.97 \text{ V}_{\text{RHE}}$. The theoretical results showed that sp^2 C in the azole ligand coordinated with Zn(II) site could be used as catalytic active center for the electrochemical reduction of CO_2 . Compared with the diazole group in ZIF-8, the faster charge transfer efficiency of the triazole ligand in CALF20 promoted the accumulation of more electrons at adjacent active sites, thereby lowering the adsorption free energy of $^*\text{COOH}$ and improving the conversion efficiency of $^*\text{COOH}$ to CO.

Two-dimensional MOFs

Recently, two-dimensional (2D) MOF nanosheets have been widely used in electrocatalytic CO_2 RR due to their outstanding advantages: (1) Compared to bulk MOFs, MOF nanosheets can expose a higher proportion of metal atom active sites on the surface for CO_2 RR catalysis. It is particularly important that the exposed coordination-unsaturated metal atoms on the surface exhibit high catalytic activity^[67]; (2) The

electronic structure of metal atoms in MOF nanosheets can be effectively controlled by selecting appropriate organic ligands^[68]. For electrocatalysis, the electronic structure of catalyst influences the binding strength of the intermediate products on the catalyst surface, and then determines the final activity and product selectivity; (3) Compared to bulk MOFs, MOF nanosheets have better conductivity^[69]; (4) The highly porous, ultrathin characteristics of MOF nanosheets are conducive to the transport of reactants and products during the catalysis reaction^[70,71]; and (5) Due to the diversity of MOF structures and the progress in material synthesis technologies, a large number of MOF nanosheets can be prepared easily to study their potential electrocatalytic properties^[72].

Two-dimensional conductive MOFs (*c*-MOFs), as a member of the 2D materials family, are developed by combining transition metal nodes with conjugated organic ligands^[73,74]. The framework of these *c*-MOFs and the corresponding physical properties are largely derived from the incorporated ligands. However, the synthesis of 2D *c*-MOFs is limited by available ligands. Macrocyclic compounds are regarded as infinite π -conjugated systems, exhibiting unique electronic behavior regardless of the presence or absence of substituents. Therefore, conjugated macrocyclic structures with well-defined shapes and non-foldable and fully π -conjugated backbones can be used to construct 2D MOFs^[75,76].

Two different ligands, 1,4-benzenedicarboxylic acid (BDC) and 2,6-naphthalenedicarboxylic acid (NDC), were selected to prepare two 2D-MOFs (Cu-UBDC and Cu-UNDC) regulating electronic structure of Cu active centers^[77]. It was found that the ratio of $\text{Cu}^+/\text{Cu}^{2+}$ was 1.12 for Cu-UNDC, far exceeding that of Cu-UBDC (0.85), indicating the change of electron densities of metal sites, thereby promoting electron migration. Consequently, FE of $\text{C}_2\text{H}_5\text{OH}$ and C_2H_4 for Cu-UNDC was 24.3% at $-1.0\text{ V}_{\text{RHE}}$, far exceeding that of Cu-UBDC (13.2%). In addition, for Cu-UBDC, Cu_2O as a photocatalyst could be generated under the condition of CO_2 reduction. Therefore, more efficient charge separation efficiency and more electrons can be used for CO_2 reduction under illumination, resulting in an improved FE of 26.2% for the C_2 product of Cu-UBDC, which was better than that of Cu-UNDC (21.8%).

Metalloporphyrin organic ligands exhibit tetrapyrrole macrocyclic conjugated structures. When they are used to construct MOFs, different topological structures can be formed by changing the number of nodal metal clusters or connections, which greatly improves the structural diversity of the porphyrin-metal framework materials. The metal centers of metalloporphyrins are easily reduced to a low-oxidation state during CO_2 reduction, and the macrocyclic ligand skeleton helps maintain chemical stability^[78]. Moreover, the structure of metalloporphyrins can be tuned and functionalized using redox-active molecular catalytic linkers^[79]. Metalloporphyrin-based 2D MOFs have been widely studied as CO_2RR electrocatalysts^[80]. Han *et al.* synthesized well-defined ultrathin 2D nanosheets (STPyP-Co) by axial coordination assembly of tetra(4-pyridyl) porphyrin Co(II)^[81]. Originating from the ultrathin characteristics of 2D MOFs, the nanosheets exhibited excellent conductivity and unsaturated five-coordinated single sites on their surface. The axial pyridine coordination led to the increase of the d_z^2 energy level in the Co 3d orbit, which enhanced the Lewis basicity of the surface Co center, thus allowing more electrons to be transferred from Co to CO_2 , which was beneficial to the activation of CO_2 and reduced the free energy required for the $\text{CO}_2^* \rightarrow \text{COOH}$ process. As a result, STPyP-Co could convert CO_2 into CO with a high FE of 96% at $-0.62\text{ V}_{\text{RHE}}$. This sample had good stability with FE of above 90% throughout the reaction process.

It has been reported that the Co- N_4 site in the porphyrin ring can be used as an active site, with strong $^*\text{COOH}$ binding energy and moderate $^*\text{CO}$ adsorption energy in the process of electrocatalytic CO_2RR . Therefore, a 2D-MOF based on Co-porphyrin is an excellent electrocatalyst for achieving the transformation of CO_2 to CO^[82]. Chen *et al.* prepared 2D Co-based porous porphyrin nanolayer (Co-

PPOLs) catalyst with Co-N₄ sites through a bottom-up self-assembly strategy^[83] [Figure 4A]. The ultrathin nanolayer showed an average thickness of 3.8 nm [Figure 4B], which was conducive to the exposure of more active sites and faster electron transfer, so it could promote the adsorption, activation and transformation of reactants/intermediates, thereby improving the activity, selectivity and stability of electrocatalytic CO₂RR. Therefore, the highest FE_{CO} was 94.2% at -0.9 V *vs.* RHE [Figure 4C]. Moreover, the electrocatalytic CO₂ reduction performance of Co-PPOLs under industrial currents was also studied. At a full battery voltage of 2.7 V (higher than the industrial grade current of 200 mA), the CO FE of CO-PPOLs could still reach 92% for 20 h in MEA cells [Figure 4D and E]. In addition, the electrocatalytic process with the assistance of light was conducive to the stabilization of CO intermediates bound to the catalyst, and promoted the formation of high-electron product CH₄. Based on the above conditions, MOFs based on cobalt 5, 10, 15, 20-tetri (4-carboxyphenyl) porphyrin (CoTCPP) (Co-MOF-525) achieved an FE_{CH₄} of 14% at -0.49 V *vs.* NHE^[84] [Figure 4F and G]. Under light conditions, the generation of [Co(III) TCPP]⁺ species could stably bind to CO, and then be electroreduced to CH₄.

A Cu-MOF nanosheet, Cu₂(Cu-TCPP), with porphyrinic Cu and Cu paddle wheel in two different chemical environments, was synthesized under cathodization conditions^[85]. Due to cathodized reconstruction, the Cu-MOF nanosheets exhibited an FE_{HCOOH} of 68.4% at -1.55 VAg/Ag⁺, superior to those of CuO, Cu₂O, Cu, and Cu-TCPP. Similarly, a 2D porphyrin organometallic framework nanozyme (PPF-100) with Cu-paddle-wheels, Cu₂(COO)₄ structure could realize highly selective CO₂RR and significantly inhibit the HER^[86]. The FEs of CO and HCOOH were 72.4% and 24.1% at -3.0 V *vs.* Ag/Ag⁺ with no generation of H₂, attributed to the hydrophobicity of PPF-100, which was conducive to inhibiting the HER, thereby improving the electrocatalytic performance of CO₂ reduction. Furthermore, Wu *et al.* prepared ultrathin 2D nickel (Ni)-based ZIF nanosheets [Ni(Im)₂] by exfoliating bulk MOFs to nanosheets of varying thicknesses as electrocatalysts to convert CO₂ to CO^[87]. Due to the existence of more Ni sites and rapid mass and electron transfer by ultrathin nanosheet structure, the CO FE for the 2D Ni(Im)₂ nanosheets with thickness of 5 nm reached ~78.8% at -0.85 V_{RHE}, much higher than that of bulk Ni(Im)₂ ZIF (33.7%).

Metallophthalocyanines (MePc) have also been used for the preparation of 2D-MOFs with thermal/chemical stability and structural tunability at the molecular level^[88,89]. 2D NiPc-NiO₄ nanosheet MOF was previously constructed using Ni phthalocyanine (NiPc)-2,3,9,10,16,17,23,24-octanol (NiPc-OH) and Ni(II) ions^[90]. The NiPc linked with nickel-catecholate [Ni(C₆H₄O₂)₂] served as an active site in this MOF; the high d- π orbital overlap between the two increased the conductivity of the nanosheets to $\sim 4.8 \times 10^{-5}$ S m⁻¹. The adsorption energy of CO₂ on NiPc was 0.23 eV, much higher than that on NiO₄ (0.02 eV), indicating that CO₂ molecules were more easily bound to NiPc through non-covalent interactions. Furthermore, the electron-rich environment in NiPc was more favorable for the reduction of CO₂. In addition, the COOH* formation energy barrier (1.93 eV) on NiPc was lower than that of H* (1.98 eV), whereas on NiO₄, it (2.53 eV) was higher than that of H* (1.58 eV), indicating that CO₂RR occurred preferentially on NiPc. While HER was dominant on NiO₄. Owing to rapid electron transport capacity, these nanosheets exhibited a FE_{CO} of 98.4% and partial current density of 34.5 mA cm⁻². This study showed that the catalytic ability of Ni active sites can be improved by inserting phthalocyanine (H₂Pc) molecules into 2D *c*-MOF materials. The well-maintained NiPc active sites after CO₂RR allowed the electrocatalyst to show superior stability with a high FE_{CO} of 86%.

To further improve the electrical conductivity of H₂Pc-based MOFs, NiPc-Ni(NH)₄ nanosheets have been synthesized by using 2,3,9,10,16,17,23,24-octaaminophthalocyaninato nickel(II) [NiPc-(NH₂)₈] and Ni(II) ions^[91]. Due to the NiPc links with Ni(NH)₄ nodes, the electronic conductivity of NiPc-Ni (NH)₄ can reach up to 2.39×10^{-4} S m⁻¹, improving the electron transfer capacity. Controlled experiments and density

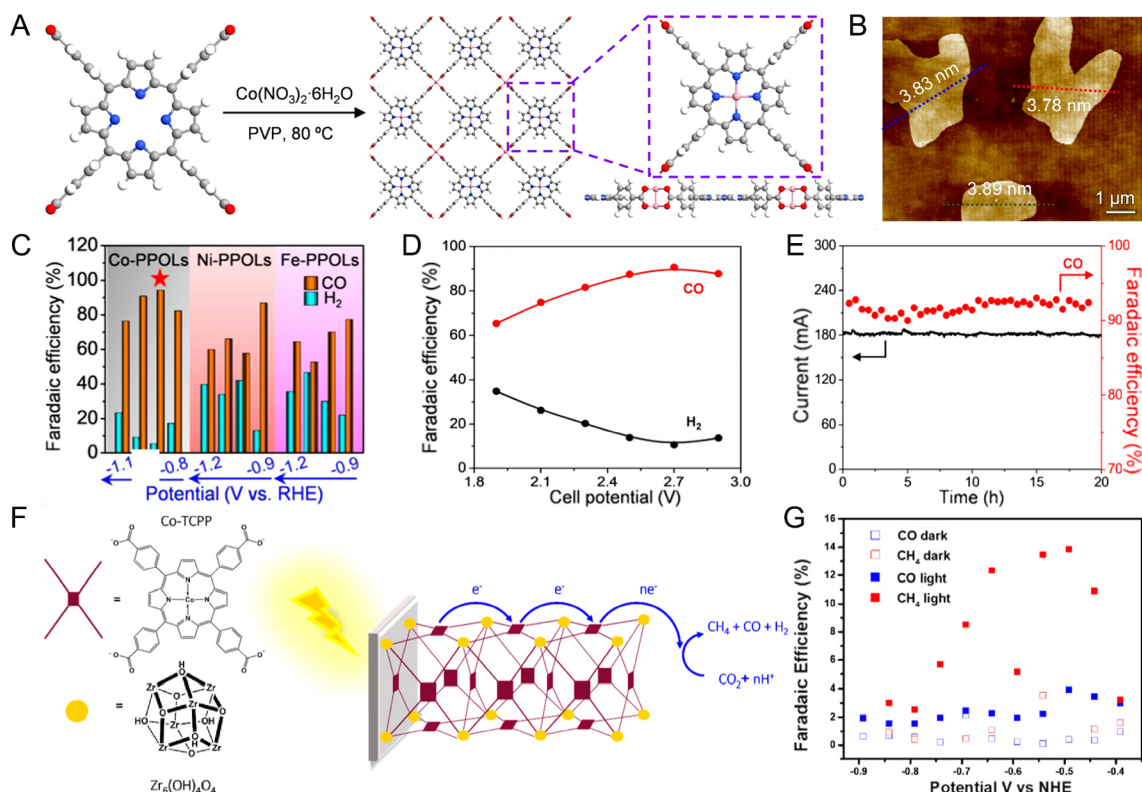


Figure 4. (A) The synthesis of ultrathin 2D Co-PPOLs. (B) AFM image of Co-PPOLs. (C) FE of CO and H₂ at different potentials. (D) FE_{CO} of Co-PPOLs in MEA under different potentials. (E) Long-term stability of Co-PPOLs in MEA^[83]. Copyright 2023 Wiley-VCH. (F) Schematic illustration of the photo-assisted CO₂RR on Co-MOF-525. (G) The FE of CH₄ and CO under dark and light^[84]. Copyright 2023 Wiley-VCH.

functional theory (DFT) calculations indicated that, unlike NiPc-NiO₄ nanosheets, a Ni-N₄ unit in the H₂Pc ring acted as catalytic active center, while the Ni(NH)₄ node accelerated transport of protons/electrons to the active site, thereby promoting the process of CO₂-to-CO. The FE_{CO} for this catalyst reached 96.4% at -0.7 V_{RHE} with a current density of 24.8 mA cm⁻² at -1.1 V_{RHE}, which were remarkably good characteristics for H-type electrolytic cells among the reported 2D MOFs.

The conversion of CO₂ to C₂H₄ has great significance for sustainable energy production. However, this process can be quite difficult due to high energy barriers for the hydrogenation of *CO and C-C coupling steps^[92]. For such cases, electrocatalysts with dual active sites are expected to be a better choice. By assembling metallo-ligand (2,3,9,10,16,17,23,24-octahydroxyphthalocyaninato) Cu(II) (PcCu-(OH)₈) with CuO₄ nodes, a PcCu-Cu-O 2D MOF was prepared for conversion of CO₂ to C₂H₄^[93]. It exhibited a high FE of 50(1)% and current density of 7.3 mA cm⁻² at -1.2 V_{RHE} with the synergistic effects of CuPc and CuO₄; i.e., the CO formed on the CuO₄ site could rapidly diffuse on CuPc site and dimerize with *CHO to form *OCCHO, thereby reducing C-C dimerization energy barrier. In summary, this study provided a strategy for designing and utilizing electrocatalysts with dual active sites to reduce CO₂ into C₂₊ compounds.

Ligands with heteroatoms, such as tricycloquinazoline (TQ) and hexaazatrinaphthylene (HATNA), have also been reported for the 2D *c*-MOF preparation. Liu *et al.* selected an electron-deficient TQ moiety in the ligand incorporated into the 2D MOF framework and coordinated it with Cu²⁺ and Ni²⁺ to prepare M₃(2,3,7,8,12,13-hexahydroxytricycloquinazoline) [M₃(HHTQ)]^[94]. The Cu₃(HHTQ)₂ exhibited a cellular

2D network that passes through π - π interaction, which was further stacked along the *c*-axis; the crystal edge with a ligand terminal was observed, indicating good crystallinity and conductivity. In CO₂-saturated electrolytes, the current density of Cu₃(HHTQ)₂ can reach 45 mA cm⁻² at -1.2 V_{RHE}. Meanwhile, the Cu₃(HHTQ)₂ showed FE of 53.6% for CH₃OH under low overpotential conditions (-0.4 V_{RHE}). Similarly, a HATNA-Cu-MOF by assembling HATNA as a ligand with electron-deficient conjugated molecule with Cu catecholate node could efficiently convert CO₂ to CH₄, with FE of 78% and current density of 8.2 mA cm⁻² at -1.5 V_{RHE}^[95].

Single-atom MOFs

Atomically dispersed metal sites (ADMSs) in metal nodes of the coordinatively unsaturated sites are isolated metal atoms with well-defined local coordination structures, whose coordination bonds, bond lengths, and coordination numbers can be tuned to change the electrocatalytic CO₂ selectivity/activity. The maximum atomic utilization and the unsaturated coordination environment reduce the excess metal cost and improve the catalyst performance. The design of monatomic catalysts with good electrical conductivity, discrete active centers, and good mass transfer performance for efficient electrocatalysis can be a challenging process. ADMSs can be easily introduced into (i) metal nodes and organic ligands due to their highly ordered arrangements; and (ii) the pores of MOFs. This property leads to advantages in several reactions, making ADMSs an important component of heterogeneous catalysis research.

Chen *et al.* prepared an electrocatalyst (2Bn-Cu@UiO-67) by embedding N-heterocyclic carbene (NHC)-linked Cu single-atom sites (SAs) (2Bn-Cu) into porous MOF shell (UiO-67) for CH₄ electrosynthesis^[96]. It had FE of ~81% for CH₄ at -1.5 V_{RHE}, with a corresponding current density of 420 mA cm⁻², due to the following properties: (i) Cu-SAs as the catalytic center of CO₂RR were anchored on NHC by metal-carbon bonds. The electron donor effect of the NHC increased the charge density around metal sites which was beneficial to the adsorption of CHO* intermediate, thus promoting the CH₄ formation; and (ii) The MOF framework had a strong ability to capture CO₂ molecules and provided multiple channels to facilitate the diffusion of CO₂ to 2Bn-Cu. These two aspects synergistically promoted efficient electrocatalytic CO₂RR.

SA coordination with diverse heteroatoms exhibits advantages for the selectivity of various hydrocarbons^[97]. Zhang *et al.* synthesized Cu-based *c*-MOF (Cu-DBC) consisting of a conjugated graphene-like ligand (dibenzo-[g, p]chrysene-2,3,6,7,10,11,14,15-octaol, 8OH-DBC) and Cu-O₄ active sites to study the effects of coordination environment on CO₂RR^[97]. It was found that highly conjugated organic ligands imparted distinctive redox properties and electrical conductivity to Cu-DBC, while the abundant and uniformly distributed Cu-O₄ sites contributed to highly selective transformation of CO₂ to CH₄. The Cu-DBC catalyst had FE of ~80% for CH₄ with partial current density of 162.4 mA cm⁻² at -0.9 V_{RHE}. The relationship between the selectivity of CO₂RR and coordination environment of a separate Cu site was studied by DFT. The results showed that Cu-O₄ site in Cu-DBC had a lower energy barrier than the N-coordinated Cu site in 2BN-Cu@UiO-67, showing better CO₂RR performance.

SAs are more likely to reduce CO₂ into C₁ products, such as HCOOH, CO, CH₄, *etc.*, while the formation of C₂₊ products by C-C coupling often requires double active sites^[98]. Based on the above considerations, a MOF with Ir-porphyrin and Cu-SAs double active sites (Cu-SAs@ Ir-PCN-222-PA) was formed by confining Cu SAs in a nano-framework of Ir-porphyrin-based MOF (Ir-PCN-222), realized the tandem catalytic process of CO₂→CO→C₂H₄^[99] [Figure 5A]. As a result, Cu-SAs@Ir-PCN-222-PA could promoted the transformation of CO₂ to C₂H₄ with high FE of 70.9% and current density of 20.4 mA·cm⁻² at -1.0 V_{RHE} [Figure 5B]. However, no C₂H₄ but CO products were produced at Ir-PCN-222 and Cu-SAs@PCN-222-PA, demonstrating that Cu-SAs and Ir-porphyrin worked together to promote the reduction of CO₂ to C₂H₄.

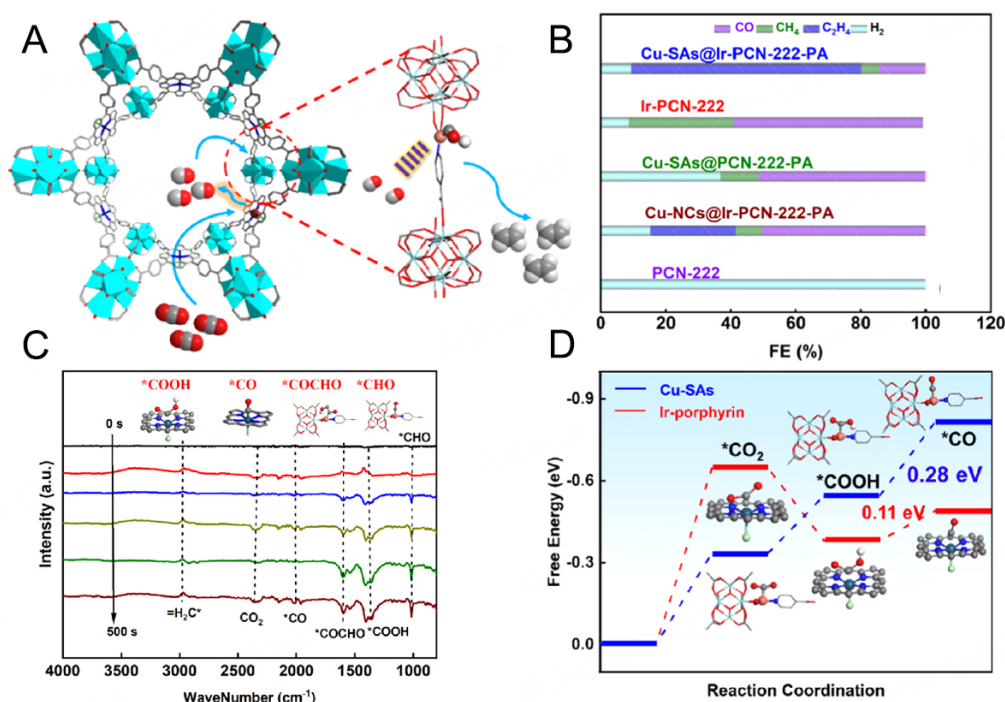


Figure 5. (A) Synergistic tandem electrocatalytic CO₂ to C₂H₄ for Cu-SAs@Ir-PCN-222-PA. (B) FE at -1.0 V_{RHE}. (C) *In situ* FTIR spectrum for the electrocatalytic CO₂RR on Cu-SAs@Ir-PCN-222-PA. (D) CO formation on Cu-SAs and Ir-porphyrin of Cu-SAs@IrPCN-222-PA^[99]. Copyright 2024 the American Chemical Society.

The reaction mechanism was investigated by *in-situ* diffuse reflectance infrared Fourier transform spectroscopy (DRIFT) and DFT calculations. The signals of Cu-*CO, Ir-*CO where *CO was the intermediate in the process of CO₂-to-C₂H₄, and free CO and Cu-*COCHO were found [Figure 5C]. In addition, CO molecules first appeared in Ir-PCN-222 and then transferred on Cu-SAs with a large diffusion coefficient ($2.3 \times 10^{-7} \text{ m}^2 \text{ s}^{-1}$), and then underwent C-C coupling reaction with *CO^[100], which was consistent with DFT calculation. Specifically, CO adsorption energy on Ir-porphyrins (-0.70 eV) was significantly lower than that of Cu-SAs (-0.82 eV) [Figure 5D], proving that CO was formed on Ir-porphyrins sites. Then, CO molecules desorbed from the Ir-porphyrin site and reacted with Cu-*CO to form *COCHO due to the low barrier energy of *COCHO formation, followed by multiple dehydrogenation and hydrogenation steps to form C₂H₄.

The electronic structure adjustment of *sp*² C sites in imidazole organic ligands influences the performance of electrocatalytic CO₂RR. M_xZn_y/ZIF-8 (M: transition metal) was prepared by substituting a portion of Zn²⁺ in ZIF-8 into Ni²⁺, Fe²⁺, and Cu²⁺ through a doping strategy^[101]. As a result, the optimum Cu_{0.5}Zn_{0.5}/ZIF-8 could convert CO₂ to CO with the highest FE_{CO} of 88.5% and partial current density of 11.57 mA cm⁻² at -1.0 V vs. RHE, which was much higher than that of pristine ZIF-8 (FE_{CO}: 43.7%). The enhancement of performance was attributed to the enrichment of electrons on the *sp*² C in the imidazole organic ligands because of the introduction of additional electronic states by Cu doping, promoting the rapid transfer of electrons. Furthermore, the change in the electronic structure of *sp*² C made Cu_{0.5}Zn_{0.5}/ZIF-8 more strongly bound to COOH*, promoting the transformation process of CO₂-to-CO. Furthermore, the electronic properties of SAs, such as binding energy and reaction coordinates, are considered the key factors determining their catalytic performance^[102]. Xue *et al.* created a model to study these properties by confining a series of 3d transition metal SAs into the microporous cavity of UiO-66-NH₂ for electrocatalytic CO₂RR^[103].

MOF composites

Traditional MOFs exhibit poor conductivity and lack electron-donating components in their structures, which greatly limit their catalytic efficiency for electrochemical CO₂RR. These characteristics can be tuned by introducing guest species, including conductive substrates, metals, metal oxides, or functional molecules to construct MOF composites^[104].

Metal-MOF composites

MOF films can be deposited on highly reactive catalytic materials, such as gold nanostructured microelectrodes (AuNMEs), silver (Ag), and other solid electrodes, to obtain high catalytic efficiency^[105]. Ag, as an electrocatalyst, can reduce CO₂ to CO^[106]; however, this process can be impeded by competitive HER and selectivity of electrochemical reductive products^[107]. Non-catalytic Zr₆-oxo-based MOF (UiO-66) thin films with different thicknesses and chemical compositions have been assembled on Ag electrodes^[108]. The existence of MOF membranes can systematically regulate the chemical environment of the active site on a molecular level, resulting in a significant improvement of electrocatalytic performance. Three key mechanisms have been used to verify such an improvement in electrocatalytic activity. Firstly, porous MOF membranes weakened the mass transfer of CO₂ and H⁺ to Ag electrocatalysts. Compared to the reactants in the bulk solution, the local concentration of reactants near the catalyst changed significantly, thereby changing the catalytic path. Secondly, Zr₆-oxo nodes of MOF contained brønsted acidic groups close to the catalytic activity surface. These groups accelerated electrocatalysis by stabilizing the activated *COOH intermediates. Thirdly, the decoration of MOFs with a positively charged ligand, such as (3-carboxypropyl) trimethylammonium (TMA), can control the proton transfer at the catalytic activity site, thereby improving the electrocatalytic selectivity. The combination of these three mechanisms increased the selectivity of CO for Ag from 43% to 89% at -0.8 V_{RHE}.

Considering that the solubility of CO₂ in acetonitrile was higher than that in water, coating the Bi electrode with UiO-66 film decorated by nitrile functional groups (Bi-UiO-66-CN) as a CO₂ enrichment layer can increase the local concentration to 0.82 M, which was 27 times the concentration of CO₂ in the bulk phase, and further improved the electrocatalytic rate and product selectivity^[109]. By optimizing the thickness of the film, the maximum HCOOH FE could reach 93% at -0.75 V_{RHE} for Bi-UiO-66-CN. Especially, the partial current density of HCOOH could reach 166 mA cm⁻² at -0.9 V vs. RHE, more than seven times that of a bare Bi electrode. The improved activity was attributed to the change of the Bi surface microenvironment because of the anchor of UiO-66-CN membranes. At first, coating a UiO-66-CN membrane could enhance the CO₂ adsorption capacity of the catalytic site, thus accelerating the catalytic reaction. Furthermore, the interfacial structure between Bi and UiO-66-CN promoted CO₂ activation and intermediate stabilization, thereby promoting the selective formation of HCOOH.

The high SSA and periodic framework chemical functionality of MOFs provide the possibility of embedding metal active sites within their framework at a high density to include the characteristics of nanocrystals (NCs) for CO₂RR^[110]. Kung *et al.* coated MOF films (NU-1000) with Cu nanoparticles (NPs) to prepare an electrocatalyst (Cu-SIM NU-1000) for CO₂RR using the following process^[111]: Initially, Cu(II) was uniformly coated onto the NU-1000 film through solvothermal deposition in MOFs (SIM). Subsequently, Cu(II) was partially reduced to Cu(0) through an electrochemical process. Cu embedded in the MOF film did not change its crystallinity and morphology, but the SSA reduced compared to that of pure NU-1000. As a result, Cu-SIM NU-1000 primarily produced HCOOH as main product with FE of 31% at potential of -0.82 V_{RHE}. The size of Cu NPs in this sample was limited to < 10 nm because of the MOF film channel size, so the inhibition of HER was less obvious.

The heterogeneous interface constructed by the intimate contact between MOFs and Cu nanowires (NWs) can adjust the adsorption energy of specific intermediates, thus achieving precise regulation of product selectivity. Additionally, porous structure of MOFs facilitates the local enrichment of reactants, the exposure of active sites, and promotes the interfacial diffusion of reactants between Cu-NWs and MOFs, thereby improving catalytic performance. *In-situ* encapsulation of ZIF-8 on the Cu-NW surface to synthesize the composite Cu@ZIF-8 NWs with core-shell structure resulted in an $\text{FE}_{\text{CH}_4 + \text{C}_2\text{H}_4}$ of 57.5% at -0.7 V *vs.* RHE^[112] [Figure 6A and B]. However, it only produced CO for ZIF-8. For pure Cu-NWs, the mixed total FE of products CO, CH₄, C₂H₄ and HCOOH, C₂H₅OH was low, but for H₂, it was more than 50% at -0.5~-0.9 V. The difference in catalytic activity and product distribution between the composite structure and the single material suggested that the existence of the interface between ZIF-8 and Cu-NWs enabled the regulation of product selectivity and the effective inhibition of HER. In addition, wrapping of ZIF-8 on Cu regulated the adsorption energy of the reaction intermediate, which was also verified by DFT calculation. The combination of *CO and H to produce *CHO was regarded as a crucial stage in the process of CO₂ to hydrocarbon products. The energy barrier of *CHO for Cu@ZIF-8 NWs was 0.62 eV, significantly lower than that of pure Cu (0.79 eV), proving that the formation and stabilization of *CHO was facilitated at the interface between Cu and ZIF-8, promoting the process of CO₂→CH₄+C₂H₄ [Figure 6C].

It was reported the capture form of CO₂ molecules on MOFs was also one of the factors affecting the efficiency of CO₂ reduction^[113]. Bi NPs, as an electrocatalyst, were loaded on UiO-66 (Bi/UiO-66) for the transformation of CO₂ to HCOOH. The FE of HCOOH could reach 65%-85% at -0.4~-0.7 V_{RHE} for both Bi and Bi/UiO-66. Notwithstanding, the current density of Bi/UiO-66 was -265 mA cm⁻² at -0.7 V_{RHE}, 4.6 times higher than that of pure Bi, which was attributed to the presence of CO₂ adsorbed on the UiO-66 in the form of carbonate to promote CO₂ conversion. The mechanism of CO₂RR based on Bi/UiO-66 was also proposed. The CO₂ enriched on Bi/UiO-66 reacted with OH⁻ (KOH electrolyte) to form HCO₃⁻ which combined with UiO-66 falling from the electrode to form [Zr₂(OH)₂(CO₃)₄]²⁻^[114], representing the CO₂ capture process accompanied by the structural transformation of UiO-66. Meanwhile, HCOOH produced on Bi ionizes to release H⁺. The H⁺ then reacted with the carbonate ion to release CO₂, which could be used directly in the CO₂ conversion process [Figure 6D].

Ag NP catalysts are prone to sintering or agglomerating during the reaction, leading to a decrease in their activity. Confining NPs in the MOF is a good means of preventing aggregation while providing a path for product diffusion in its pores. To increase the pore size of MOFs, Aparna *et al.* replaced the BDC linker in UiO-66 with 2-mercaptobenzoic acid (2-MBA) to create defective MOFs (UiO-66-SH) [Figure 6E]^[115]. Due to the strong interaction between the thiol group and Ag, it helped anchor Ag NPs on MOFs to prepare Ag@UiO-66-SH, which could promote the transformation of CO₂ to CO with 74% FE and high partial current density of 19.5 mA cm⁻² at -1.1 V *vs.* RHE. To strongly inhibit the HER, Guntern *et al.* embedded Ag NCs into Al-PMOF ([Al₂(OH)₂-(TCPP)]) [tetrakis(4-carboxyphenyl) porphyrin (TCPP)] to prepare Ag@Al-PMOF, ensuring close contact between the Ag NCs and MOF^[110]. The CO FE of the Ag@Al-PMOF composites was more than twice that of the plain Ag NCs, and the HER was inhibited significantly. Due to the tunability of the synthesis process, the close contact between the Ag NCs and MOF interface acted as a crucial factor in facilitating charge transfer between them and enhancing the catalytic performance.

Metal-oxide-MOFs composites

Metal oxide NPs can act as effective electrocatalysts for CO₂RR^[116,117]. However, their low SSA limits the adsorption of reactant molecules. Moreover, they tend to agglomerate during the reaction, which limits the CO₂ conversion. By embedding metal oxide NPs into MOFs, the porous structure is maintained and the interaction between the NPs and MOFs is enhanced, significantly boosting the strong electrocatalytic performance for CO₂ reduction^[118,119].

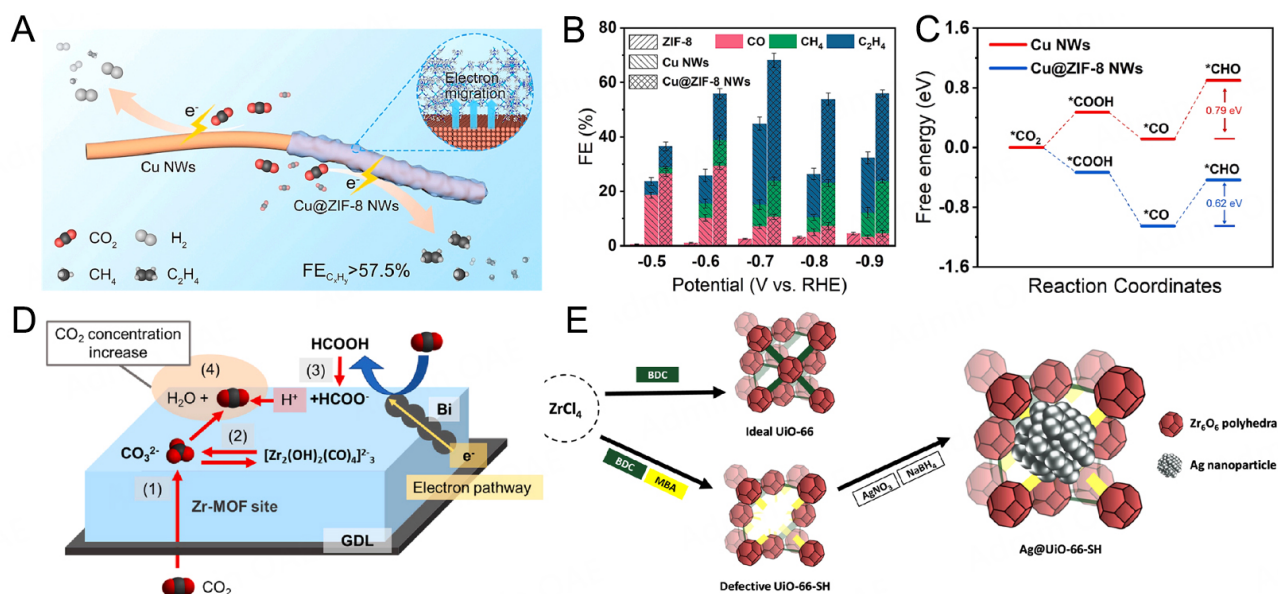


Figure 6. (A) Schematic diagram of Cu@ZIF-8 NWs for electrocatalytic CO₂RR. (B) FE of CO, CH₄, and C₂H₄. (C) Free energy of CO₂RR on Cu NWs and Cu@ZIF-8 NWs^[112]. Copyright 2024 Elsevier. (D) The possible mechanism of Bi/UIO-66 for CO₂RR^[113]. Copyright 2023 Elsevier. (E) The synthesis of Ag@UIO-66-SH^[115]. Copyright 2023 the American Chemical Society.

Cu₂O, as an electrocatalyst, can convert CO₂ into C₂H₄ with low FE and poor stability. CO₂ capture and adsorption are key steps in the heterogeneous catalytic process; therefore, it is a feasible strategy to combine Cu₂O with MOFs with high SSA to form an integrated catalyst, which can improve the CO₂ adsorption capacity of Cu₂O to realize the conversion of CO₂→hydrocarbons with high selectivity and stability. Tan *et al.* combined Cu-MOF with Cu₂O to prepare a hybrid electrocatalyst for CO₂RR^[120]. The composite Cu₂O@Cu-MOF exhibited high SSA of 1,467 cm² g⁻¹ and CO₂ adsorption capacity of 83.6 cm³ g⁻¹, about ten times higher than that of Cu₂O (8.3 cm³ g⁻¹). The catalyst showed an excellent performance with an FE_{CH₄+C₂H₄} of 79.4%, with the FE for CH₄ being 63.2%. The unsaturated coordination active centers in Cu₂O@Cu-MOF led to a large CO₂ adsorption capacity and the embedded Cu₂O contributed to efficient charge transfer. To further increase the selectivity for C₂H₄, Cu₂O/Cu-CuTCPP heterostructures (Cu₂O/CPFs) with three Cu-active centers (Cu₂O, Cu-N₄, Cu-O₄) were constructed^[121]. The FE of C₂H₄ for Cu₂O/CPFs was 61.8% at -1.3 V_{RHE}, significantly higher than that of pure MOF (32.6%) and Cu₂O (18.1%). The current density of C₂H₄ was -7.96 mA cm⁻², far exceeding that of CPFs and Cu₂O, respectively. The presence of the built-in electric field between Cu₂O and CPFs promoted the rapid transfer of electrons from CPFs to Cu₂O and was beneficial to the stabilization of Cu-O₄ sites in MOFs. Meanwhile, Cu₂O and Cu-O₄ sites were connected by Cu²⁺-O-Cu⁺-O bond, promoting adsorption, consumption of reactant molecules, as well as C-C coupling of *CHO and *CO, and finally C₂H₄ products could be generated at Cu₂O and Cu-N₄ sites.

Owing to slow C-C coupling reaction kinetics and complex intermediates, C₂H₅OH selectivity over Cu-based catalysts is usually relatively low. To further improve the C₂H₅OH selectivity of the Cu-based electrocatalyst, the construction of asymmetric refined structures can enhance the charge polarization effect, which acts as a critical factor in promoting the proton-coupled electron transfer (PCET) process of CO₂ to produce C₂H₅OH^[122]. Zhang *et al.* coated Cu₂O NPs with a NiCu-MOF grown on a Cu foam to synthesize Cu₂O@MOF/CF with an asymmetric fine structure^[123]. Cu₂O@MOF/CF could serve as a cathode for CO₂ reduction, providing high FE of 44.3% for C₂H₅OH at -0.615 V vs. RHE. The internal electric field induced by the existence of multiple self-polarization units in Cu₂O@MOF/CF led to the asymmetric distribution of

electrons and promoted C-C coupling process in CO₂RR. The free energy of *OCCOH formation (1.26 eV) at the Cu site of Cu₂O in Cu₂O@MOF/CF was significantly lower than that of pure Cu₂O/CF (2.13 eV) and Cu₂O@CuMOF/CF (1.39 eV), indicating that the dimerization of *OCCOH tended to proceed at the Cu site of Cu₂O and the introduction of MOF contributed to the C₂H₅OH formation.

The unusual flaky structure and electronic characteristics of 2D MOFs lead to several advantages in the construction of novel high-performance composites^[118,119]. Liu *et al.* employed bismuth oxide (Bi₂O₃) NWs as active sites to be uniformly deposited on a metal-organic layer (MOL) to prepare a Bi₂O₃/MOL composite for CO₂RR^[118]. This composite had FE of > 85% for HCOOH at potential of -0.87~-1.17 V_{RHE}, far more than that of Zr-based MOF (Bi₂O₃/UiO). The structural and chemical stability of the MOL and NWs allowed the composite to maintain its FE at -0.97 V for more than 21 h. Ultrafine CuO NPs were uniformly deposited on a 2D copper 1,4-dicarboxybenzene (1,4-BDC) MOF by hydrothermal method to prepare CuO/Cu-MOF composites^[119]. The Cu-MOF contained a large number of channels with pore structures larger than the molecular size of CO₂. It led to a CO₂ adsorption capacity of the CuO/Cu-MOF composite at 1.0 atm to be ~5.0 mg g_{cat}⁻¹, significantly higher than that of the commercially available CuO NPs. The C₂H₄ FE for this composite reached 50.0% at potential of -1.1 V_{RHE}, compared to CuO (25.5%) and Cu-MOF (37.6%). The improved electrocatalytic performance of the composite came from the improvement of adsorption and activation of CO₂ molecules at the interface between Cu-MOF and CuO.

Functional-molecule-MOFs composites

The electron-rich units are embedded into the MOF to construct MOF-based composites with multiple electron transfer channels, which change the charge distribution around the active sites of MOF and further improve the performance of CO₂RR. Metallocene (MCp₂) is an electron-rich molecule with 18 delocalized electrons due to the presence of two cyclopentadienes (Cp) and a transition metal, making it a good electron donor. Meanwhile, MOFs with metalloporphyrin (M-TCPP), such as MOF-545-Co, may be a suitable electron acceptor. The metallocene molecule (CoCp₂) modification into the MOF-545-Co channel (CoCp₂@MOF-545-Co) overlapped with the large ring conjugated π -electron system of the Co-TCPP group to increase its electron density, which greatly facilitated the electron transfer from the Co-active center to CO₂, and improved the catalytic efficiency and selectivity [Figure 7A]^[124]. Although the CO₂ adsorption capacity of the composite decreased due to the intercalation of CoCp₂, the adsorption energy of CO₂ for CoCp₂@MOF-545-Co (-0.92 eV) was nearly four times higher than that of MOF-545-Co (-0.24 eV) because of the strong interaction between CoP₂ and Co-TCPP via C-Co bond (C in CoCp₂ and Co in Co-TCPP) [Figure 7B and C]. As a result, FE of CO for CoCp₂@MOF-545-Co composite was 97% at -0.7 V *vs.* RHE, much higher than that of MOF-545-Co (54.6%) [Figure 7D]. Moreover, polypyrrole (PPy) is a highly conducting polymer that can be used as an ideal additive for hybridization with MOFs to achieve efficient CO₂ conversion. Xin *et al.* inserted PPy molecules into the channels of MOF-545-Co to synthesize PPy@MOF-545-Co, improving the electron transport capability due to the strong π - π interaction [Figure 7E]^[125]. Therefore, FE of CO for PPy@MOF-545-Co was 98% at -0.8 V *vs.* RHE, twice that of MOF-545-Co [Figure 7F].

For Zn-MOFs (such as ZIF-8), the catalytic active site for CO₂ reduction is located on the ligand coordinated with Zn; therefore, the electrocatalytic activity of such catalysts can be improved by adjusting the ligands. As a nitrogen-containing heterocyclic compound, 1,10-phenanthroline has strong electron donating ability. Doping it into the ligand of ZIF-8 enables the formation of stable coordination bonds with metal ions in MOFs, thereby enhancing the stability and functionality of the material^[126]. The *sp*² C atom in methylimidazole ligand of ZIF-8 was the catalytic active site for CO₂RR, which was still the best catalytic active site after doping with phenanthroline molecules. Due to the doping of the electron donor unit, charge

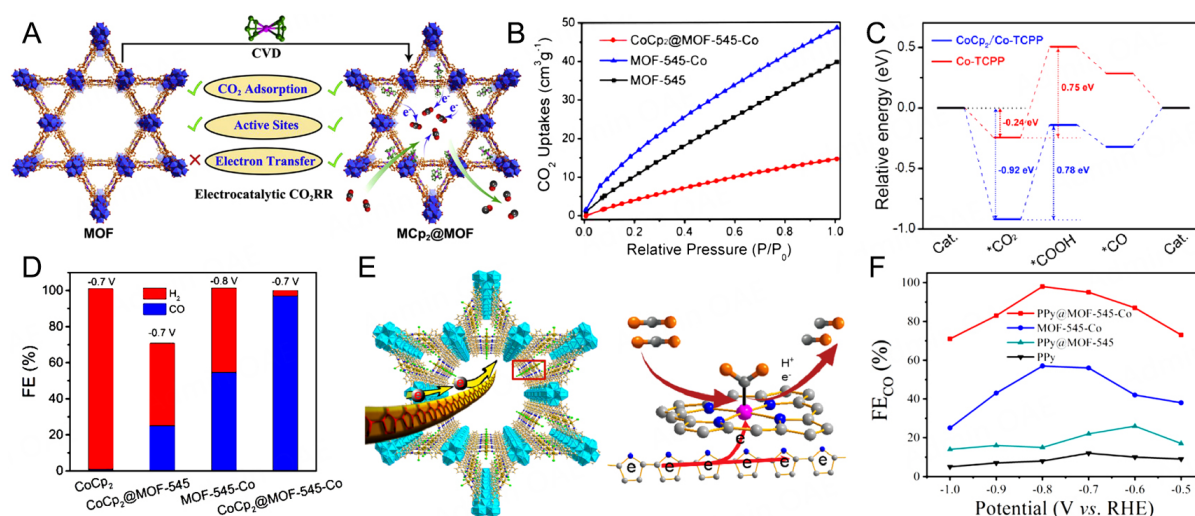


Figure 7. (A) Comparison of $\text{MCP}_2\text{@MOF}$ and MOF for CO_2RR . (B) CO_2 adsorption at 298 K. (C) The free energy of CO_2RR to CO for Co-TCPP and $\text{CoCp}_2/\text{Co-TCPP}$. (D) FE for CO and H_2 . Copyright 2020 Elsevier. (E) Schematic presentation of PPY in the channel of MOF-545-Co. (F) FE_{CO} at different voltages. Copyright 2021 the American Chemical Society.

density of catalytic active site was significantly enhanced (3.702 to 4.884), so that the doped ZIF-8 (ZIF-A-LD) exhibited excellent CO FE (90.57%) at -1.1 V vs. RHE. The theoretical calculation further made known that doping of electron-donating molecules reduced the formation energy of intermediate $^*\text{COOH}$ on the catalytic active site and promoted the activation of CO_2 molecules, thus improving its CO_2 electrocatalytic activity.

MOF derivatives

The conversion of MOFs into different derivatives through post-synthesis strategies can achieve novel properties compared to original MOFs^[127]. Several nanostructure materials, such as MOF-derived porous carbon materials^[128], metal/metal oxides^[129], and metal/metal oxide/carbon nanocomposites^[130], have been developed using 8UMOF as a sacrifice template through heat treatment methods. Notably, MOF-derived materials can not only maintain porous structure and high SSA and enhanced electrical conductivity and structural stability, but also offer many unrivaled advantages, including controllable chemical composition and reduced electron and ion transport distances.

Heteroatom-doped carbon materials

Porous carbon materials have been widely employed in energy storage equipment due to their large SSA, stability, wide source of raw materials, and environment-friendly aspects^[131]. Porous carbons prepared from MOFs as precursors have the advantages of controllable porous structure and high SSA. MOFs can also be used to prepare heteroatom-doped porous carbon, and the existence of heteroatoms can improve the electron density and interface wettability of the porous carbon material, which is conducive to the supply of electrolyte ions, thereby improving the electrochemical performance of the porous carbon.

As a low-cost material, N-doped carbon (NC) materials have a high SSA and adjustable electrochemical activity and conductivity, along with a strong inhibition of HER, thereby attracting much attention as electrocatalysts for CO_2RR . Guo *et al.* prepared ZIF-8/MWCNTs by growing ZIF-8 on multi-walled carbon nanotubes (MWCNTs), and pyrolyzed them to prepare NC materials (ZIF-CNT-FA-p) for selective electrocatalysis of CO_2 to CO against the HER^[132]. This composite had a FE of 100% and total current density of 7.7 mA cm^{-2} at -0.86 V vs. RHE. The superior selectivity could originate from the enhancement of

electron transport and CO₂ mass transfer exhibited by the MWCNTs.

The existence of the N heteroatom can change electronic environment of the C atom, promote CO₂ adsorption, and stabilize intermediate. It has also been found that the number and types of the doping N atoms determine the number of active centers, and ultimately affect the catalytic activity of the material^[133]. Mesoporous NC (MNC-D) materials with adjustable structures and different N dopants have been constructed for CO₂RR through the pyrolysis of ZIF-8, followed by treatment with N, N-dimethylformamide (DMF)^[134]. MNC could efficiently promote the conversion process from CO₂ to CO with FE of ~92% and current density of -6.8 mA cm⁻² at -0.58 V_{RHE}. Further studies showed that the pyridinic-N and defects produced by DMF treatment acted as active centers of the MNC catalyst, which was beneficial to adsorption and activation of CO₂ molecules, further promoting electrocatalysis. In general, co-doping of pyridinic and graphitic N (active N) can synergistically improve the electrochemical CO₂RR performance. Porous NC materials with a large number of active N sites have been prepared via calcinating O-rich MOF (Zn-MOF-74) and melamine (C₃H₆N₆)^[135]. The active N content in the composite was adjusted by regulating temperature and time. This catalyst well inhibited the HER, and had high FE_{CO} of 98.4% at -0.55 V vs. RHE for the sample prepared at 1,000 °C (NPC-1000). The lower number of pyridinic-N had a significant effect on reducing the absolute overpotential^[128]. NC materials, rich in pyridinic-N and quaternary-N species, have been prepared by pyrolysis of ZIF-8 at 700~900 °C in N₂ atmosphere^[136]. The CO FE for the samples pyrolyzed at 900 °C reached ~78%. The pyridinic-N and quaternary-N in the carbon matrix lowered energy barriers of the COOH* for the CO generation, leading to its high selectivity.

Metal/metal oxide interfaces

MOF-derived metal/metal oxide interfaces have a unique porous micro-/nanostructure and a high SSA. Their special morphology is conducive to uniform distribution of reactant molecules, adsorption, and activation, resulting in high selectivity and long cycle life for CO₂RR^[129,137]. A series of Cu/Cu₂O hybrids with porous octahedral structures and varying ratios of Cu⁰ and Cu⁺ were prepared by the pyrolysis of Cu-MOF octahedrons in N₂ atmosphere at different temperatures and heating rates^[138]. The optimal catalyst (Cu-MOF_{20/300}) with higher SSA (129.11 m² g⁻¹) and more Cu⁺ sites could reduce CO₂ to CO and H₂, where the highest FE of CO was 43.8% at -0.76 V vs. RHE for H-type cells. It was worth noting that compared with H-type fuel cells, the activity of the catalyst in the flow MEA reactor was significantly improved due to the smaller gas diffusion resistance. The current density was 34.97 mA cm⁻² at -0.64 V_{RHE}, ~3 times higher than that of in H-type cells. Moreover, the energy loss was also greatly reduced due to the shorter distance between the electrodes in the MEA reactor.

Transition metal oxides as electrocatalysts may have low product selectivity and stability due to the deactivation of the cathode; the catalytic efficiency can be further improved by exposing more active sites through the construction of bimetallic oxides. Porous bimetallic oxides with desired composition and structure by MOF pyrolysis can be synthesized to facilitate the electrochemical reaction^[129,139]. Payra *et al.*^[129] prepared cerium dioxide (CeO₂) and cerium-doped titanium oxide (Ce_{1-x}Ti_xO₂) spherical particles by thermal decomposition of Ce-UiO-66^[140,141] and Ce_{1-x}Ti_x-UiO-66-NH₂ MOFs for CO₂RR^[142]. CeO₂ served as an electrocatalyst to efficiently reduce CO₂ to CH₃COOH, whereas Ce_{1-x}Ti_xO₂ exhibited excellent inhibitory effect on HER. MOF-derived porous indium (In)-Cu bimetallic oxides with adjustable Cu/In ratios have been employed as efficient electrocatalysts (InCuO-*x*, *x* denotes the Cu/In molar ratio) to reduce CO₂ to CO^[139]. InCuO-0.92 had a CO₂ adsorption capacity of 59.4 mg g⁻¹ at 298 K, 5.7 times greater than that of In₂O₃. The smaller Nyquist plots indicated efficient electron migration between In₂O₃ and Cu₂O during the conversion of CO₂, consistent with the electrocatalytic performance of the composite^[143]. Therefore, a good electrocatalytic performance could be obtained by the synergistic effects of In and Cu oxides, which

promoted CO₂ adsorption capacity, mass transport, and charge transfer. The HER could also be inhibited by adjusting Cu/In ratios in MOFs. The InCuO-0.92 composite had 92.1% of FE for CO and total current density of 11.2 mA cm⁻² at -0.8 V_{RHE}. Additionally, InCuO-0.92 showed no cathode deactivation and significant decrease in activity and selectivity during the 24 h continuous test, indicating better stability.

Metal/metal-oxide/carbon nanocomposite interfaces

The carbonization of MOFs provides a direct method for fabricating functional and porous metal/metal-oxide/carbon hybrid materials. Through high-temperature treatment, the MOFs can be directly calcinated into porous carbon materials, and the metal centers can be *in situ* incorporated into the carbon matrix^[144,145]. Thus, the structure provides an excellent electronic connection between the metal/metal oxide interface and carbon skeleton.

Metal NPs deposited on carbon materials

Due to their significant electronic conductivity and high SSA, porous carbons can be used as substrates to load metal NPs^[146], which can prevent NP aggregation, and enhance interface contact to provide better electrical conductivity. Therefore, increasing the density of active sites and interactions between metal NPs and carbon nanomaterials can further improve the catalytic performance^[147]. MOFs are considered a promising precursor to synthesize metal NPs that can be distributed on the carbon substrate. For example, Bi NPs (~4.4 nm) have been grown *in situ* and uniformly distributed on functionalized MWCNTs to prepare Bi NP@MWCNT catalysts for CO₂RR^[146] [Figure 8A and B]. For this composite, the optimal FE and current density for HCOOH reached 95.2% and 10.7 mA cm⁻², respectively, at -1.5 V vs. SCE (saturated calomel reference electrode) [Figure 8C and D]. It was speculated that the MWCNTs in this composite significantly increased the charge density on Bi NPs, promoting the rapid transfer of electrons from Bi to CO₂, thus facilitating the selective conversion of CO₂ to HCOOH^[148]. Moreover, Ni NPs coated with carbon loaded onto NC (Ni-NC_ATPA@C) could effectively reduce CO₂ to CO with FE of ~94% at overpotential of 0.59 V^[149]. At -1.1 V_{RHE}, the CO current density and TOF of the catalyst reached 22.7 mA cm⁻² and 697 h⁻¹, respectively. The direct contact between Ni NPs and aqueous electrolytes could be avoided due to the encapsulation of Ni NPs by carbon, which could significantly inhibit HER. The experimental results combined with the DFT calculations revealed that the carbon layer coated with Ni and N stabilized *COOH without affecting the ability to easily desorb *CO, which acted as a critical factor in promoting electrocatalytic performance.

In previous studies, it was found that smaller metal NPs are more likely to produce *COOH with lower energy. In addition, small metal clusters exhibit thermodynamic stability to avoid aggregation, thereby leading to high catalytic efficiency^[150]. Wang *et al.* employed a Ni-Zn bimetallic MOF as a precursor to prepare Ni nanoclusters with a high dispersion of ~2 nm on NC material^[151]. The particle size and content of Ni catalyst can be effectively regulated by adjusting Ni:Zn ratios in MOF precursors [Figure 8E]. The Ni nanoclusters (diameter = 1.9 nm) loaded on NC material from a MOF with a Ni:Zn ratio of 1:150 created a catalyst (Ni_{1/150}NCs@NC) with FE of 98.7% for CO and partial current density of 40.4 mA cm⁻² at -0.88 V [Figure 8F], attributing to the enrichment of CO₂ originating from hybridization of *COOH and Ni and enhanced electron mobility from Ni to NC. The catalyst also showed long-term stability (~40 h) without decay of activity and selectivity and Ni aggregation [Figure 8G]. The DFT calculations revealed that Ni particles supported on NC facilitated the formation of *COOH, which promoted the process of CO₂-to-CO [Figure 8H].

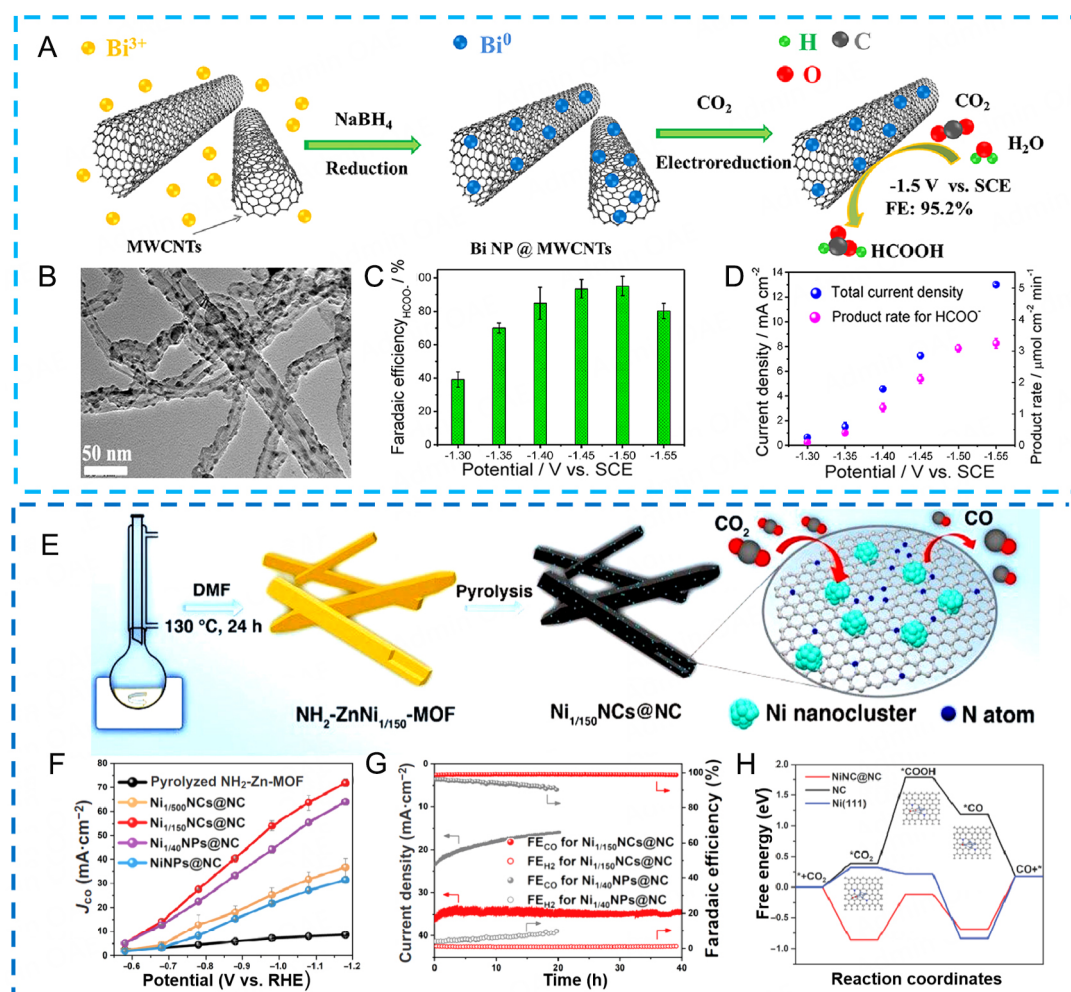


Figure 8. (A) The preparation process of Bi NP@MWCNT; (B) TEM image, (C) FE and (D) Current density of HCOOH for Bi NP@MWCNTs at different potentials^[146]. Copyright 2020 the American Chemical Society. (E) The preparation process of Ni_{1/150}NCs@NC; (F) CO current density and (G) Stability. (H) The calculated free energy of CO₂RR^[151]. Copyright 2023 Springer Nature.

The reduction of CO₂ to syngas (CO and H₂) in a specific ratio is an important industrial feedstock for the synthesis of some chemicals (e.g., methanol, acetic acid, dimethyl ether, *etc.*)^[152]. HER and CO₂RR are two competitive processes, so regulating the adsorption energy of catalysts for H⁺ and CO₂ is the key to producing CO/H₂ with an appropriate ratio^[153]. It was reported that by optimizing the electronic structure of metal alloy composites such as Cu-Co alloys, the adsorption energy of H⁺ and CO₂ could be adjusted, and then a specific ratio of CO and H₂ could be produced. Song *et al.* introduced Cu²⁺ into the synthesis process of ZIF-67 to synthesize bimetallic CoCu-MOFs, which were carbonized at high temperatures to synthesize CoCu@C composite catalysts^[154]. The FE and current density of CO for the optimal sample Co₁Cu₃@C (34%, 11.67 mA cm⁻²) at -0.7 V_{RHE} were significantly higher than those of Co@C (28%, 3.5 mA cm⁻²), originating from the rapid transfer of electrons from Co to Cu in the Co-Cu alloys. It was worth noting that the ratio of CO:H₂ generated for Co₁Cu₃@C was about 1:1.7~1:4, which met the industrial demand. In the CO₂RR process, a CO₂ molecule combined with one electron to synthesize *CO₂⁻, which captured H⁺ to form *CO₂H. It was observed that there was a strong interaction between the carbon atoms in *CO₂H and metal sites on the catalyst surface by DFT calculation, which facilitated the conversion of *CO₂H to *COOH, thus promoting the conversion of CO₂ to CO.

The Bi-based catalyst shows better selectivity and current density in HCOOH^[155], but due to the presence of competing HER, the FE_{HCOOH} at low overpotential is low, and can only exceed 90% at a narrow potential window (< 750 mV)^[156]. Combining different metals with Bi to form alloys by doping strategy can adjust the electron cloud distribution of the catalyst, thereby affecting its affinity for reactants and the stability of reaction intermediates, and further improving the generation efficiency of HCOOH. Ma *et al.* substituted partial Bi sites in Bi-MOF with Sb to prepare Sb-doped Bi-MOF ($Sb_x/Bi-MOF$)^[157], which was carbonized to prepare $Sb_x/Bi@C$. $Sb_{2.5}/Bi@C$ with Sb doping of 2.5% showed excellent FE_{HCOOH} of 94.8% at $-1.4 V_{Ag/AgCl}$, far exceeding that of $Bi@C$. Furthermore, the FE_{HCOOH} of $Sb_{2.5}/Bi@C$ remained above 92% in the range from -1.3 to $-1.6 V$. The doping of a small amount of Sb could effectively promoted the generation of $*OCHO$ and inhibited the formation of $*H$, thus significantly enhancing the selective formation of HCOOH in Bi materials. Furthermore, a series of Ce-doped $Bi@C$ nanorod (NR) electrocatalysts were prepared by pyrolysis of Ce-doped Bi-MOFs^[158]. Firstly, due to the doping of Ce, the number of active sites and adsorption of CO_2 were increased; secondly, the increase of electron density around Bi sites promoted rapid electron transport and reduced the formation energy barrier of $*OCHO$. Therefore, $Ce_{0.05}Bi_{0.95}@C$ NRs achieved high FE_{HCOOH} of 96.1% at $-1.5 V_{RHE}$, accompanied by high stability for 36 h. It was important that FE_{HCOOH} could exceed 90% at an ultra-wide potential window (1,000 mV).

Carbon-supported metal composite catalysts are known to be quite active in producing C_2 and C_3 products due to the high CO_2 pressure that can be generated at the three-phase boundary^[159]. Zhao *et al.* prepared an oxide-derived (OD) Cu/C catalyst by carbonization of HKUST-1 precursors^[159]. The FE of the obtained composite for CO_2 conversion to alcohols was in the range of 45.2%–71.2% at potential of $-0.1 \sim -0.7 V_{RHE}$. For OD Cu/C-1000 catalyst obtained by carbonizing HKUST-1 at $1,000^\circ C$, the CH_3OH and C_2H_5OH production rates were $5.1 \sim 12.4$ and $3.7 \sim 13.4$ mg $L^{-1} h^{-1}$, respectively. Equally notable was that the initial potential for generation of C_2H_5OH was $\sim -0.1 V_{RHE}$, corresponding to overpotential of ~ 190 mV. The increased performance of OD Cu/C originated from interaction between the uniform distribution of Cu and porous carbon matrices.

Metal oxides deposited on carbon

Carbon nanotubes (CNTs) are a type of carbon material with graphene layers that exhibit semiconducting/metallic properties and tubular morphology. Theoretical studies have shown that the curling of the graphene layer results in an inward-to-outward shift of π -electron density, resulting in an electron-rich state on the outer surface. The catalyst dispersed into the CNT cavities exhibits a confinement effect, which affects the mass transfer and distribution of the reactants, thus changing the catalyst redox properties. The ultra-small cobalt (II, III) oxide (Co_3O_4) NPs with a high dispersion were confined within CNTs to prepare a composite electrocatalyst (Co/CNTs) by the pyrolysis of ZIF-67 to effectively reduce CO_2 to CO^[160]. Owing to the excellent nanostructure of the Co/CNTs, Co_3O_4 NPs served as the maximally exposed primary active sites, greatly improving the electrocatalytic efficiency. At the cathode potential of $-0.7 V_{RHE}$, the Co/CNTs obtained 90% FE_{CO} and current density of 20.6 mA cm^{-2} . In addition, the CNTs prevented the aggregation of the Co_3O_4 NPs in the electrolysis process, thus enabling the catalyst to remain stable for a long period (40 h). Similarly, Deng *et al.* used Bi-MOFs as sacrificial precursors to prepare a composite catalyst ($Bi_2O_3@C-800$) for the reduction of CO_2 ^[161]. The composite exhibited a stable FE of 93% for HCOOH at an initial potential of $-0.28 V_{RHE}$ and a high partial current density of 208 mA cm^{-2} at $-1.1 V_{RHE}$ in a flow-cell configuration. The carbon matrix improved the activity and selectivity, while oxides were favorable to the promotion of reaction kinetics and selectivity.

Different structural catalysts with tailored porosities can be produced through MOF pyrolysis, and treatment using different etching reagents provides efficient ways to generate specific active sites^[130]. Sn/SnO₂/C composites with exposed Sn (101) faces have been synthesized by the carbonization of a Sn-based MOF under an argon (Ar) atmosphere and different temperatures as CO₂RR electrocatalysts^[130] [Figure 9A]. The Sn (101)/SnO₂/C-500 (pyrolysis at 500 °C) catalyst had 93.3% FE and current density of 8.2 mA cm⁻² for HCOOH at -0.8 V_{RHE} with no performance decay for 13 h [Figure 9B and C]. With the increase of calcination time (30 to 120 min), the peak intensity of Sn (101) in Sn (101)/SnO₂/C-500 gradually rose, while the FE of HCOOH improved from 45.4 to 93.3% at -0.8 V_{RHE}. This suggested that the Sn (101) could be used as an active site to improve the selectivity of HCOOH. In order to show the superiority of Sn (101) for CO₂RR, Sn (200) was used as a comparative sample and further verified by DFT. The activation of CO₂ to *OCHO occurred spontaneously on both Sn (101) and Sn (200). However, the binding energy for *OCHO on Sn (101) was -0.28 eV, significantly stronger than that on Sn (200) (-0.08 eV), so it was more conducive to the transformation of *OCHO to *HCOOH on Sn (101). Simultaneously, the adsorption energy of H* on Sn (101) (0.23 eV) was much higher than that of *OCHO, proving that Sn (101) could suppress HER well [Figure 9D].

Single-atom catalysts

In recent years, transition-metal SACs (TM-SACs) have been extensively studied owing to their superior electrocatalytic performance, low cost, and stability. TM-SACs can act as adsorption and activation sites for H₂O, O₂, CO₂, etc., and facilitate redox of adsorbed molecules^[162]. The choice of support is particularly important for the formation of TM-SACs because individual atoms tend to agglomerate in the preparation process. In addition, the electron and mass transfer during electrocatalytic reaction are also affected by the substrate. With the advantages of adjustable structure and various available modification methods, MOF precursors/templates can be potentially employed in the synthesis of TM-SACs with high loading capacity, stability, and electrocatalytic activity^[163].

Well-defined metal-nitrogen (M-N_x) sites confined into a carbon matrix (M-N-C) have been successfully obtained by the thermal decomposition of MOFs^[164]. A Fe-doped MOF has been used to synthesize a carbon nano-skeleton with a hierarchical pore structure (micropores to large mesopores) and atomically dispersed metalloporphyrin-like Fe-N₄ active centers^[165]. The presence of mesopores in the nano-framework improved the amount and accessibility of monoatomic active sites and facilitated mass and charge transport. The FE for this composite reached 86.9% at -0.47 V_{RHE} for CO. Isolated M-N_x sites could serve as active centers for CO₂RR. However, the content of the isolated M-N_x active sites in the carbon matrix was generally limited, and they can be maximally exposed using various feasible strategies to achieve efficient catalysis. The functionalization of ZIF-8 NPs was first achieved by the selective restriction of ammonium ferric citrate (C₆H₁₁FeNO₇, AFC) on its surface using a post-synthesis modification strategy (PSMS)^[166]. Subsequently, isolated Fe-N sites were confined into the carbon matrix after the MOF thermal decomposition (C-AFC@ZIF-8). The maximally exposed Fe-N active sites showed excellent selectivity and mass transfer ability for conversion of CO₂ to CO with FE of 91.6% at -0.63 V_{RHE}, superior to most reported noble metal catalysts. The study of CO₂RR mechanism and the site specificity of TM-SACs could instruct the design of M-N-C electrocatalysts to obtain higher product selectivity of CO₂RR. The Fe-N-C catalyst prepared by employing ZIF-8 as a template had FE of > 93.5% for CO at 90 mV of overpotential^[167]. The location of Fe-N₄ may influence the activity of CO₂ reduction, which was verified by DFT calculation [Figure 10A]. The conversion of CO₂ to *COOH on Fe-N₄ groups at the bulk (bulk-Fe-N₄) and edge (edge-Fe-N₄) sites of graphite layers without defects occurred spontaneously, which was beneficial to the CO₂ reduction at low overpotential. However, the adsorption energy of the intermediate *CO on bulk-Fe-N₄ (-1.71 eV) and edge-Fe-N₄ (-1.55 eV) was particularly high, which was not conducive to the desorption of CO, thus causing the

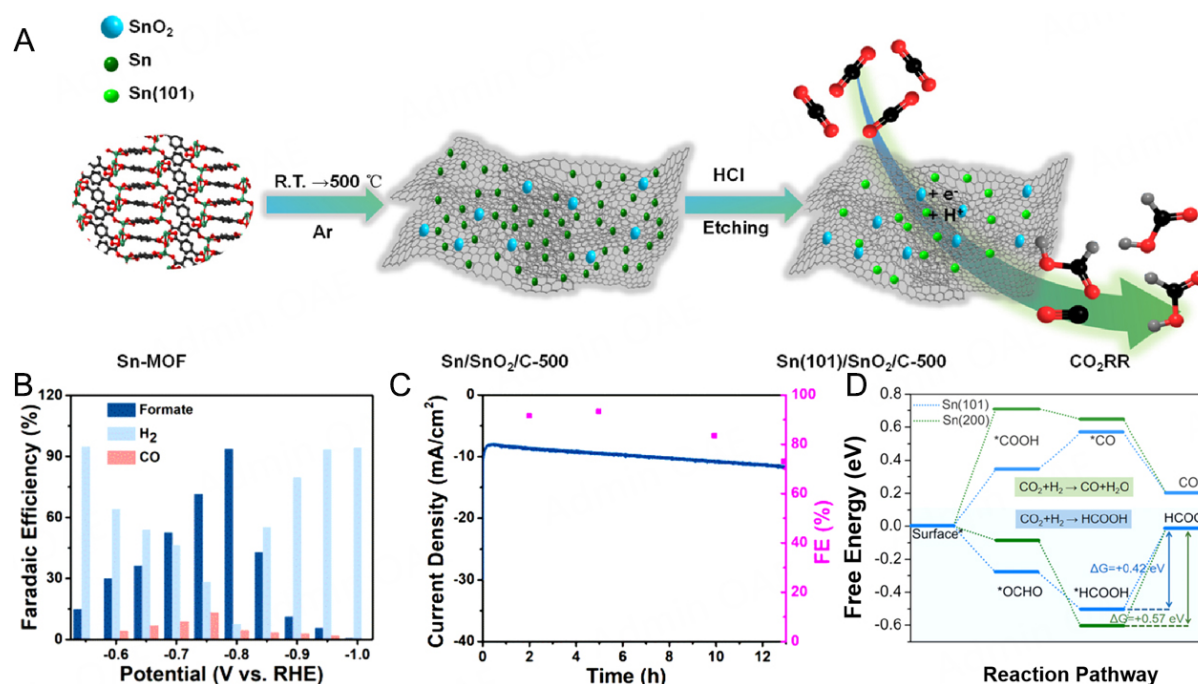


Figure 9. (A) The Sn (101)/SnO₂/C-500 preparation process for CO₂RR. (B) FE and (C) long-term stability of Sn (101)/SnO₂/C-500. (D) The free energy of HCOO⁻, CO formation^[130]. Copyright 2021 the American Chemical Society.

poisoning of the Fe center. However, for Fe-N₄ in the graphite layer with defects (Fe-N₄-pore), the low energy barrier (0.30 eV) of the CO₂-to-*COOH process could ensure the realization of CO₂RR at low overpotential, while the small barrier (0.37 eV) of *CO-to-CO conversion could effectively promote the CO desorption [Figure 10B]. Therefore, it can be considered that Fe atoms in Fe-N₄-pore were the active sites of CO₂RR. The more appropriate binding strength of Fe-N₄-pore for the intermediates *COOH and *CO promoted the conversion of CO₂ to CO.

Although M-N-C as an effective electrocatalyst can promote the process of CO₂-to-CO, the current of the competitive HER grows sharply with the increase of the overpotential, resulting in a rapid decline in the FE of CO, and it is difficult to obtain a high partial current density of CO. Therefore, obtaining high current density and FE for CO₂RR simultaneously is an important challenge for M-N-C. Based on the above considerations, Yan *et al.* embedded unsaturated Ni-N units into porous carbon by pyrolyzing ZIF-8 doped with different Ni contents (Zn_xNi_y ZIF-8) [Figure 10C]^[168]. The FE of CO for all the C-Zn_xNi_y ZIF-8 could be maintained 92.0%~98.0% at a range of -0.53~-1.03 V vs. RHE, and the current density of CO increased with potential, reaching $71.5 \pm 2.9 \text{ mA cm}^{-2}$ at -1.03 V_{RHE} [Figure 10D and E]. The theoretical calculations clarified that unsaturated Ni-N active sites possessed lower *COOH free energy and higher *H adsorption energy, thus exhibiting high CO₂RR activity and inhibiting competitive HER. The catalyst breaks the "seesaw" effect limitation of selectivity and activity on the M-N-C material, and realizes efficient catalysis of CO₂RR. In addition, Ni-N₄ sites have two forms: embedded at the edge (Ni-N₂₊₂) and in the bulk (Ni-N₄) of the carbon matrix^[169,170]. However, the catalytic active sites for CO₂RR between these two types are difficult to distinguish. Over these considerations, Pan *et al.* used ZIF-based Ni-N-C catalyst to achieve highly selective conversion of CO₂ to CO with FE of 96% at overpotential of 570 mV^[171]. The DFT calculations revealed that the Ni-N₂₊₂-C₈ with active C atoms possessing dangling bonds were considered to be the active sites due to lower activation energy in the dissociation of COOH* intermediates. In contrast, Ni-N₄-C₁₀, which was tightly embedded into graphite layers, may not be active. Moreover, Ni-N₂₊₂-C₈ could efficiently inhibit the competitive HER as well.

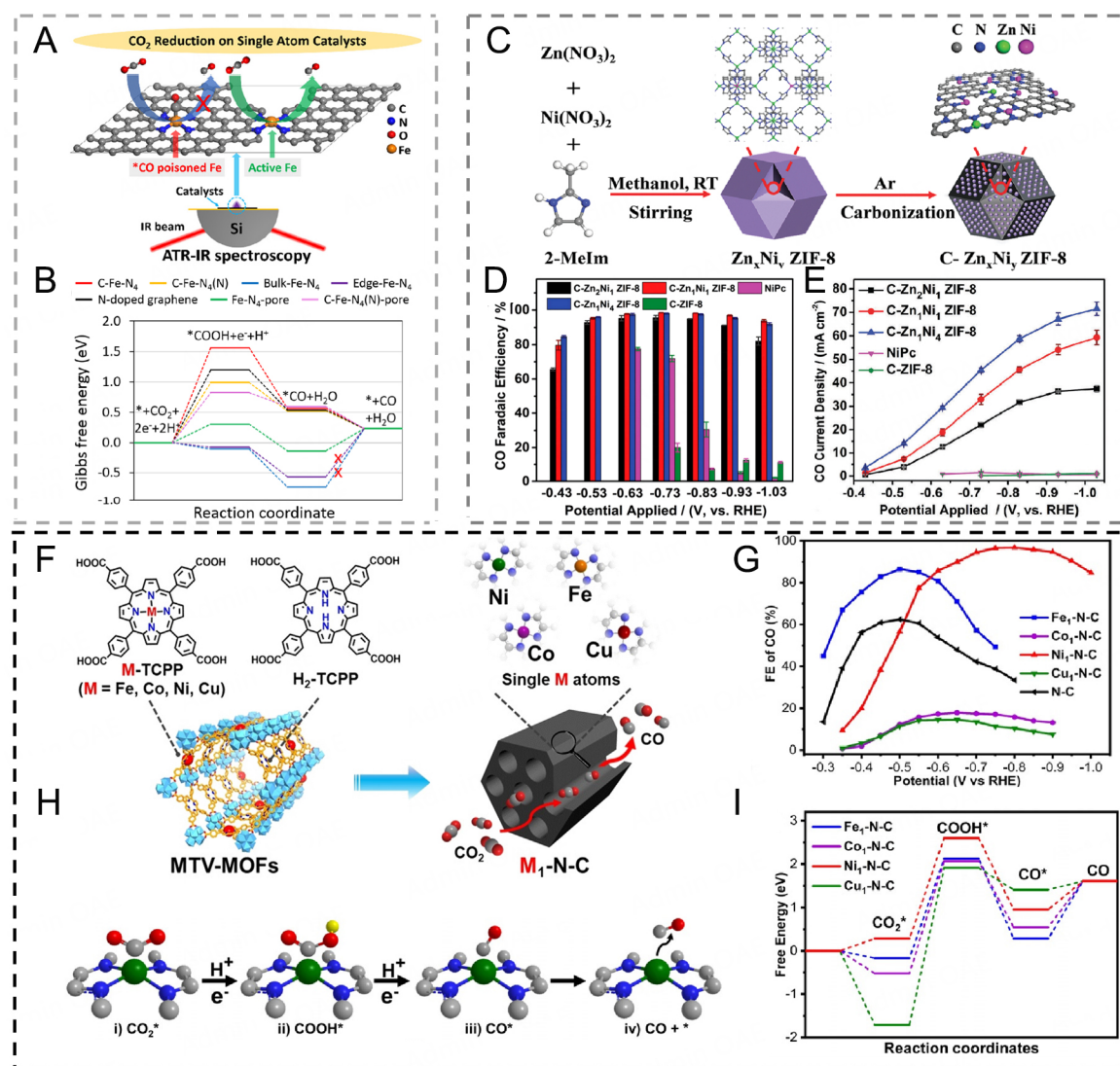


Figure 10. (A) Fe-N₄ moiety in the defective porous graphitic layer (Fe-N₄ pore). (B) Gibbs free energy on various sites^[167]. Copyright 2019 the American Chemical Society. (C) The preparation process of C-Zn₂Ni₂ ZIF-8. (D) FE and (E) current density of CO at different potentials^[168]. Copyright 2018 Royal Society of Chemistry. (F) The synthesis of M₁-N-C by pyrolysis of MTV-MOFs. (G) FE of CO for M₁-N-C in pure CO₂. DFT calculations of (H) reaction paths and (I) free energy^[172]. Copyright 2020 Wiley-VCH.

Influence of coordination metal

Owing to the diversity in MOF structures and compositions, M-N-C catalysts containing different metal elements could be constructed using the tunability of the ligand central metal. By only changing the types of monatomic metals, the physicochemical properties of MOF-derived monatomic materials can be strictly controlled, thus creating a prerequisite for identifying and comparing the catalytic performance^[172].

M-N-C with different M-N₄ groups (M = Mn, Fe, Co, Ni and Cu) was prepared to explore the influence of metal centers on electrocatalytic performance^[173]. It was found that the current density of CO₂ reduction to

CO was significantly different among the five catalysts, in which Co-N-C showed the best intrinsic activity (at $-0.6 V_{\text{RHE}}$), followed by Fe-N-C, Ni-N-C, Mn-N-C and Cu-N-C. Due to similar structure of these five model catalysts, the binding affinity of metal sites for the key intermediates might be the reason for the difference in the electrocatalytic CO_2RR activity. The binding ability of Mn-N₄ and Fe-N₄ to CO was too strong, so the desorption of CO^* determined its activity. However, Ni-N₄ was weakly bound to CO, so the activation of CO_2 to form CO_2^{*-} was the main process affecting their activity. The more suitable energy barrier of Co-N₄ for CO_2^{*-} and CO^* was the reason for its best activity. Mn-O₄-O could be formed due to the strong adsorption of Mn-N₄ on O, and Mn-O₄-O had a high energy barrier for CO_2 adsorption, which explained the poor activity of Mn-N-C for CO_2RR . For Cu-N-C, the central Cu ion was reduced to Cu (0), resulting in low activity. In terms of selectivity, the FEs of Fe-N-C, Ni-N-C and Mn-N-C were $> 80\%$, whereas Co-N-C exhibited lower selectivity (48%), which was attributed to the different binding energies between CO_2^{*-} and H^* .

The structural and functional diversity of multivariate MOFs (MTV-MOFs) provides the possibility to construct M-N-C with multiple metal centers to achieve electrocatalytic conversion under low CO_2 concentration. Based on this, a series of MOFs with metal species at the center have been constructed by introducing both porphyrin and metalloporphyrin ligands using a mixed ligand strategy^[172]. M-N-C (M = Fe, Co, Ni, and Cu) with the same chemical environment and substrate was prepared using MTV-MOFs with porphyrin groups as templates [Figure 10F]. The FE of Ni₁-N-C catalyst reached 96.8% for CO, far exceeding that of Fe₁-, Co₁- and Cu₁-N-C in pure CO_2 [Figure 10G]. The free energy calculation for the intermediate path from CO_2 to CO towards different catalysts revealed that free energy of COOH^* formation along with CO desorption in the RDS of Ni₁-N-C was optimized [Figure 10H and I]. Ni₁-N-C inhibited the competitive HER most effectively, explaining the high FE for the CO_2RR . Furthermore, upon application for the more challenging reduction of low-concentration CO_2 (15%), Ni₁-N-C maintained 80% of FE for CO.

Effect of coordination environment

The metal active center in M-N-C interacts with its surrounding atoms to form a certain coordination environment, which can regulate electron density of the metal site, and then affect adsorption behavior of key reaction intermediates on the monatomic active center, thereby optimizing catalytic performance^[174,175]. At present, the change of coordination environment of metal active centers mainly includes the regulation of number, species of coordination atoms, and cooperation of adjacent metal sites.

Regulation of coordination number

The variation in the coordination numbers of SAs in M-N-C leads to differences of the local electron density of the central metal atom, which greatly affects adsorption and configuration of the reaction intermediates during CO_2RR , thus resulting in varying catalytic activities of SACs^[176,177]. A PSMS strategy was adopted to prepare Ni-N_x-C with different N coordination numbers^[176]. For Ni-N₃-C catalyst used in the CO_2RR , the FE reached 95.6% for CO at $-0.65 V_{\text{RHE}}$, surpassing Ni-N₄-C catalyst (89.2%). DFT calculations suggested that free energy of COOH^* formation on Ni-N₃-C was 0.66 eV, significantly lower than that of Ni-N₄-C, thus promoting the CO formation. SACs have also been synthesized by inserting PPy into bimetallic MOFs^[177]. The distance between two Ni atoms was elongated by the presence of Mg^{2+} in MgNiMOF-74. In the pyrolysis process, isolated Ni atoms could be stabilized by the PPy guest as a N source. Therefore, coordinated Ni-N_x inserted NC (Ni_{SA}-N_x-C) was prepared at different pyrolysis temperatures. For CO, the FE (98%) and TOF ($1,622 \text{ h}^{-1}$) of Ni_{SA}-N₂-C catalysts were significantly higher than those of the Ni_{SA}-N₃-C and Ni_{SA}-N₄-C.

Atomically dispersed Co SAs with different N coordination numbers have been used to further understand the CO₂RR intermediates and active sites^[178]. The number of N atoms around that central Co site was regulated by control of volatile C-N fragment in the pyrolysis process at different temperatures. A decrease in the N coordination number increased the unoccupied 3d orbital of the Co atom, which favored the adsorption of CO₂* and then improved the performance of CO₂RR. The catalyst with the Co-N₂ site showed higher FE of 94% for CO and current density of 18.1 mA cm⁻² at a low overpotential of 0.52 V than the catalyst with Co-N₄ sites.

Regulation of coordination species

Based on the above research, the construction of M-N_x structure with a low unsaturated coordination number can obtain higher CO₂ reduction performance. However, due to the limitation of M-N_x structure, the adjustable space is limited, making it very difficult to further improve the performance of unsaturated M-N_x sites. Introducing heteroatoms (O, S, *etc.*) into the unsaturated coordination structure to further adjust the local environment is also a feasible scheme to further improve electrocatalytic performance^[179]. The electronegativity of heteroatom O is stronger than that of N, which plays an important role in regulating the microenvironment of Fe single atoms and improving the catalytic performance. Zhao *et al.* first doped oxygen-rich Zn-MOF-74 with Fe to obtain Fe/Zn-MOF-74, where Fe occupied the Zn site in Zn-MOF-74 and coordinated with O atoms of organic ligand^[180]. After introducing melamine as a N source to MOFs, M@Fe/Zn-MOF-7 was formed, and then Fe-N coordination replaced part of Fe-O through calcination. Finally, Fe₁N₂O₂/NC catalyst was obtained. The FE of CO for Fe₁N₂O₂/NC was higher than 95% in the wide potential range of -0.4~ -0.8 V_{RHE}, and reached a maximum of 99.7% at -0.5 V_{RHE}. The CO current density of Fe₁N₂O₂/NC could reach 6.5 mA cm⁻² at -0.7 V_{RHE}. According to the calculation, the CO₂ adsorption energy of Fe₁N₂O₂ site (-1.41 eV) was significantly lower than that of other sites (FeN₄: -1.65 eV, FeO₄: -2.69 eV), indicating that CO was more easily adsorbed at FeN₄ and FeO₄ sites, which was not conducive to CO desorption. At the same time, FeO₄ has strong spin polarization, less electron loss, and most electrons are concentrated on CO, resulting in difficulties in CO desorption.

Wei *et al.* prepared a MOF-derived monatomic Cu catalyst (plasma-activated CuDBC, PA-CUDBC-1) using a plasma activation strategy to achieve efficient electrocatalysis of CO₂RR to produce CH₄^[181]. The plasma bombardment led to abundant O-vacancies on the catalyst, and the number of low coordination Cu sites increased significantly. In addition, the plasma treatment resulted in a layered porous structure, which allowed the catalyst to adsorb the reactant molecules efficiently. The synergistic effect of the porous structure and low coordination Cu sites significantly increased the production of CH₄ using PA-CUDBC-1 with a high FE of 75.3% at -1.1 V_{RHE}. The low coordination of Cu-O₃-C and Cu-O₂-C lowered the energy barrier for the decisive step (CO₂→COOH*) and other key intermediates (*CO and *CHO), thus accelerating the kinetic process of CO₂ conversion to CH₄.

Cooperation of adjacent metal sites

The concentration of SAs can affect the distance between single atoms, leading to different catalytic pathways and even distinct catalytic products. Cu-N_x-C catalysts are effective CO₂RR catalysts for producing hydrocarbons, including CH₄ or C₂H₄^[182]. Based on this, Cu-N_x-C catalysts with different Cu contents were prepared by optimizing the pyrolysis process. When the concentration of Cu was 4.9 mol%, the distance between the adjacent Cu-N_x species was small, so the C-C coupling could be realized, thus forming C₂H₄. On the contrary, if the Cu concentration in the Cu-N_x structure was less than 2.4 mol%, the distance between the Cu-N_x components increased, making the catalyst more conducive to producing CH₄. The calculations further suggested that the formation of C₂H₄ was related to two intermediates CO bound on two adjacent Cu-N₂ sites, and individual Cu-N₄, Cu-N₂ and adjacent Cu-N_x sites were related to the formation of CH₄.

MOF-derived M-N-C has a planar and conjugated carbon structure, which can realize long-range electron delocalization and is considered as an ideal material for constructing adjacent SAs. Jiao *et al.* precisely constructed a Fe₁-Ni₁-NC catalyst in which adjacent Fe-N₄ and Ni-N₄ sites were decorated on NC support by pyrolysis of MOF composites (Fe&Ni-ZnO/ZIF-8) [Figure 11A]^[183]. Due to the synergy of neighboring Fe and Ni SAs, the activity of Fe₁-Ni₁-NC for conversion of CO₂ to CO was enhanced, and FE of CO at -0.5 V vs. RHE was 96.2%, much better than that of Fe₁-NC and Ni₁-NC with individual Fe or Ni SAs [Figure 11B]. Single Fe atoms in Fe₁-Ni₁-NC could be activated by the neighboring monatomic Ni through non-bonding interactions, so that electrons were enriched in the region between Fe and CO₂, promoting CO₂ activation [Figure 11C]. The free energy of forming COOH* at Fe site in Fe₁-Ni₁-NC was calculated to be 0.64 eV, much lower than that at Ni sites in Fe₁-Ni₁-NC (1.53 eV), Ni-NC (1.95 eV) and Fe-NC (0.75 eV) [Figure 11D], thereby promoting the reduction of CO₂ to CO. This work provides an idea for the construction of SACs containing multiple metal elements.

By introducing different metal atoms to form diatomic sites (DSs), the electronic structure of a single metal active site can be changed by precisely regulating the low-coordination microenvironment at the atomic level, and ultimately the selectivity and activity of CO formation on DSs can be improved^[184]. Pei *et al.* pyrolyzed ZIF-8 at 1,000 °C to synthesize NC with N defects to provide sites for the anchoring of Co²⁺ and Mn²⁺, and then prepared a series of Co-Mn DS catalyst with low coordination (labeled as L-Co₁Mn₁-NC) [Figure 11E]^[185]. Co₁Mn₁-NC, Co₁-NC and Mn₁-NC as reference samples were prepared by saturated coordination of Co-Mn, Co and Mn on NC. The maximum FE_{CO} of Co₁Mn₁-NC and Co₁-NC was 84.7% and 64.6% at -0.57 V_{RHE}, respectively, while for Mn₁-NC, it was 52.8% at -0.67 V_{RHE}. It was noteworthy that the FE of CO for L-Co₁Mn₁-NC was significantly improved, even reaching 97.6% at -0.47 V_{RHE} [Figure 11F]. The low coordination structure of L-Co₁Mn₁-NC promoted the enhancement of charge interaction between Co and Mn sites, which was beneficial to the direct electron transfer from Co to Mn. Moreover, d-d orbital coupling between Co and Mn led to electron delocalization, which was beneficial to *CO desorption, thereby promoting the process of CO₂-to-CO. In addition, Jin *et al.* prepared MoFe-N₆ with Mo-Fe DS coordination on NC, breaking the constraint of linear correlation of intermediate adsorption energy in the process of CO₂RR to obtain higher CO selectivity (95.96%) and TOF (3,336 h⁻¹)^[186]. The existence of the "bridge" adsorption mode of *COOH on Mo-Fe DS increased the adsorption energy of *COOH [Figure 11G]. Meanwhile, Mo-Fe DS had the lowest adsorption energy for *CO compared with Mo-N₄ and Co-N₄, originating from d-orbital coupling between Mo and Fe, realizing electron delocalization of metal sites, and ultimately benefiting the desorption of *CO.

POP-BASED ELECTROCATALYSTS

Similar to MOFs, POPs inherit excellent physical and chemical tunability provided by various functionalized monomers in their structures^[187]. In addition, their strong covalent bond is an important sign that POPs differ from other porous materials to ensure the chemical stability of polymers, and with high SSA, they can bind specific catalytic sites, which is more suitable for CO₂ capture and conversion^[188]. Based on the adjustable porous structure and larger SSA of POPs, metal can be complexed or loaded in the POP framework through pre-design and post-modification strategies to realize the metallization of POPs, which can not only increase the exposure of the active center of the POPs, but also protect metal centers from aggregation in the reaction process, thus improving the electrocatalytic performance of CO₂RR. Moreover, the introduction of heteroatoms into POPs or the combination of POPs with conductive carbon materials (such as graphene and CNTs) or metal electrodes (such as Au and Ag) can adjust the POP structure to promote the enrichment of CO₂ and electron transport in the electrocatalytic process; In addition, porous POPs can be employed as sacrificial templates for the synthesis of porous catalysts with high dispersion of catalytic active sites. POPs exhibit good electrocatalytic activity in CO₂RR due to their well-preserved structure and composition, and there has been considerable progress towards their development^[189].

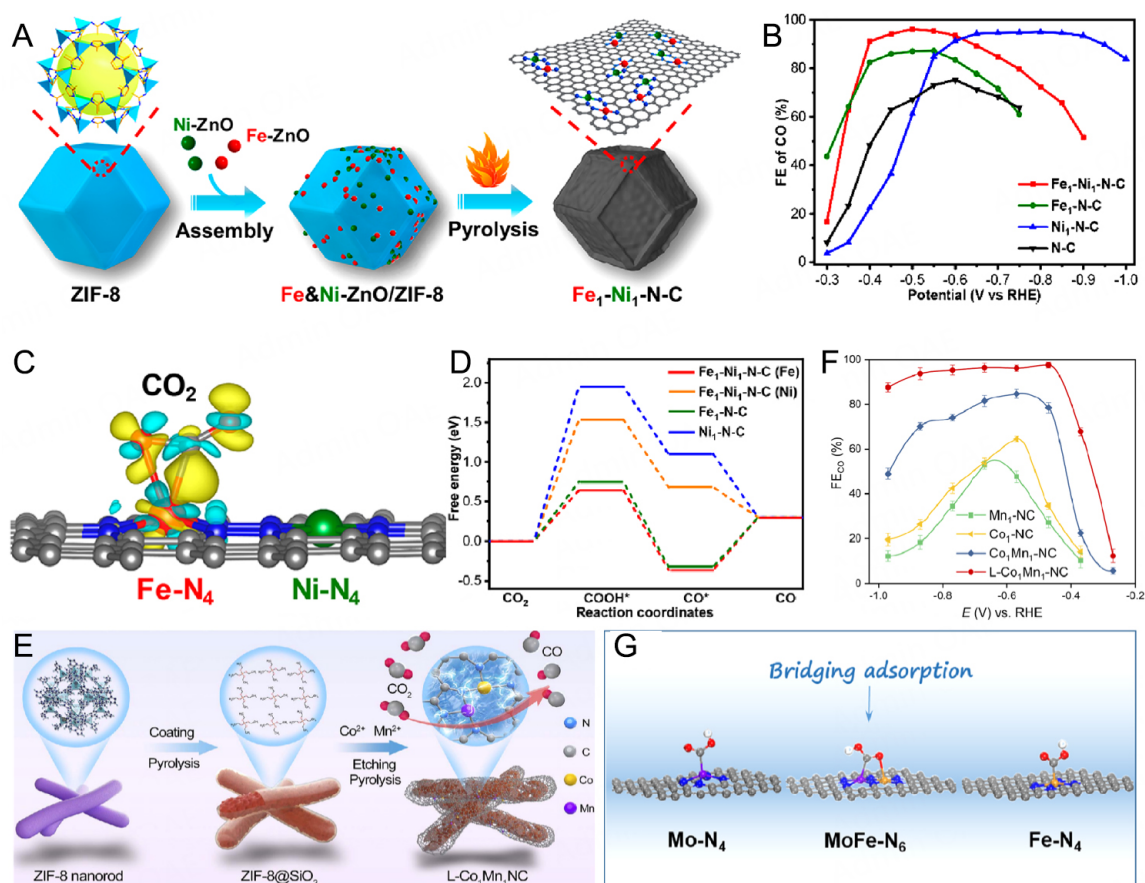


Figure 11. (A) The construction of $\text{Fe}_1\text{-Ni}_1\text{-N-C}$. (B) FE_{CO} at different potentials. (C) Electron density difference analysis for CO_2 adsorbed onto the Fe-N_4 sites of the $\text{Fe}_1\text{-Ni}_1\text{-N-C}$. (D) Free energy of CO_2RR ^[183]. Copyright 2021 the American Chemical Society. (E) The construction of $\text{L-Co,Mn}_1\text{-NC}$ catalysts. (F) FE_{CO} curves^[185]. Copyright 2024 the Royal Society of Chemistry. (G) Optimized catalytic models and reaction pathways on MoFe-N_6 ^[186]. Copyright 2024 Springer Nature.

Pristine POPs

Non-metallic POPs

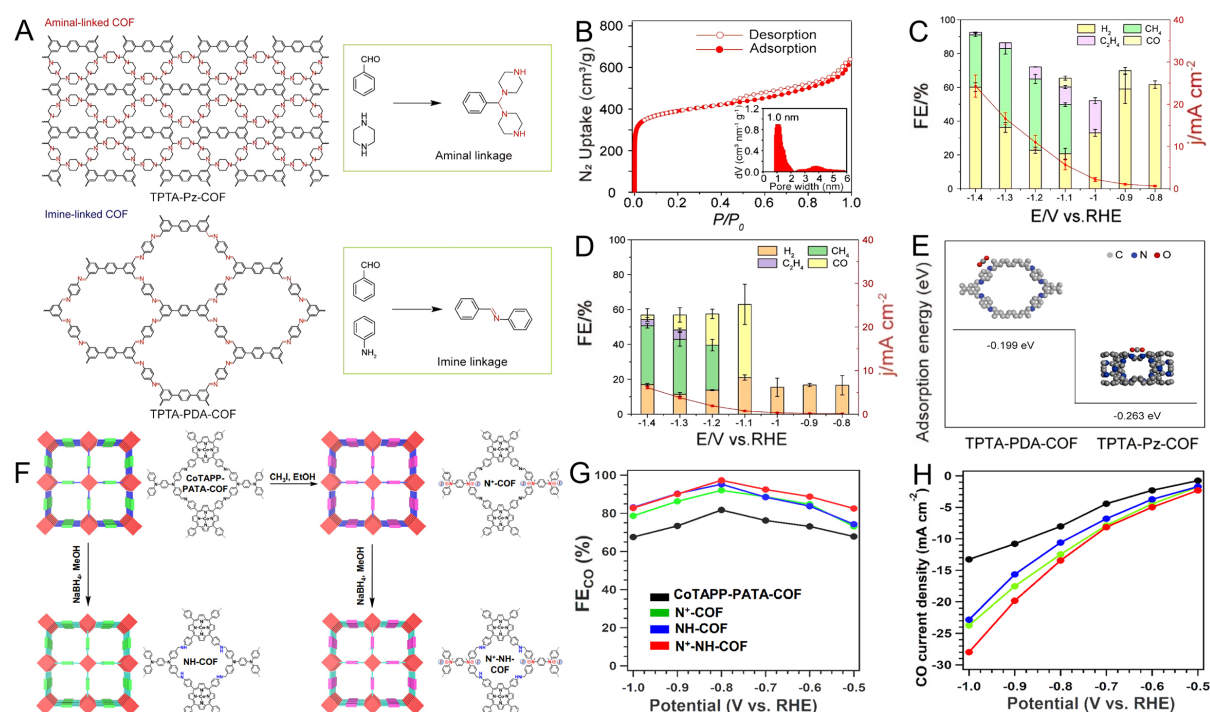
Conjugated triazine frameworks (CTFs), as porous polymeric materials linked by strong triazine bonds, possess favorable porous structure, high stability, and intrinsic N-rich doping. In addition, the conjugated structure of CTFs is beneficial to electron transport and mass transfer, so they are considered as potential electrode materials for the electrocatalytic reduction of CO_2 ^[190]. Zhu *et al.* prepared triazine-based frameworks (TTF-1 and TTF-2) by ZnCl_2 ionothermal method at 600 °C using 2,6-dicyanopyridine and 1,3-dicyanobenzene as monomers, respectively^[190]. The abundant porous structure and large SSA of TTF-1 (1,234 $\text{m}^2 \text{g}^{-1}$) and TTF-2 (2,522 $\text{m}^2 \text{g}^{-1}$) endowed the electrode and electrolyte with a large contact surface, which was conducive to charge and mass transfer. However, the content of pyridinic N that served as active sites in TTF-1 was 13.8 atom%, much higher than that of TTF-2 (6.8 atom%). Therefore, CO FE of 82% was achieved at -0.68 V_{RHE} for TTF-1, far exceeding the highest CO FE of 22% at -0.43 V_{RHE} for TTF-2. In addition, TTF-1 could maintain about 75% FE_{CO} for 12 h, indicating its long-term stability.

Covalent organic frameworks (COFs) are a type of organic polymer with porous crystal structures and strong covalent bonds, and their properties such as CO₂ adsorption capacity and electronic conductivity can be achieved by adjusting the building units or linkages. It is noted that N sites (pyridine N, pyrrole N, etc.) are considered as active centers for electrocatalysis, while *sp*³ N sites show higher CO₂ adsorption capacity compared to *sp*² N sites^[191]. Therefore, the design of amine-linked crystalline COFs containing *sp*³ N can be used as electrocatalysts to achieve efficient CO₂ reduction. Based on the above considerations, Ke *et al.* introduced piperazine (Pz) linking motifs into the crystalline COF to construct TPTA-Pz-COF (TPTA: [1,1':4',1''-terphenyl]-3,3'',5,5''-tetracarbaldehyde) with amination linkage and high density of *sp*³ N for efficient electrocatalytic reduction of CO₂ to C₂H₄^[192]. To demonstrate the superiority of the presence of *sp*³ N, an imine-based TPTA-PDA-COF with *sp*² N was prepared as a reference sample [Figure 12A]. TPTA-Pz-COF had a higher SSA of 1,470 m² g⁻¹ compared to TPTA-PDA-COF (1,110 m² g⁻¹) ensured a high electrochemical active surface area (ECSA) (12.7 μF cm⁻²) [Figure 12B], while TPTA-Pz-COF showed strong CO₂ capture ability due to obvious adsorption hysteresis based on the presence of *sp*³ N, which can promote mass transfer in the CO₂ reduction process. As a result, TPTA-Pz-COF could convert CO₂ to C₂H₄ as a gas-phase product and C₂H₅OH and HCOOH as liquid-phase products with FE of 19.1%, 21.86%, and 3.94% at -1.0 V_{RHE} [Figure 12C]. However, TPTA-PDA-COF could not reduce CO₂ to C₂H₄ under the same conditions [Figure 12D], suggesting that *sp*³ N played a key role in the C₂H₄ production. It was also found that the adsorption energy of CO₂ on TPTA-Pz-COF was -0.263 eV, lower than that on TPTA-PDA-COF (-0.199 eV) [Figure 12E]. At the same time, the existence of high-density *sp*³ N sites in TPTA-Pz-COF was conducive to charge accumulation, which further facilitated the activation of CO₂ and intermediates. Moreover, good hydrophilicity of TPTA-Pz-COF promoted the formation of hydrogen bonds, which was beneficial to the stabilization of intermediates *COOH and *CO, and then the C-C coupling process.

The linkage and linker of COF are simultaneously modified by post-modification strategy to enhance the CO₂ binding capacity and conductivity, thus improving CO₂RR performance^[188]. Firstly, a crystalline COF (CoTAPP-PATA-COF) was prepared by utilizing 5,10,15,20-tetrakis(4-aminophenyl) porphinato]-cobalt (CoTAPP) and 4,4',4'',4'''-(1,4-phenylenebis(azanetriyl)) tetrabenzaldehyde (PATA) as raw materials^[193]. Then, ionization of PATA was conducted by *in-situ* ammonium groups to form N⁺-COF, while NaBH₄ was used to reduce the C=N in COF to C-N to prepare N⁺-NH-COF [Figure 12F]. The conductivities of N⁺-NH-COF and N⁺-COF were 6.7 × 10⁻⁹ and 8.1 × 10⁻⁹ S m⁻¹, far exceeding that of NH-COF (3.0 × 10⁻¹⁰ S m⁻¹), indicating that ionic modification was beneficial to electron transport and further improved the activity of CO₂ reduction. In addition, the minimum Tafel slope of N⁺-NH-COF indicated that the dual modification can significantly elevate CO₂RR kinetics. As a result, N⁺-NH-COF could efficiently convert CO₂ to CO with the highest FE of 97.32% at -0.8 V_{RHE}, which was higher than that of NH-COF (95.26%), N⁺-COF (92.07%) and CoTAPP-PATA-COF (81.75%) [Figure 12G]. The presence of C-N bond promoted the adsorption of CO₂, while the hydrophobicity of the catalyst can inhibit the competitive adsorption of water, thus improving the selectivity. Meanwhile, the best current density of CO was 28.01 mA cm⁻² for N⁺-NH-COF at -1.0 V, significantly higher than that of NH-COF (22.83 mA cm⁻²), N⁺-COF (23.73 mA cm⁻²), CoTAPP-PATA-COF (13.26 mA cm⁻²) [Figure 12H]. The *COOH formation energy barrier on N⁺-NH-COF was lower than that of N⁺-COF, CoTAPP-PATA-COF and NH-COF, which promoted the *COOH→*CO process.

Metalized POPs

Metal complexation and PSMS are two common methods for preparing metalized POPs. The PSMS of POPs is generally achieved by introducing metal ions through cation exchange or coordination^[194]. Zhang *et al.* used a rigid N-containing ligand 2-(5-(3-(5-(pyridin-2-yl)-1H-1,2,4-triazol-3-yl) phenyl)-1H-1,2,4-triazol-3-yl) pyridine (H₂bptb) and Cu⁺ to synthesize two stable coordination polymers NNU-32 and



NNU-33 (S) (where S = sulfate)^[195]. During CO_2 RR, NNU-33 (S) can be converted to NNU-33 (H) (where H = hydroxyl radical) by the substitution of (SO_4^{2-}) by OH^- by anion exchange, further strengthening cuprophilic interactions within the catalyst structure. NNU-33 (H) efficiently catalyzed the process of CO_2 -to- CH_4 with 82.17% FE at $-0.9 V_{RHE}$. In addition, the DFT calculations revealed that energy barrier in the $*H_2COOH \rightarrow *OCH_2$ process could be lowered by the cuprophilic interactions, effectively promoting the CH_4 production. Moreover, it has been reported that the catalyst prepared by changing the ligand type can generate C_2 products during the CO_2 RR^[196], and the selectivity of these products can also be adjusted by changing the distance between two adjacent metal atoms in the coordination polymer^[197]. Sakamoto *et al.* synthesized binuclear coordination polymers $[Cu_2(\mu-X)_2(PPh_3)_2(\mu-BPY)]_n$ ($CuX-BPY$) ($X = Cl, Br, I$) with different distances between two adjacent Cu atoms by changing halogen bridging elements on which the catalytic properties of polymers depend^[197]. The catalytic efficiency of copper chloride $CuCl-BPY$ with shorter Cu-Cu distance for C_2 product was > 8 times higher than that of copper iodide $CuI-BPY$. On the one hand, the binding force between Cu and Cl was weaker due to the smaller ionic radius of Cl compared with Br and I, so the bridged Cl was easily desorbed from $Cu-\mu X-Cu$, and each Cu atom was coordinated with two CO_2 molecules, facilitating C-C coupling reaction; On the contrary, the charge repulsion caused by larger radius of I increased the distance between two adjacent Cu atoms and reduced electron density around the Cu atoms, which was not conducive to the coordination of CO_2 on Cu atoms.

H_2Pc ^[198] and porphyrin^[199,200] polymers containing SA centers ($M-N_4$) are promising electrocatalysts for CO_2 RR, and their electrocatalytic activities can be enhanced by tuning ligands or metal centers. Wei *et al.* prepared a 2D conjugated NiPc polymer (NiPcP) with sheet structure under vacuum at high temperature of $400^\circ C$, which served as an efficient electrocatalyst for CO_2 RR^[201]. The conjugated structure endowed strong binding affinity between the Ni sites in the polymer and CO_2 and fast electron transfer within the catalyst,

ensuring high selectivity (> 98%) of CO for NiPcP at potential of -0.15~-0.60 V vs. RHE. NiPcP had ~100% FE at -0.5 V, maximum CO current density of 232 mA cm⁻² at -0.60 V, and high TOF of 23,148 h⁻¹ at 0.39 V overpotential. The intrinsic electronic structure, conjugation properties of Ni, and hydrophobic properties of NiPcP promoted CO formation during CO₂RR and inhibited the competitive HER.

The strong π - π stacking between layers in polymer structure may cause the aggregation of the bulk structure, which hinders the full play of the catalytic activity of the catalytic center and reduces the electrocatalytic performance. The construction of an ultra-thin polymer structure may be a good solution^[198]. Song *et al.* prepared an ultrathin covalent organic polymer (COP) with a thickness of ~1.7 nm by condensation of Co tetraaminophthalocyanine (CoPc-(NH₂)₄) and squaric acid (SA) as monomers [Figure 13A and B]^[198]. However, the COP-BDA prepared by replacing SA with 1,4-benzenedicarboxaldehyde (BDA) exhibited a significant stacking structure with a thickness of > 4 nm [Figure 13C]. Compared with COP-BDA, ultrathin COP-SA ensured higher active site exposure and electron transfer efficiency. As a result, the CO FE of COP-SA reached 96.5% at -0.65 V_{RHE}, slightly higher than that of COP-BDA (84.4%) [Figure 13D]. It was worth noting that the CO partial current density of COP-SA was 8.16 mA cm⁻², far exceeding that of COP-BDA (0.59 mA cm⁻²) [Figure 13E]. Moreover, the TOF of COP-SA was 46.3 s⁻¹, 30.8 times that of COP-BDA. A smaller Tafel slope of COP-SA (118 mV Dec⁻¹) compared to COP-BDA (265 mV Dec⁻¹) suggested that the ultrathin structure contributed to enhanced CO₂RR kinetics [Figure 13F]. In addition, theoretical calculations suggested that higher binding energy of the Co center with *COOH (0.86 eV) and the weaker binding energy with *CO (0.12 eV) favored the desorption of the product CO [Figure 13G].

The regulation of CO₂RR performance can be achieved by adjusting the microenvironment around the electrocatalytic site. Pz-linked NiPc COFs (NiPc-NH-TFPN, NiPc-NH-TFPN-COOH, NiPc-NH-TFPN-NH₂, TFPN: tetrafluoroterephthalonitrile) with different ligands comprising -CN, -COOH, and -CH₂NH₂ groups were prepared to achieve the regulation of microenvironment near the active sites^[202]. The presence of Pz linkage made COF have better conductivity and stability, while the adsorption capacity of NiPc-NH-TFPN-NH₂ (80.6 cm³ g⁻¹) for CO₂ at 298 K was significantly higher than that of NiPc-NH-TFPN (19.4 cm³ g⁻¹) and NiPc-NH-TFPN-COOH (38.2 cm³ g⁻¹) due to the interaction between -NH₂ groups in NiPc-NH-TFPN-NH₂ and CO₂. The FE of CO for these three catalysts from -0.4 to -0.7 V_{RHE} showed an increasing trend with the rise of potential. The highest CO FE of NiPcNH-TFPN-NH₂ was 99.6% at -1.0 V, higher than the maximum FE of NiPc-NH-TFPN-COOH (71.4%). Meanwhile, NiPc-NH-TFPN-NH₂ exhibited a higher CO partial current density compared to NiPc-NH-TFPN and NiPc-NH-TFPN-COOH. In addition, the FE_{CO} and current density of the NiPc-NH-TFPN-NH₂ at -0.8 V showed almost no decay within 60 h, indicating good long-term stability. Compared with -CN and -COOH as electron-withdrawing groups, the introduction of electron-donating group -CH₂NH₂ can make more electrons participate in the electrocatalytic process. Moreover, the energy barrier of *COOH formation near the active site (-CH₂NH₂) was 1.35 eV, lower than that of NiPc-NH-TFPN (1.63 eV) and NiPc-NH-TFPN-COOH (1.57 eV), promoting the formation of CO.

In addition, the reduction of H₂Pc ligands during the electroreduction of CO₂RR at high overpotential may greatly affect the long-term stability of the electrocatalyst. The COP-CoPc was prepared by reacting viologen ligands with different redox states with cobalt polyphthalocyanine (CoPc-NH₂), which showed good electrocatalytic selectivity (FE_{CO} > 90%) for CO₂RR at a range of -0.68~-1.28 V_{RHE} in the H-type cell, reaching up the highest FE_{CO} of 97.3% at -0.88 V^[203]. The CO current density of COP-CoPc reached 90 mA cm⁻² at -1.4 V_{RHE}, higher than that of CoPc (45 mA cm⁻²) and CoPc-NH₂ (57 mA cm⁻²). Remarkably, a high FE_{CO} of more than 95% can also be obtained under the condition of 150 mA cm⁻² in the MEA system,

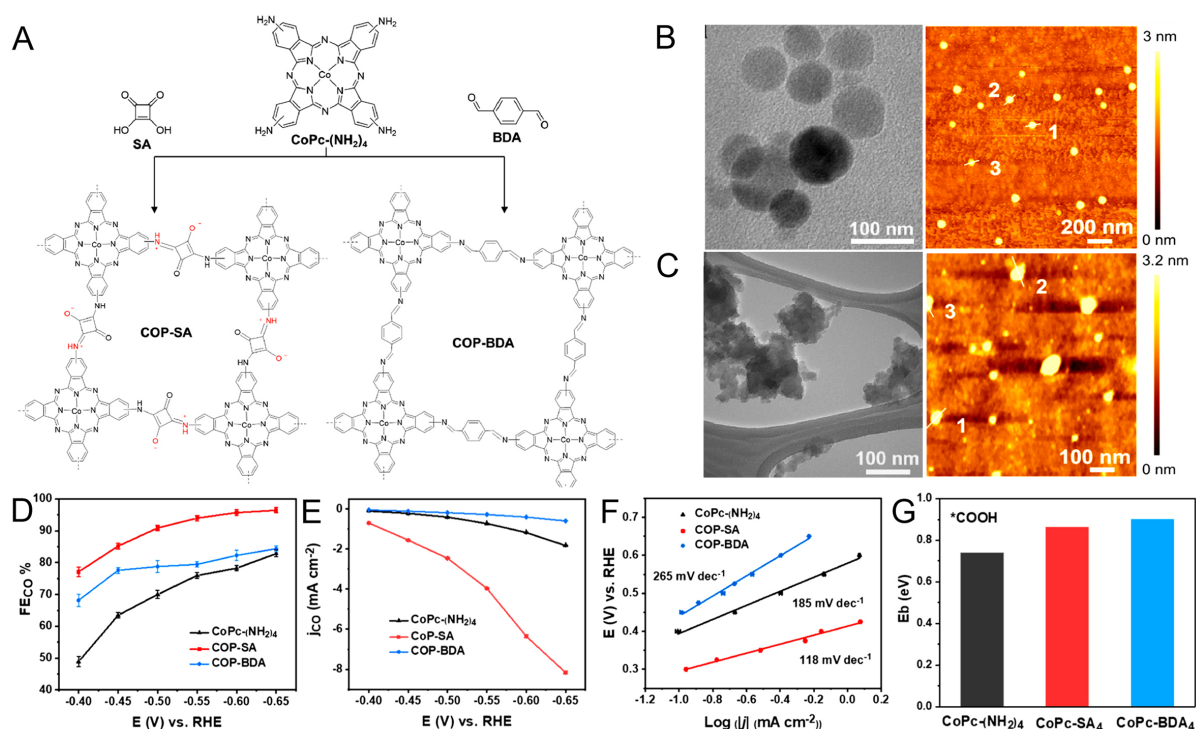


Figure 13. (A) The synthesis of COP-SA and COP-BDA. TEM and AFM images of (B) COP-SA and (C) COP-BDA. (D) FE and (E) CO current density from -0.4 to -0.65 V_{RHE}. (F) Tafel plots. (G) The binding strength of *COOH^[198]. Copyright 2021 Elsevier.

showing great application potential. More importantly, at a constant current of 0.25 A, COP-CoPc maintained more than 90% FE_{CO} over 48 h period.

A porphyrin complex with M-N₄ sites is also a promising CO₂RR electrocatalyst. Lu *et al.* prepared a Ni porphyrin CTF (NiPor-CTF) with NiN₄ units for the effective reduction of CO₂ to CO^[204]. The CO FE of NiPor-CTF exceeded 90% at -0.6~-0.9 V_{RHE}, reaching up the highest FE of 97% at -0.9 V with current density of 52.9 mA cm⁻². The calculations indicated that the kinetic energy barrier of *CO₂ to *COOH transition on NiN₄ active sites could be reduced. Furthermore, Wang *et al.* prepared a large π -conjugated polymer (CoPor-N₃) by coupling an electron-rich ligand (2, 6-bis (5-amino-1h-benzimidazole-2-yl) pyridine, N₃) with meso-tetra (p-formylphenyl) porphyrin cobalt (CoPor) containing Co-N₄ unit via strong covalent imine bonds (C=N)^[205]. H₂Por-N₃ with no Co sites only had a low FE_{CO} of 5.4% at -0.65 V_{RHE}, while the highest FE of the CoPor monomer for CO reached 78% at -0.55 V_{RHE}, suggesting that the high CO selectivity of CoPor-N₃ may be mainly contributed by the CoPor unit as an active site for CO₂RR. It was worth noting that CoPor-N₃ showed a significantly higher FE_{CO} of 96% at a lower potential of -0.50 V_{RHE} than that of CoPor, which was mainly attributed to coupling between electron-rich N₃ ligands and CoPor ensuring that electrons can be enriched around the Co center, facilitating the electron transfer from the Co center to CO₂ for activation and reduction. In addition, the superior optical driving characteristics of the CoPor unit enabled CoPor-N₃ to be used as a photosensitive electrocatalyst for the reduction of CO₂ to CO, so that partial current density of CO reached -42.1 mA cm⁻² at -0.60 V_{RHE} under illumination, which was higher than the partial current density (-28.2 mA cm⁻²) with no illumination.

The use of different linkers can adjust the catalytic effect of metal centers and control CO₂RR performance to a certain extent. However, the linker itself is generally not catalytically active. The performance of CO₂RR can be improved in principle by linking metalloporphyrin groups with catalytic monomers (such as metal

bipyridine) to synthesize polymers with two metal sites^[206,207]. Porphyrin-bipyridine bifunctional COF (COF-Re) was constructed by Schiff base reaction between bipyridine rhenium [obtained by the reaction of 2,2'-bipyridine-5,5'-formaldehyde and pentacarbonyl chlororhenium (I)] and 5,10,15,20-tetra(4-aminophenyl) porphyrin (TAPP)^[206]. Further modifications with cobalt chloride (CoCl₂) or ferric chloride (FeCl₃) led to the addition of the Co²⁺ or Fe³⁺ into the porphyrin unit, resulting in COFs with bimetallic sites (COF-Re-Co or COF-Re-Fe). COF-Re-Co had higher FE_{CO} of 18(2)%. The low selectivity may be related to the competition between the two metal centers, while the considerable distance between the two sites limited the migration of carriers. Based on the above considerations, a 3D bimetallic catalyst labeled as Co/Ni-TPNB-COF was constructed by covalently linking Ni(II)-porphyrin and Co(II)-porphyrin units with 4',4'',4'''-nitritoltris (1,1'-biphenyl) (NB) units^[208], which showed higher FE_{CO} of 95% and TOF of 4.10 s⁻¹. Theoretical calculation and experimental characterization showed that the triphenylamine unit as a linker could promote the charge migration between two metal sites, as well as the charge redistribution, which could help improve the electrocatalytic activity.

The particle size of COF is also a critical factor affecting its electrocatalytic performance, which is usually limited by the large particle size caused by particle aggregation, while the precise control of the morphology of COF catalyst is still a difficult problem. Endo *et al.* employed a trityl group-protected cobalt porphyrin precursor [Co(tppp), tppp = 5, 10, 15, 20-tetrakis (4-(tritylamino) phenyl) porphinato (2-)] for the preparation of small particle COF (COF-366-Co)^[209]. Due to the trityl protection, Co(tppp) exhibited good solubility in the solvent, which could inhibit intermolecular packing and uniform nucleation of COF particles; therefore, the size of the crystals (COF-T) prepared was reduced to 162 ± 41 nm, much smaller than that of the COF particles (COF-A, about 10 μm) prepared by the unprotected porphyrin precursor. As a result, the smaller size of COF showed excellent electrocatalytic performance of CO₂-to-CO with FE of 86%-95% at -0.58~-0.88 V vs. RHE, much greater than that of COF-A (38%~67%).

The binding strength between reactants and intermediates is considered to be one of the factors affecting the catalytic performance of COFs for CO₂RR. Many methods have been used to promote the charge transfer within the framework, thereby regulating the binding strength of intermediates, and ultimately improving the electrocatalytic performance. Bimetallic COFs with dioxin-linkage were synthesized to improve the electron transfer within the framework, guaranteeing FE_{CO} of 97% and TOF of 2.87 s⁻¹^[210]. A conductive 2D H₂Pc COF with isolated Cu-H₂Pc active sites, as an electrocatalyst, can convert CO₂ to acetate with FE of 90.3(2)% and current density of 12.5 mA cm⁻² at -0.8 V vs. RHE^[211]. Theoretical calculations showed that isolated Cu-H₂Pc had a high electron density, ensuring the migration of d electrons from Cu to C. At the same time, due to the strong interaction between COF and *CH₃ intermediates, the C-C coupling between *CH₃ and CO₂ was promoted, and the formation of ethylene and ethanol by the interaction between *CO and other intermediates was avoided. Furthermore, the COF containing an imidazole group as the catalyst for electrocatalytic CO₂RR enhanced the stabilization of the key intermediate *COOH and the electron transfer, thereby facilitating the catalytic reaction and ultimately achieving nearly 100% FE_{CO}^[212,213]. Due to the single donor and acceptor units of the above COF, the regulation of the binding strength of intermediates was inaccurate. To accurately adjust the interaction between the catalyst and the intermediate, Liu *et al.* constructed a three-component COF by adding the electron-rich diarylamine unit, the electron-deficient benzothiazole and the Co-porphyrin unit^[214]. The COF had higher electronic conductivity and more efficient charge transfer, and thus high CO FE of 97.2% at -0.8 V vs. RHE, which was attributed to favorable *COOH formation and *CO desorption.

POPs-based composites

POPs/C composites

Although the electrocatalysts of metalized POPs have well-defined and tunable active sites, the efficiency of their CO₂RR is usually much lower than that of metal catalysts due to poor conductivity, which largely limits their practical applications. The combination of POPs with substrates to construct composites is seeking to confront poor electrical conductivity of POPs and obtain high electrocatalytic performance. The interaction of POPs and graphene or CNTs has been used to enhance the electron transport capability^[215]. Lu *et al.* prepared a composite material (COF-366-Co@CNTs) by *in-situ* polymerization of COF with Co porphyrin units on amino-functionalized CNTs via covalent bonding to ensure close contact between COFs and CNTs^[216], thereby promoting rapid electron transfer from the Co center to CNTs [Figure 14A]. To further adjust electronic structure of the Co center, COF-366-(OMe)₂-Co@CNT was prepared by introducing an electron-withdrawing group (methoxy) into the porphyrin units during the preparation of the composite. In addition, COF-366-(OMe)₂-Co@CNT had higher binding capacity for CO₂ due to the hydrophobicity of the methoxy group and CO₂. The ultrathin COF nanolayer with a thickness of 0.9 nm wrapped on the CNT greatly shortened the electron transport distance from the COF to the CNT [Figure 14B]. For these reasons, COF-366-(OMe)₂-Co@CNT showed the best performance of CO₂→CO, with FE of 93.6% at -0.68 V_{RHE}, current density of 40 mA cm⁻² at -1.05 V and TOF of 11,877 h⁻¹ at 770 mV overpotential [Figure 14C-E]. For the same purpose, the composites CoP@CNT, CoP-Ph@CNT and CoP-F@CNT were prepared by *in-situ* growth of covalent Co porphyrin polymers with different porphyrin substituents on CNTs through the coupling between the alkynyl groups of porphyrins and CNTs to adjust the electronic structure of the polymers^[217] [Figure 14F]. As a result, FE_{CO} of CoP@CNT (~95%) and CoP-Ph@CNT (~80%) was significantly higher than that of CoP-F@CNT (~20%) in a large potential window of -0.57~-0.87 V [Figure 14G], attributed to electron-rich Co^I center in CoP and CoP-Ph which facilitated the binding and activation of CO₂ to improve CO₂RR selectivity compared with electron-deficient CoP-F. In addition, the activity and selectivity of CoP@CNT hardly decreased at -0.57 V within 100 h, exhibiting excellent stability.

MePc and its derivatives as electrocatalysts are capable of selectively electroreducing CO₂ to CO. In contrast, the polymerization of metal H₂Pc can improve the stability of the catalyst, but it can not effectively control electronic properties and microenvironment of the metal active center, so the catalytic activity is often weaker than that of small H₂Pc molecules. Therefore, it is of great significance to regulate the polymerization of metal H₂Pc molecules so as to give consideration to both stability and activity in the selective electrocatalytic reduction reaction of CO₂. Guo *et al.* synthesized a CNT@conjugated microporous polymer (CMP) (CoPc-H₂Pc) composite electrocatalyst with both catalytic activity and stability by copolymerizing H₂Pc and cobalt H₂Pc (CoPc) molecules on the CNT surface through Scholl coupling reaction^[218]. The addition of H₂Pc in the polymerization process can not only effectively avoid the metal shedding of CoPc in the reaction, but also promote the dispersion of metal Co in the ultra-thin shell of CMP at atomic level. The catalytic performance results suggested that the material had the lowest onset potential, achieving CO current density of 15.2 mA cm⁻² at -0.6 V_{RHE}, far exceeding of CNT@CMP(CoPc) with 9.9 mA cm⁻². In addition, FE_{CO} of 96% can be maintained even at high current densities (> 200 mA cm⁻²) from -0.6 to -1.1 V_{RHE}. In the study of catalytic mechanism, it was found that, on the one hand, the H₂Pc unit as electron donor improved the nucleophilicity of the neighboring monatomic Co and enhanced the interaction between the metal and CO₂. On the other hand, the H₂Pc unit can also be used as a proton donor to stabilize the intermediate of CO₂ through intermolecular hydrogen bonding, improve the proton transfer ability of the electrocatalyst, and promoted the activation process of CO₂, thus improving the selective reduction of CO₂ by cooperating with the active metal center.

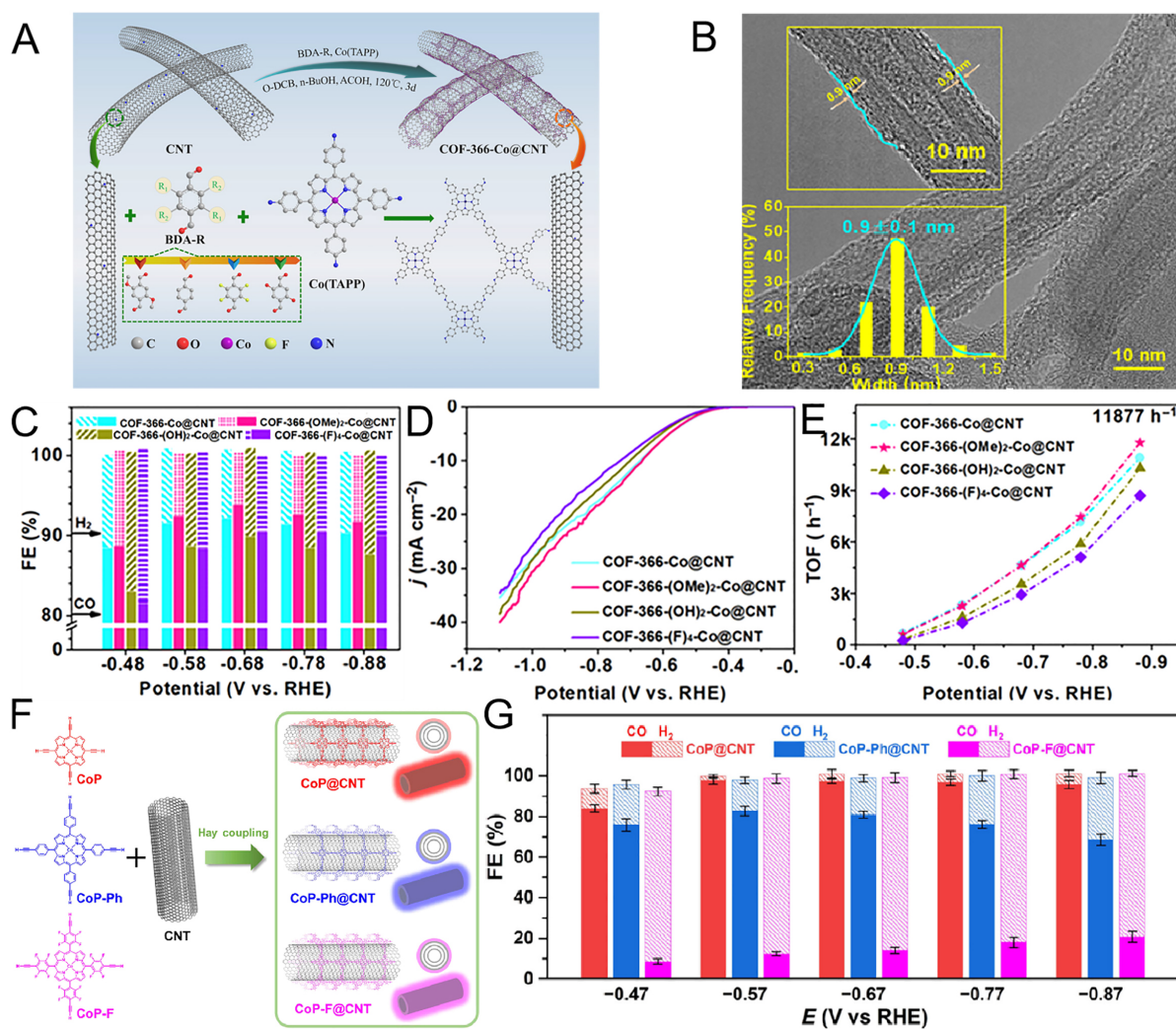


Figure 14. (A) The construction of COF-366-Co@CNT. (B) HRTEM images of COF-366-(OMe)₂-Co@CNT. (C) FEs (D) Current densities and (E) TOFs^[216]. Copyright 2020 the American Chemical Society. (F) The synthesis of CoP@CNT, CoP-Ph@CNT, and CoP-F@CNT. (G) FEs at -0.47~ -0.87 V^[217]. Copyright 2022 Chinese Chemical Society.

The electrocatalytic activity of M-N_x sites in POPs may be affected by the carbon substrate, and it is reported that CNTs with highly curved surfaces may provide a unique curvature effect for M-N_x, which in turn improves the electrocatalytic performance^[219]. Ao *et al.* prepared NiN_x by high temperature pyrolysis of Ni particles in N-doped CNTs, and then coated CTF nanosheets to synthesize electrocatalyst Ni-N/CNT@CTF^[220]. The close contact between ultra-thin 2D CTFs and CNTs could inhibit the accumulation of carbon layers and give full play to the curvature effect of CNTs. The Ni-N bond length (1.90 Å) in the Ni-N/CNT@CTF was slightly larger than that of the common NiN_x site (1.84~1.88 Å) due to the compressive strain of the curved CNTs on the Ni-N sites. DFT data showed that NiN₃ site was active site for electrocatalytic CO₂RR, and its electronic structure could be adjusted by the curvature effect of CNTs, thereby improving the kinetics of electrocatalytic CO₂RR. The current density and FE of CO were 201 mA cm⁻² and 98% at -0.9 V vs. RHE for Ni-N/CNT@CTF in flow cells.

Metal/POP composites

Metal NPs suffer from problems such as easy aggregation, low mass and electron transfer, and poor stability in the reaction process, which significantly reduce their catalytic performance^[221]. Metal/polymer hybridization is a feasible way to solve the above problems. The modification of metal NPs by POPs with large SSA and excellent stability is not only beneficial to the high dispersion of metal particles, thereby improving the accessibility of active sites, but also can improve the stability of metal catalysts in the catalytic process. The introduction of POPs can also regulate the catalytic microenvironment of metal sites. Therefore, it is highly desirable to design metal/polymers with higher mass and electron transfer efficiency through different strategies. Polymer ligands can control the surface accessibility of metal nanocatalysts, which provides a way to improve their cycle life and catalytic performance. Zhang *et al.* used Au and palladium (Pd) nanocatalysts stabilized by two polymer NHCs (mono- and polydentate) for CO₂RR^[222]. Compared to traditional thiols, amines, and other ligands, the stable metal-carbene bond at the reduction potential prevented the aggregation of metal NPs. The NHC-ligand-modified Au catalyst had 86% CO FE at -0.9 V for 11 h, whereas that of the unmodified Au was < 10%. Moreover, the hydrophobicity of polymer ligands and the surface electron density of NPs greatly improved the selectivity of C via the σ -donation of NHCs.

Cu-based catalysts can be used in the electrocatalytic reduction of CO₂ to produce CH₄, *etc.*^[223]. However, due to complicated reaction process and poor structural stability, the selectivity and stability of CH₄ are poor, which limits its practical application^[224]. By adjusting the catalytic microenvironment of Cu sites, including the coverage of reaction intermediates^[225], the adsorption of CO₂, H₂O^[226], *etc.*, the path of CO₂RR can be regulated to improve the selectivity of CH₄ products. The sheet-like structure and open channels of 2D COFs provide an ideal platform for regulating the catalytic microenvironment^[227]. Cu NPs were modified by 2D COF nanosheets (NUS9) with high density of heteroatoms and sulfonic acid groups to prepare Cu-NUS9, which can adjust the selectivity and activity of its products. As a result, the Cu-NUS9 catalyst reduced CO₂ to CH₄ with 66% FE and 296 mA cm⁻² of current density in an acidic electrolyte (pH = 2) and 61.6% FE and 308 mA cm⁻² of current density in an alkaline electrolyte (pH = 14). The introduction of NUS9 with a porous structure and ionic group could promote the local accumulation of CO₂ and K⁺ around the surface of the catalyst, which significantly reduced adsorption energy of *CO on Cu-NUS9 (-0.22 eV) compared with Cu (-0.27 eV) and prevented the occurrence of C-C coupling reaction. On the other hand, the enhanced adsorption of H₂O significantly promoted the dissociation of H₂O which was beneficial to the hydrogenation reaction in the CO₂RR process. Additionally, the presence of NUS9 significantly lowered energy barrier of *CO + *H → *CHO, which was RDS for CH₄ production (Cu-NUS9: 1.02 eV, Cu: 1.35 eV), and promoted the reduction of CO₂ to CH₄.

In addition, Meng *et al.* proposed an effective tandem catalytic strategy to improve the selectivity of reducing CO₂ to C₂H₄^[228]. Combined with the advantages of non-noble metal monatomic Ni to produce CO and Cu nanocatalyst to conduct CO-CO coupling, the selectivity of CO₂ to ethylene was improved by tandem catalysis. Based on the above considerations, non-noble PTF (Ni)/Cu was prepared by loading Cu NPs on Ni monatomic porphyrin-triazine framework (PTF-Ni) [Figure 15A and B]. In the catalytic process, monatomic Ni efficiently reduced CO₂ to intermediate CO, and the generated CO was immediately converted to ethylene by the adjacent Cu nanocatalyst through C-C coupling reaction. As a result, compared with non-tandem catalyst PTF/Cu which mainly produced CH₄, FE of C₂H₄ increased from 9.6% to 57.3% at -1.1 V vs. RHE [Figure 15C]. Furthermore, PTF (Ni)/Cu could still maintain ~91% of the initial activity after 11 h [Figure 15D]. PTF (Ni) was beneficial to increasing the generation of active intermediates of *CO on Cu NPs, thereby improving the probability of C-C coupling, and significantly reducing energy barrier required for the production of C₂H₄, thus improving activity of converting CO₂ to C₂H₄ through tandem catalysis.

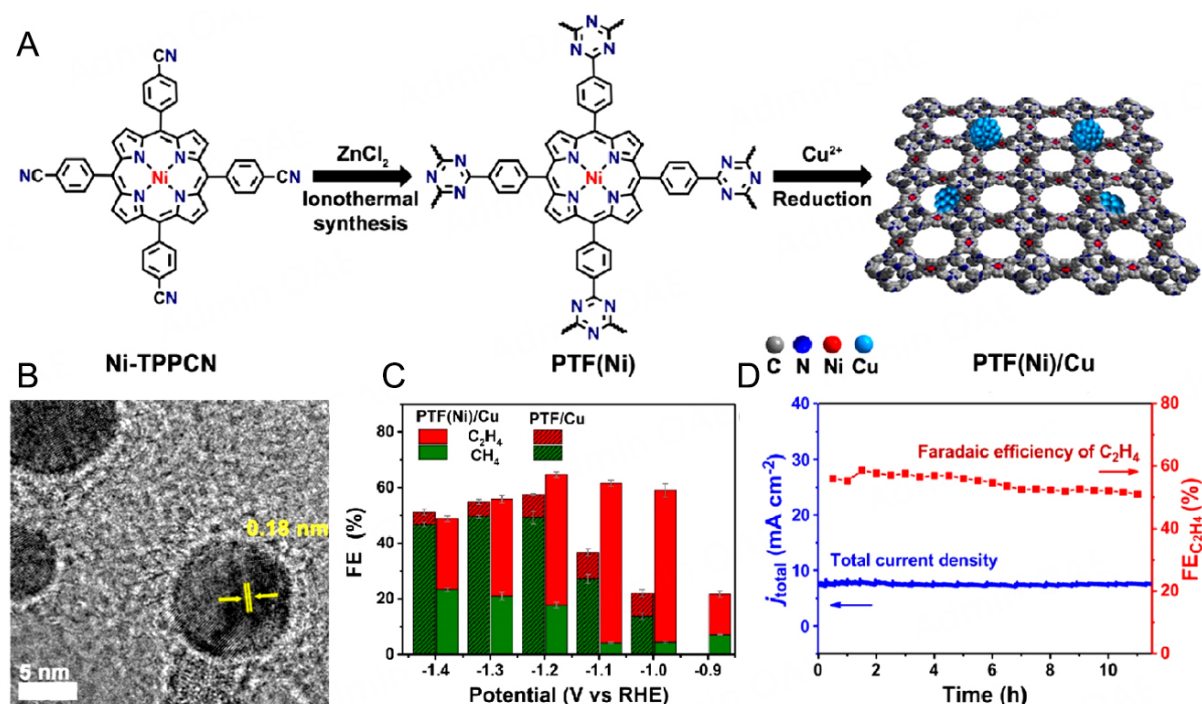


Figure 15. (A) Fabrication of PTF(Ni)/Cu. (B) HRTEM images of PTF(Ni)/Cu. (C) FEs of C₂H₄ and CH₄ at different potential. (D) The long-term stability for 11 h on PTF(Ni)/Cu catalyst^[228]. Copyright 2021 Wiley-VCH.

Molecular catalyst/POP composites

The porous structure of POPs allows the insertion of molecular electrocatalysts via rapid diffusion to obtain sufficient active sites, thereby improving the electrocatalytic activity and stability^[229]. To verify these characteristics, rhenium (Re)-based Re (2,2'-bpy-5,5'-diamine) (CO)₃Cl was inserted into the framework of COF-2,2'-bp with non-metallic 2,2'-bpy moiety to segregate COF-2,2'-bpy-Re^[230]. COF-2,2'-bpy-Re combined with carbon black and polyvinylidene fluoride (PVDF) actively catalyzes the reduction of CO₂ to CO at -2.8 V only for a Re concentration of 29.38 wt%. After 30 m of controlled potential electrolysis (CPE), the CO FE for the catalyst reaches 81%. After 30 m, the electrocatalytic performance of the composite decreases due to the inhibition of mass transfer and substrate diffusion. Moreover, Co porphyrin molecules have been embedded into cationic POPs with bipyridyl ligands (POP-Py) by anion exchange to generate strong secondary coordination sphere interactions to improve CO₂RR performance^[231]. In this study, Co meso-tetra (4-carboxyphenyl) porphyrine (Co-TCPP) was uniformly encapsulated in POP-Py under electrostatic attraction. The hybrid exhibited a CO FE of 83%, current density of 4.0 mA cm⁻², and TOF of 1.4 s⁻¹ at 0.49 V of overpotential, which was attributed to the synergistic interaction between the cationic polymer substrate and the molecular catalyst. The electrostatic effect of the positively charged framework of the cationic POPs could not only promote the dispersion and stable loading of the negatively charged molecular catalyst, but also stabilize the intermediate of the electrocatalytic reaction and improve the catalytic activity.

The strategy of integrating the photosensitive donor Ru(bpy)₃Cl₂ and the acceptor CO₂ reduction activator Co-Por into the crystalline COF framework can effectively prolong excited state lifetime of Co-Por and improve the catalytic performance of electrocatalytic CO₂ reduction under illumination. Wu *et al.*

constructed Ru (bpy)₃Cl₂ photosensitizer into 2,2'-bipyridine-functionalized Co porphyrin-based COF (Co-Bpy-COF) by post-synthesis method, and obtained Co-Bpy-COF-Ru_x (*x* represented molar ratio of Ru to Co)^[232]. Due to the large polarity difference of building units and the high crystallinity of 2D COF, the built-in electric field in Co-Bpy-COF-Ru_{1/2} was created to facilitate the migration of photoexcited electrons from Ru (bpy)₃Cl₂ to Co-Por on the one hand, and on the other hand, the excited state lifetime of Co-Por was 3.4 times longer than that of Co-Bpy-COF, and therefore the formation energy of CO was effectively reduced under the illumination. Thus, Co-Bpy-COF-Ru_{1/2} had the highest FE_{CO} of 96.7% at -0.7 V_{RHE}, and CO partial current density of 16.3 mA cm⁻² at -1.1 V_{RHE}, both far exceeding the value with no illumination (84.6%, 11.9 mA cm⁻²).

MOF/POP hybrids

COFs and MOFs, as two kinds of porous crystalline materials, have received extensive attention and research in electrocatalytic reduction of CO₂. Despite many similarities between them, there are still obvious differences in structure and functionality, and each has its own shortcomings. It is possible to combine their own advantages and form synergistic catalytic effect in electrocatalysis to overcome their respective shortcomings. In recent years, there have been many reports on MOF and COF hybrid materials, which have opened up a wide range of frontier applications for the synthesis and application of these materials^[33]. However, MOFs/COFs reported in the literature have some problems, such as less exposure of active sites and insufficient research on interface effect or synergistic mechanism. Therefore, it is of great value and significance to explore MOF@COF hybrid materials with fully exposed active sites to realize electrocatalytic CO₂RR and produce high-value-added products.

Based on the above considerations, Yang *et al.* prepared a series of composite electrocatalysts MCH-X by epitaxially growing an ultrathin Cu-Por-based COF (COF-366-OH-Cu) layer with nanoscale thickness on the surface of a mesoporous honeycomb UiO-66-NH₂ template via covalent bonds (imine linkage)^[233]. The morphology of MCH-X and the exposure of active sites were optimized by adjusting the amount of MOFs, which endowed the composite with high electrocatalytic performance. The optimum MCH-3 was still able to maintain the honeycomb structure due to the thinner COF layer with a thickness of ~8.5 nm, which was favorable for the exposure of the active sites. The CO₂ adsorption capacity of MCH-3 was higher than that of COF-366-OH-Cu but lower than that of UiO-66-NH₂, suggesting that the introduction of UiO-66-NH₂ improved the affinity of the hybrid material for CO₂. The results showed that UiO-66-NH₂, COF-366-OH-Cu and MCH-3 could reduce CO₂ to CH₄ and a very small amount of C₂H₄. The maximum FE_{CH₄} and total current density of MCH-3 was 76.7% and -398.1 mA cm⁻² at -1.0 V, far exceeding that of UiO-66-NH₂ (15.9%, -187.8 mA cm⁻²) and COF-366-OH-Cu (37.5%, -374.4 mA cm⁻²), demonstrating the advantage of the honeycomb heterostructure possessed by MCH-3. Due to the introduction of MOFs, the formation energy barrier of the *COOH, acting as RDS for the CH₄ generation for MCH-3, was 1.18 eV, lower than that of COF-366-OH-Cu (1.41 eV), further promoting the formation of the intermediates *CO, *CHO, and *CH₂O. This work provides a reference for applications of porous crystalline hybrid materials in the efficient electrocatalytic reduction of CO₂.

POP derivatives

COFs are ideal templates for the construction of carbon materials due to their 2D layered structure and high porosity. However, only massive 3D carbon materials can be obtained by direct pyrolysis, resulting in low conductivity and stacking structure. Therefore, it is highly desirable to control the structure of the derived carbon to obtain an electrocatalyst with high porosity, high electrical conductivity, and abundant atomic doping sites. In this context, Liu *et al.* used different templates (CNT, graphene) to prepare different sizes of COFs-derived carbon structures (1D to 3D) and studied their effects on CO₂RR performance^[234]. Firstly, trialdehyde phloroglucinol (TP) and [2,2'-bipyridine]-5,5'-diamine (BPY) were employed as monomers to

prepare TP-BPY-COF, which was directly pyrolyzed at 800 °C to obtain 3D derived carbon materials. Then, the composites constructed by *in-situ* growth of COFs on CNTs and graphene were pyrolyzed under the same conditions to obtain 1D COF@CNT₈₀₀ and 2D COF@Gr₈₀₀, respectively. Finally, Co porphyrin units with CoN₅ catalytic sites were anchored on carbon materials as electrocatalysts (Co-COF₈₀₀, Co-COF@CNT₈₀₀, Co-COF@Gr₈₀₀) to reduce CO₂ to CO [Figure 16A]. Due to the collapse of the pore structure for TP-BPY-COF after pyrolysis, the SSA of Co-COF₈₀₀ decreased from 1,318 m² g⁻¹ of TP-BPY-COF to 43.97 m² g⁻¹, resulting in a lower CO₂ adsorption capacity (9.17 cm³ g⁻¹). In contrast, the CO₂ adsorption capacities of Co-COF@CNT₈₀₀ and Co-COF@Gr₈₀₀ were 17.10 and 16.25 cm³ g⁻¹, respectively, showing higher CO₂ binding capacity [Figure 16B]. Moreover, the charge transfer resistance of Co-COF@CNT₈₀₀ was 9.76 Ω, significantly lower than that of Co-COF₈₀₀ (18.30 Ω) and Co-COF@Gr₈₀₀ (16.04 Ω), indicating that Co-COF@CNT₈₀₀ had a faster electron transfer efficiency. As a result, the FE_{CO} of Co-COF@CNT₈₀₀ was higher than 82% at -0.6~-1.0 V_{RHE}, reaching a maximum of 94.5% at -0.7 V_{RHE} [Figure 16C]. However, the FE_{CO} values of Co-COF@Gr₈₀₀ and Co-COF₈₀₀ at -0.7 V_{RHE} were only 88.0% and 86.2%. Moreover, the CO partial current density and TOF of Co-COF@CNT₈₀₀ reached the highest values of 25.8 mA cm⁻² and 1,151 h⁻¹ at -1.0 V_{RHE}, much higher than those of Co-COF@Gr₈₀₀ (19.5 mA cm⁻², 762 h⁻¹) and Co-COF₈₀₀ (7.6 mA cm⁻², 323 h⁻¹) [Figure 16D].

Efficient CO₂ reduction can be achieved by introducing new metal atoms to form bimetallic catalytic sites in carbon-supported SACs^[235]. Metal atoms with high loading can break the weak interaction between single atomic sites, which is conducive to the synergistic effect between different metal atoms, thereby improving the selectivity and activity of CO₂ reduction and inhibiting HER. COF@MOF hybrid materials with core-shell structure are ideal precursors for the formation of active sites with high loadings. In this context, Liu *et al.* used ZIF-8 as a template and then *in-situ* grown TP-BPY-COF shell on its surface to construct COF@MOF hybrid materials^[236]. Under the protection of COF shell, the hollow carbon material COF@MOF₈₀₀ containing ZnN₄ sites was prepared by pyrolysis at 800 °C in N₂ atmosphere, which effectively avoided the loss of Zn ions and N atoms. Finally, the CoPc unit was immobilized on COF@MOF₈₀₀ by coordination to obtain the bimetallic catalyst COF@MOF₈₀₀-Co with ZnN₄ and CoN₄O sites of 11.05 and 2.47 wt% [Figure 16E]. The results showed that the maximum value of FE_{CO} of COF@MOF₈₀₀-Co was 92.6% at -0.8 V, significantly higher than that of COF@MOF₈₀₀ (13.95%). On the contrary, COF@MOF₈₀₀ had a higher hydrogen evolution selectivity (86.05%) than COF@MOF₈₀₀-Co (7.4%) at the same potential, indicating that the synergistic effect of CoN₄O and ZnN₄ not only improved the selectivity of CO₂ reduction but also inhibited HER.

CONCLUSION

Summary

Porous MOF- and POP-based materials have been widely employed in electrocatalytic CO₂RR because of their high SSA, customizable structure, adjustable functions, and good stability. In this report, we reviewed the development of MOF/POP-based nanoporous organic framework catalysts for electrochemical CO₂RR in recent years.

For MOFs/POPs, the higher SSA enables them to disperse more electrochemical active sites, while their rich pore structure can promote the enrichment of reactants and mass transfer, thus accelerating the electrocatalytic reaction. To further improve conductivity of MOFs/POPs, MOF/POP composites are constructed by introducing guest species into MOFs/POPs to adjust the electron transport efficiency. Besides, compared with individual POPs/MOFs, the MOFs/POPs-derived materials can not only retain the original porous structure, but also improve the stability. Moreover, MOFs/POPs-derived materials have precisely controlled structures, which provide a clear model for the study of their active sites, structure-

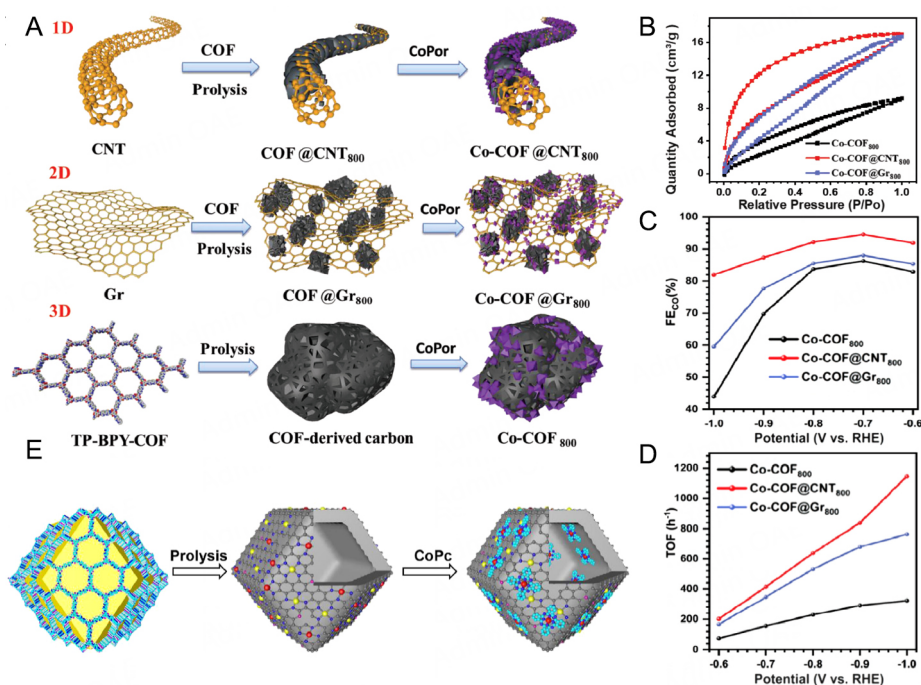


Figure 16. (A) Synthesis of Co-COF@CNT₈₀₀, Co-COF@Gr₈₀₀ and Co-COF₈₀₀. (B) CO₂ sorption curves. (C) FE_{CO} and (D) TOF values at -0.6--1.0 V vs. RHE^[234]. Copyright 2023 Wiley-VCH. (E) Preparation of COF@MOF₈₀₀-Co^[236]. Copyright 2023 Wiley-VCH.

activity relationship, and basic mechanism. In general, MOFs/POPs involved in CO₂RR are mainly classified into three categories: (1) pristine MOFs/POPs; (2) MOF/POP-based composites; and (3) MOF/POP derivatives.

In pristine MOFs, tunable metal ions or clusters and organic ligands are employed as active centers or electron transport agents. The metal centers are dispersed by organic ligands at the atomic level to tailor the original MOFs. The catalytic performance of MOFs can be improved by strategies such as adjusting/varying ligands, encapsulating active metal centers, and modifying electronic structure. The adjustment of the morphology of the MOFs, the exposure of specific crystal faces, and the particle size in the synthesis process also play critical roles in improving CO₂RR performance. The choice of organic ligands can control the valence and coordination environment of metal nodes in MOFs, which act as important factors in the activation of CO₂ and stabilization of key intermediates, further regulating the product selectivity of CO₂ electrocatalytic reduction. By employing planar macrocyclic conjugated systems such as porphyrins and H₂Pc, 2D MOFs with good crystallinity and abundant pores can be obtained. These frameworks can be formed using (i) a rigid, macrocyclic, conjugated molecule with charged, delocalized carriers; or (ii) an active metal center with mixed valence and organic ligand with redox reactivity that facilitates electron transfer. Such materials exhibit increased current densities for electrochemical CO₂RR at lower overpotentials.

Pristine POPs, as porous frameworks with strong covalent bonds, have better chemical stability than MOFs. Additionally, POPs with high SSA can bind specific catalytic sites, making them more suitable for CO₂ capture and conversion. Properties such as CO₂ adsorption capacity and electronic conductivity can be achieved by adjusting the building units or linkages. In addition, metal complexation of building blocks and PSMS are two common strategies used to synthesize metalized POPs. POPs with macrocyclic molecules, such as metalloporphyrins and MePc, are usually metalized by using building blocks, while PSMS is usually

achieved by introducing metal ions through cation exchange or coordination. Introducing metal ions into POPs by means of coordination can greatly lower the amount of metal and obtain atomically dispersed sites, which is the key to achieving high selectivity in electrocatalytic reactions. By introducing different groups (such as electron-withdrawing/donating groups and hydrophilic/hydrophobic groups) into the ligands, the microenvironment around the metal sites can be adjusted to improve the electrocatalytic efficiency. In order to break through the limitation of POP particle aggregation and bulk structure stacking on the electrocatalytic CO₂RR performance, the precise control of the morphology of POP catalysts, such as the synthesis of ultra-thin sheet structure and smaller particle size, can ensure higher active site exposure and electron transfer efficiency.

The original MOFs and POPs exhibit poor electrical conductivity, which can be adjusted by introducing guest substances, such as conductive substrates (metal electrodes), conductive carbon materials (carbon black, graphene, and CNTs), metal NPs (e.g., Pt, Co, Cu, Ag, *etc.*), metal oxides (Cu₂O, Ag₂O, Bi₂O₃, CuO, *etc.*), and functional molecules. Grafting or depositing MOFs/POPs on a substrate with good conductivity can significantly improve the charge transfer efficiency of the catalyst to improve the catalytic performance. Using MOFs/POPs as the substrates for metal catalysts can improve their stability and SSA, thereby maximizing the exposure of active sites while inhibiting the NP aggregation. In addition, the synergy of MOFs/POPs and carbon materials can adjust binding strength of key reaction intermediates, thus improving the electrocatalytic performance. Electron-rich units are embedded into MOFs/POPs to construct MOF/POP-based composites with multiple electron transfer channels, which changed the charge distribution around the active sites in MOFs/POPs and further improved the selectivity of the electrocatalytic CO₂ reaction. In addition, MOF@COF hybrid materials can combine the high chemical stability of COFs and the adjustable functionality of MOFs, which is conducive to the further improvement of electrocatalytic efficiency.

MOF/POP-derived catalysts have excellent transport capacity, widely dispersed active sites, and good electrical conductivity. MOF-derived electrocatalysts based on structural and functional properties can be divided into metal oxides, metal NPs on carbon substrates, metal coordination NC materials (e.g., SACs), and metal-free electrocatalysts and nanocomposites. In addition, it has been reported that MOF-derived carbon materials as electrocatalysts can improve the CO₂RR performance. Such materials retain the characteristics of the original MOFs to a large extent, and possess the superiority of abundant pores, large SSA, and adjustable electronic structure after doping. These properties can originate from high dispersion of active sites in the electrochemical CO₂RR, which promote the adsorption and binding of the intermediates. In summary, regardless of MOFs/POPs (i) used directly as electrocatalysts; or (ii) designed to prepare single-atom embedded carbon materials as precursors, the resulting electrocatalysts exhibit enhanced inherent catalytic activity at the active site, improved mass transfer, and high stability, all of which are key characteristics required for the improvement of CO₂RR performance.

Challenges and perspectives

Despite the vast development of MOF/POP-based electrocatalysts for CO₂RR, there remain challenges in expanding their practical and commercial applications. Based on the existing literature, we present our views on the main challenges to be faced in the future and the corresponding feasible research directions:

1. Reasonable design and efficient preparation methods are key to ensuring the performance of MOF/POP electrocatalytic materials and their large-scale applications. Notably, most of the studied catalysts have not yet been commercialized. The rational design includes the selection of appropriate metal ions and organic ligands, and the control of crystal structure and pore characteristics by regulating the synthesis method, so

as to optimize the electrocatalytic performance. The synthesis of most POP/MOF monomers and ligands is complex and costly, which has seriously limited their wide electrocatalytic applications. Future studies must particularly consider the cost factor. There is an urgent need to develop low-priced monomers, explore new synthetic strategies, and improve existing synthetic methods to achieve cost-effective large-scale production. Further, the wide electrocatalytic applications of POPs/MOFs are also limited by their low electrical conductivity, so the choice of surface modification and support materials is crucial to facilitate rapid electron transfer. Therefore, it is necessary to explore new preparation methods to obtain robust frameworks suitable for harsh environments to simultaneously improve their long-term stability.

2. MOF-derived materials show a strong structure-activity relationship, and the coordination metal and the coordination environment (coordination number and coordination species) exhibit a very significant impact on the performance of the electrocatalysts, but in the current literature, DFT calculations or *in-situ* infrared are mainly used to speculate the reaction process and catalytic mechanism. It is impossible to accurately observe how a single metal atom catalytic site catalyzes the whole process of CO₂ reduction in real time, and few researchers have explored the effects of the morphology of MOF or POP-derived SACs on the electrocatalytic performance. Therefore, we should make full use of the increasingly advanced characterization instruments to provide real monitoring of the structural changes of catalysts and important intermediates in the catalytic process under working conditions, obtain more accurate and non-ambiguous electrocatalytic reaction paths, and provide more powerful technical support for the future industrial application of electrocatalytic CO₂ reduction. Advanced *in-situ* characterization techniques, such as real-time X-ray diffraction (XRD), high-resolution transmission electron microscopy (HRTEM), and atomic force microscopy (AFM), can measure interfacial phenomena at the microscopic level and capture real-time changes at the atomic level. The dynamic evolution process of the multi-dimensional microstructure of the material from the nanometer to the atomic scale and the dynamics of the surface atoms under the operation condition are revealed. *In situ* Fourier-transform infrared spectroscopy (FTIR), X-ray absorption near-edge structure (XANES), Raman spectroscopy, X-ray absorption spectroscopy, and ambient-pressure X-ray photoelectron spectroscopy are important for understanding the evolution of intermediates, the effects of electrolyte and environment on intermediates, and interfacial electrochemistry during CO₂ reduction. However, since the CO₂ reduction is performed in a liquid electrolyte, other intermediates, besides *CO, *COOH, are generally difficult to detect. The distribution of intermediates and different products can be directly observed by *in situ* spectroscopy assisted with online product analysis. In addition, when the characteristic peaks of CO₂RR intermediates/products overlap with other peaks, *in situ* spectroscopic techniques with higher resolution may be required. However, in general, the reaction path and products of CO₂ reduction are complex. Although the intermediates in the reaction process can be identified by advanced *in-situ* spectroscopy technology, the best reaction path among many possibilities can not be determined. Therefore, by combining deep learning algorithms with various *in-situ* spectroscopic techniques, we can fully understand the path of CO₂RR and promote the study of structure-property relationship to a new height.

3. High metal loading in carbon-supported SACs does not necessarily guarantee better catalytic performance, and a large number of metal atoms may be embedded in carbon materials, reducing the accessibility of metal single atoms. Since MOF or POP-derived SACs are mostly prepared by pyrolysis at high temperatures, it is necessary to use precursors with low metal content to inhibit the agglomeration of metal components during the synthesis. Therefore, it is indispensable to propose new technical methods to synthesize SACs with high density of active sites in large quantities while avoiding the aggregation of metal species. In addition, the introduction of new metal atoms into carbon-supported SACs by a post-modification strategy to form multi-metal catalytic sites can break the weak interaction between monatomic sites and achieve effective CO₂ reduction by utilizing the synergistic effect between different metal atoms.

4. MOF/POP-based catalysts reported in the literature have a high selectivity (more than 90%) for CO or HCOOH in the electrocatalytic reduction of CO₂, but their selectivity for high-electron C₁ (such as CH₄, etc.) or C₂ products is not high due to the complex proton and electron transfer process involved. Therefore, it is necessary to deeply explore the formation mechanism of CH₄ and other products, adjust the electronic structure of the active center, and thus achieve high selectivity. Meanwhile, among the materials reported so far, Cu is the only metal electrocatalyst that can promote the C-C coupling reaction to realize the process of CO₂-to-C₂ or C₂₊ products. Therefore, it is urgent to develop new efficient electrocatalysts to achieve high selectivity of C₂ products. In addition, tandem catalysis through two-step reactions is an effective strategy to achieve CO₂ reduction to C₂ or C₂₊ products with high efficiency. By designing and optimizing the catalytic ability of each step, the highly selective generation of C₂ or C₂₊ products can be achieved, which is very important and meaningful in commercial applications.

DECLARATIONS

Acknowledgments

The authors thank TopEdit (www.topeditsci.com) for its linguistic assistance during the preparation of this manuscript.

Authors' contributions

Methodology, writing-original draft, investigation, validation, resources, conceptualization: Ma, Y.

Review & editing, supervision: Zhang, G.; Yu, Q.; Lyu, S.; Duan, X.

Project administration, funding acquisition, conceptualization, review, editing, supervision: Zhang, S.

Availability of data and materials

The materials are available from the corresponding author upon request.

Financial support and sponsorship

This work was financially supported by the National Natural Science Foundation of China (Nos. 22309096, 22102220 and 22272105), Henan Provincial Science and Technology Research Project (Nos. 242102230013, 242102320146), Natural Science Foundation of Shanghai (No. 23ZR1423900), Natural Science Foundation of Shandong province (No. ZR2021QB070) and PhD Research Startup Foundation (PXY-BSQD-2022034).

Conflicts of interest

All authors declared that there are no conflicts of interest.

Ethical approval and consent to participate

Not applicable.

Consent for publication

Not applicable.

Copyright

© The Author(s) 2025.

REFERENCES

1. Cui, X.; Li, H.; Wang, Y.; et al. Room-temperature methane conversion by graphene-confined single iron atoms. *Chem* **2018**, *4*, 1902-10. DOI

2. Daiyan, R.; Saputera, W. H.; Masood, H.; Leverett, J.; Lu, X.; Amal, R. A disquisition on the active sites of heterogeneous catalysts for electrochemical reduction of CO₂ to value-added chemicals and fuel. *Adv. Energy. Mater.* **2020**, *10*, 1902106. DOI
3. He, H.; Perman, J. A.; Zhu, G.; Ma, S. Metal-organic frameworks for CO₂ chemical transformations. *Small* **2016**, *12*, 6309-24. DOI PubMed
4. Wang, F.; Dreisinger, D.; Jarvis, M.; Hitchins, T.; Trytten, L. CO₂ mineralization and concurrent utilization for nickel conversion from nickel silicates to nickel sulfides. *Chem. Eng. J.* **2021**, *406*, 126761. DOI
5. Zhai, T.; Wang, C.; Gu, F.; Meng, Z.; Liu, W.; Wang, Y. Dopamine/polyethylenimine-modified silica for enzyme immobilization and strengthening of enzymatic CO₂ conversion. *ACS. Sustain. Chem. Eng.* **2020**, *8*, 15250-7. DOI
6. Ma, Y.; Yi, X.; Wang, S.; et al. Selective photocatalytic CO₂ reduction in aerobic environment by microporous Pd-porphyrin-based polymers coated hollow TiO₂. *Nat. Commun.* **2022**, *13*, 1400. DOI PubMed PMC
7. Sun, S.; Mao, Y.; Liu, F.; et al. Recent advances in nanoscale engineering of Pd-based electrocatalysts for selective CO₂ electroreduction to formic acid/formate. *Energy. Mater.* **2024**, *4*, 400027. DOI
8. Feng, D.; Li, Z.; Guo, H.; et al. Conjugated polyimides modified self-supported carbon electrodes for electrochemical conversion of CO₂ to CO. *Energy. Mater.* **2024**, *4*, 400069. DOI
9. Xu, D.; Li, K.; Jia, B.; et al. Electrocatalytic CO₂ reduction towards industrial applications. *Carbon. Energy.* **2023**, *5*, e230. DOI
10. Liu, A.; Gao, M.; Ren, X.; et al. Current progress in electrocatalytic carbon dioxide reduction to fuels on heterogeneous catalysts. *J. Mater. Chem. A.* **2020**, *8*, 3541-62. DOI
11. Zhou, L.; Lv, R. Rational catalyst design and interface engineering for electrochemical CO₂ reduction to high-valued alcohols. *J. Energy. Chem.* **2022**, *70*, 310-31. DOI
12. He, J.; Li, Y.; Huang, A.; Liu, Q.; Li, C. Electrolyzer and catalysts design from carbon dioxide to carbon monoxide electrochemical reduction. *Electrochem. Energy. Rev.* **2021**, *4*, 680-717. DOI
13. Bushuyev, O. S.; De, L. P.; Dinh, C. T.; et al. What should we make with CO₂ and how can we make it? *Joule* **2018**, *2*, 825-32. DOI
14. Fu, Y.; Xie, Q.; Wan, L.; Huang, Q.; Luo, J. Ethanol assisted cyclic voltammetry treatment of copper for electrochemical CO₂ reduction to ethylene. *Mater. Today. Energy.* **2022**, *29*, 101105. DOI
15. Zhang, Z.; Li, S.; Zhang, Z.; et al. A review on electrocatalytic CO₂ conversion via C-C and C-N coupling. *Carbon. Energy.* **2024**, *6*, e513. DOI
16. Saha, P.; Amanullah, S.; Dey, A. Selectivity in electrochemical CO₂ reduction. *ACC. Chem. Res.* **2022**, *55*, 134-44. DOI PubMed
17. Overa, S.; Ko, B. H.; Zhao, Y.; Jiao, F. Electrochemical approaches for CO₂ conversion to chemicals: a journey toward practical applications. *ACC. Chem. Res.* **2022**, *55*, 638-48. DOI
18. Liu, C.; Mei, X.; Han, C.; Gong, X.; Song, P.; Xu, W. Tuning strategies and structure effects of electrocatalysts for carbon dioxide reduction reaction. *Chin. J. Catal.* **2022**, *43*, 1618-33. DOI
19. Zhang, M. D.; Si, D. H.; Yi, J. D.; Zhao, S. S.; Huang, Y. B.; Cao, R. Conductive phthalocyanine-based covalent organic framework for highly efficient electroreduction of carbon dioxide. *Small* **2020**, *16*, e2005254. DOI PubMed
20. Xue, Y.; Guo, Y.; Cui, H.; Zhou, Z. Catalyst design for electrochemical reduction of CO₂ to multicarbon products. *Small. Methods.* **2021**, *5*, e2100736. DOI
21. Liang, F.; Zhang, K.; Zhang, L.; Zhang, Y.; Lei, Y.; Sun, X. Recent development of electrocatalytic CO₂ reduction application to energy conversion. *Small* **2021**, *17*, e2100323. DOI
22. Dai, S.; Huang, T. H.; Liu, W. I.; et al. Enhanced CO₂ electrochemical reduction performance over Cu@AuCu catalysts at high noble metal utilization efficiency. *Nano. Lett.* **2021**, *21*, 9293-300. DOI
23. Liu, L.; Akhoundzadeh, H.; Li, M.; Huang, H. Alloy catalysts for electrocatalytic CO₂ reduction. *Small. Methods.* **2023**, *7*, e2300482. DOI
24. Bui, T. S.; Lovell, E. C.; Daiyan, R.; Amal, R. Defective metal oxides: lessons from CO₂RR and applications in NO_xRR. *Adv. Mater.* **2023**, *35*, e2205814. DOI
25. Zhao, X.; Feng, Q.; Liu, M.; et al. Built-in electric field promotes interfacial adsorption and activation of CO₂ for C₁ products over a wide potential window. *ACS. Nano.* **2024**, *18*, 9678-87. DOI
26. Mukherjee, A.; Abdinejad, M.; Mahapatra, S. S.; Ruidas, B. C. Metal sulfide-based nanomaterials for electrochemical CO₂ reduction. *J. Mater. Chem. A.* **2023**, *11*, 9300-32. DOI
27. Cui, H.; Guo, Y.; Guo, L.; Wang, L.; Zhou, Z.; Peng, Z. Heteroatom-doped carbon materials and their composites as electrocatalysts for CO₂ reduction. *J. Mater. Chem. A.* **2018**, *6*, 18782-93. DOI
28. Yang, D. H.; Tao, Y.; Ding, X.; Han, B. H. Porous organic polymers for electrocatalysis. *Chem. Soc. Rev.* **2022**, *51*, 761-91. DOI
29. Hong, J.; Park, K. T.; Kim, Y. E.; et al. Ag/C composite catalysts derived from spray pyrolysis for efficient electrochemical CO₂ reduction. *Chem. Eng. J.* **2022**, *431*, 133384. DOI
30. Sun, K.; Qian, Y.; Jiang, H. L. Metal-organic frameworks for photocatalytic water splitting and CO₂ reduction. *Angew. Chem. Int. Ed.* **2023**, *62*, e202217565. DOI PubMed
31. Yang, R.; Fu, Y.; Wang, H.; et al. ZIF-8/covalent organic framework for enhanced CO₂ photocatalytic reduction in gas-solid system. *Chem. Eng. J.* **2022**, *450*, 138040. DOI
32. Liu, G.; Liu, S.; Lai, C.; et al. Strategies for enhancing the photocatalytic and electrocatalytic efficiency of covalent triazine frameworks for CO₂ reduction. *Small* **2024**, *20*, e2307853. DOI
33. Mushtaq, N.; Ahmad, A.; Wang, X.; Khan, U.; Gao, J. MOFs/COFs hybrids as next-generation materials for electrocatalytic CO₂

- reduction reaction. *Chem. Eng. J.* **2024**, *486*, 150098. DOI
34. Pan, Y.; Abazari, R.; Tahir, B.; et al. Iron-based metal-organic frameworks and their derived materials for photocatalytic and photoelectrocatalytic reactions. *Coordin. Chem. Rev.* **2024**, *499*, 215538. DOI
35. Wang, J.; Tan, H. Y.; Zhu, Y.; Chu, H.; Chen, H. M. Linking the dynamic chemical state of catalysts with the product profile of electrocatalytic CO₂ reduction. *Angew. Chem. Int. Ed.* **2021**, *60*, 17254–67. DOI
36. Li, M.; Garg, S.; Chang, X.; et al. Toward excellence of transition metal-based catalysts for CO₂ electrochemical reduction: an overview of strategies and rationales. *Small. Methods.* **2020**, *4*, 2000033. DOI
37. Al-rowaili, F. N.; Jamal, A.; Ba, S. M. S.; Rana, A. A review on recent advances for electrochemical reduction of carbon dioxide to methanol using metal-organic framework (MOF) and non-MOF catalysts: challenges and future prospects. *ACS. Sustain. Chem. Eng.* **2018**, *6*, 15895–914. DOI
38. Wang, D.; Mao, J.; Zhang, C.; et al. Modulating microenvironments to enhance CO₂ electroreduction performance. *eScience* **2023**, *3*, 100119. DOI
39. Wu, Y.; Cao, S.; Hou, J.; et al. Rational design of nanocatalysts with nonmetal species modification for electrochemical CO₂ reduction. *Adv. Energy. Mater.* **2020**, *10*, 2000588. DOI
40. Xiao, H.; Cheng, T.; Goddard, W. A. Atomistic mechanisms underlying selectivities in C₁ and C₂ products from electrochemical reduction of CO on Cu(111). *J. Am. Chem. Soc.* **2017**, *139*, 130–6. DOI
41. Zhi, X.; Vasileff, A.; Zheng, Y.; Jiao, Y.; Qiao, S. Role of oxygen-bound reaction intermediates in selective electrochemical CO₂ reduction. *Energy. Environ. Sci.* **2021**, *14*, 3912–30. DOI
42. Peng, H.; Tang, M. T.; Liu, X.; Schlexer, L. P.; Bajdich, M.; Abild-pedersen, F. The role of atomic carbon in directing electrochemical CO₂ reduction to multicarbon products. *Energy. Environ. Sci.* **2021**, *14*, 473–82. DOI
43. Garza, A. J.; Bell, A. T.; Head-Gordon, M. Mechanism of CO₂ reduction at copper surfaces: pathways to C₂ products. *ACS. Catal.* **2018**, *8*, 1490–9. DOI
44. Zang, Y.; Wei, P.; Li, H.; Gao, D.; Wang, G. Catalyst design for electrolytic CO₂ reduction toward low-carbon fuels and chemicals. *Electrochem. Energy. Rev.* **2022**, *5*, 140. DOI
45. Jin, S.; Hao, Z.; Zhang, K.; Yan, Z.; Chen, J. Advances and challenges for the electrochemical reduction of CO₂ to CO: from fundamentals to industrialization. *Angew. Chem. Int. Ed.* **2021**, *60*, 20627–48. DOI
46. Verma, S.; Kim, B.; Jhong, H. R.; Ma, S.; Kenis, P. J. A gross-margin model for defining technoeconomic benchmarks in the electroreduction of CO₂. *ChemSusChem* **2016**, *9*, 1972–9. DOI PubMed
47. Lai, W.; Qiao, Y.; Zhang, J.; Lin, Z.; Huang, H. Design strategies for markedly enhancing energy efficiency in the electrocatalytic CO₂ reduction reaction. *Energy. Environ. Sci.* **2022**, *15*, 3603–29. DOI
48. Ma, W.; He, X.; Wang, W.; Xie, S.; Zhang, Q.; Wang, Y. Electrocatalytic reduction of CO₂ and CO to multi-carbon compounds over Cu-based catalysts. *Chem. Soc. Rev.* **2021**, *50*, 12897–914. DOI
49. Yang, C.; Li, S.; Zhang, Z.; et al. Organic-inorganic hybrid nanomaterials for electrocatalytic CO₂ reduction. *Small* **2020**, *16*, e2001847. DOI
50. Zhou, Y.; Abazari, R.; Chen, J.; et al. Bimetallic metal-organic frameworks and MOF-derived composites: recent progress on electro- and photoelectrocatalytic applications. *Coordin. Chem. Rev.* **2022**, *451*, 214264. DOI
51. Chang, F.; Xiao, M.; Miao, R.; et al. Copper-based catalysts for electrochemical carbon dioxide reduction to multicarbon products. *Electrochem. Energy. Rev.* **2022**, *5*, 139. DOI
52. Zhong, H.; Qiu, Y.; Zhang, T.; Li, X.; Zhang, H.; Chen, X. Bismuth nanodendrites as a high performance electrocatalyst for selective conversion of CO₂ to formate. *J. Mater. Chem. A.* **2016**, *4*, 13746–53. DOI
53. Cao, L.; Huang, J.; Wu, X.; et al. Active-site stabilized Bi metal-organic framework-based catalyst for highly active and selective electroreduction of CO₂ to formate over a wide potential window. *Nanoscale* **2023**, *15*, 19522–32. DOI
54. Zhang, X.; Zhang, Y.; Li, Q.; et al. Highly efficient and durable aqueous electrocatalytic reduction of CO₂ to HCOOH with a novel bismuth-MOF: experimental and DFT studies. *J. Mater. Chem. A.* **2020**, *8*, 9776–87. DOI
55. Ying, Y.; Khezri, B.; Kosina, J.; Pumera, M. Reconstructed bismuth-based metal-organic framework nanofibers for selective CO₂-to-formate conversion: morphology engineering. *ChemSusChem* **2021**, *14*, 3402–12. DOI
56. Jiang, Z.; Zhang, M.; Chen, X.; et al. A bismuth-based zeolitic organic framework with coordination-linked metal cages for efficient electrocatalytic CO₂ reduction to HCOOH. *Angew. Chem. Int. Ed.* **2023**, *62*, e202311223. DOI
57. Chen, S.; Chung, L. H.; Chen, S.; et al. Efficient lead removal by assembly of bio-derived ellagate framework, which enables electrocatalytic reduction of CO₂ to formate. *Small* **2024**, *20*, e2400978. DOI
58. Wang, Y. R.; Huang, Q.; He, C. T.; et al. Oriented electron transmission in polyoxometalate-metalloporphyrin organic framework for highly selective electroreduction of CO₂. *Nat. Commun.* **2018**, *9*, 4466. DOI PubMed PMC
59. Zhu, H. L.; Huang, J. R.; Zhang, X. W.; et al. Highly efficient electroconversion of CO₂ into CH₄ by a metal-organic framework with trigonal pyramidal Cu(I)N₃ active sites. *ACS. Catal.* **2021**, *11*, 11786–92. DOI
60. Liu, Y.; Zhu, H.; Zhao, Z.; Huang, N.; Liao, P.; Chen, X. Insight into the effect of the d-orbital energy of copper ions in metal-organic frameworks on the selectivity of electroreduction of CO₂ to CH₄. *ACS. Catal.* **2022**, *12*, 2749–55. DOI
61. Deng, J.; Qiu, L.; Xin, M.; et al. Boosting Electrochemical CO₂ reduction on copper-based metal-organic frameworks via valence and coordination environment modulation. *Small* **2024**, *20*, e2311060. DOI
62. Lu, P.; Lv, J.; Chen, Y.; et al. Steering the selectivity of carbon dioxide electroreduction from single-carbon to multicarbon products

- on metal-organic frameworks via facet engineering. *Nano. Lett.* **2024**, 24, 1553-62. DOI
63. Wang, J.; Liu, J.; Song, Y.; et al. Simultaneous defect and size control of metal-organic framework nanostructures for highly efficient carbon dioxide electroreduction to multicarbon products. *ACS. Mater. Lett.* **2023**, 5, 2121-30. DOI
64. Cao, L.; Wu, X.; Liu, Y.; et al. Electrochemical conversion of CO₂ to syngas with a stable H₂/CO ratio in a wide potential range over ligand-engineered metal-organic frameworks. *J. Mater. Chem. A.* **2022**, 10, 9954-9. DOI
65. Shao, P.; Yi, L.; Chen, S.; Zhou, T.; Zhang, J. Metal-organic frameworks for electrochemical reduction of carbon dioxide: the role of metal centers. *J. Energy. Chem.* **2020**, 40, 156-70. DOI
66. Al-attas, T. A.; Marei, N. N.; Yong, X.; et al. Ligand-engineered metal-organic frameworks for electrochemical reduction of carbon dioxide to carbon monoxide. *ACS. Catal.* **2021**, 11, 7350-7. DOI
67. Zhao, S.; Wang, Y.; Dong, J.; et al. Ultrathin metal-organic framework nanosheets for electrocatalytic oxygen evolution. *Nat. Energy.* **2016**, 1, 16184. DOI
68. Zhu, D.; Guo, C.; Liu, J.; Wang, L.; Du, Y.; Qiao, S. Z. Two-dimensional metal-organic frameworks with high oxidation states for efficient electrocatalytic urea oxidation. *Chem. Commun.* **2017**, 53, 10906-9. DOI
69. Duan, J.; Chen, S.; Zhao, C. Ultrathin metal-organic framework array for efficient electrocatalytic water splitting. *Nat. Commun.* **2017**, 8, 15341. DOI PubMed PMC
70. Yuan, M.; Wang, R.; Fu, W.; et al. Ultrathin two-dimensional metal-organic framework nanosheets with the inherent open active sites as electrocatalysts in aprotic Li-O₂ batteries. *ACS. Appl. Mater. Interfaces.* **2019**, 11, 11403-13. DOI
71. Hu, Q.; Huang, X.; Wang, Z.; et al. Unconventionally fabricating defect-rich NiO nanoparticles within ultrathin metal-organic framework nanosheets to enable high-output oxygen evolution. *J. Mater. Chem. A.* **2020**, 8, 2140-6. DOI
72. Zhou, W.; Huang, D. D.; Wu, Y. P.; et al. Stable hierarchical bimetal-organic nanostructures as highperformance electrocatalysts for the oxygen evolution reaction. *Angew. Chem. Int. Ed.* **2019**, 58, 4227-31. DOI
73. Majumder, M.; Santosh, M. S.; Viswanatha, R.; Thakur, A. K.; Dubal, D. P.; Jayaramulu, K. Two-dimensional conducting metal-organic frameworks enabled energy storage devices. *Energy. Storage. Mater.* **2021**, 37, 396-416. DOI
74. Zhao, Y.; Hou, N.; Wang, Y.; et al. All-fiber structure covered with two-dimensional conductive MOF materials to construct a comfortable, breathable and high-quality self-powered wearable sensor system. *J. Mater. Chem. A.* **2022**, 10, 1248-56. DOI
75. Ball, M.; Zhang, B.; Zhong, Y.; et al. Conjugated macrocycles in organic electronics. *ACC. Chem. Res.* **2019**, 52, 1068-78. DOI
76. Lv, J.; Li, W.; Li, J.; et al. A triptycene-based 2D MOF with vertically extended structure for improving the electrocatalytic performance of CO₂ to methane. *Angew. Chem. Int. Ed.* **2023**, 62, e202217958. DOI
77. Singh, A. K.; Gu, L.; Dutta, C. A.; Indra, A. Exploring ligand-controlled C₂ product selectivity in carbon dioxide reduction with copper metal-organic framework nanosheets. *Inorg. Chem.* **2023**, 62, 8803-11. DOI PubMed
78. Zhao, J.; Lyu, H.; Wang, Z.; et al. Phthalocyanine and porphyrin catalysts for electrocatalytic reduction of carbon dioxide: progress in regulation strategies and applications. *Sep. Purif. Technol.* **2023**, 312, 123404. DOI
79. Downes, C. A.; Marinescu, S. C. Electrocatalytic metal-organic frameworks for energy applications. *ChemSusChem* **2017**, 10, 4374-92. DOI PubMed
80. Hu, X. M.; Rønne, M. H.; Pedersen, S. U.; Skrydstrup, T.; Daasbjerg, K. Enhanced catalytic activity of cobalt porphyrin in CO₂ electroreduction upon immobilization on carbon materials. *Angew. Chem. Int. Ed.* **2017**, 56, 6468-72. DOI PubMed
81. Han, J.; An, P.; Liu, S.; et al. Reordering d orbital energies of single-site catalysts for CO₂ electroreduction. *Angew. Chem. Int. Ed.* **2019**, 58, 12711-6. DOI
82. Bohan, A.; Jin, X.; Wang, M.; Ma, X.; Wang, Y.; Zhang, L. Uncoordinated amino groups of MIL-101 anchoring cobalt porphyrins for highly selective CO₂ electroreduction. *J. Colloid. Interface. Sci.* **2024**, 654, 830-9. DOI
83. Zhang, W.; Liu, S.; Yang, Y.; et al. Exclusive Co-N₄ sites confined in two-dimensional metal-organic layers enabling highly selective CO₂ electroreduction at industrial-level current. *Angew. Chem. Int. Ed.* **2023**, 62, e202219241. DOI
84. Ifraemov, R.; Mukhopadhyay, S.; Hod, I. Photo-assisted electrochemical CO₂ reduction to CH₄ using a co-porphyrin-based metal-organic framework. *Solar. RRL.* **2023**, 7, 2201068. DOI
85. Wu, J. X.; Hou, S. Z.; Zhang, X. D.; et al. Cathodized copper porphyrin metal-organic framework nanosheets for selective formate and acetate production from CO₂ electroreduction. *Chem. Sci.* **2019**, 10, 2199-205. DOI PubMed PMC
86. Lee, J.; Choi, H.; Mun, J.; et al. Nanozyme based on porphyrinic metal-organic framework for electrocatalytic CO₂ reduction. *Small. Struct.* **2023**, 4, 2370002. DOI
87. Wu, J. X.; Yuan, W. W.; Xu, M.; Gu, Z. Y. Ultrathin 2D nickel zeolitic imidazolate framework nanosheets for electrocatalytic reduction of CO₂. *Chem. Commun.* **2019**, 55, 11634-7. DOI PubMed
88. Zhang, M. D.; Huang, J. R.; Shi, W.; Liao, P. Q.; Chen, X. M. Synergistic effect in a metal-organic framework boosting the electrochemical CO₂ overall splitting. *J. Am. Chem. Soc.* **2023**, 145, 2439-47. DOI
89. Zhong, H.; Ghorbani-Asl, M.; Ly, K. H.; et al. Synergistic electroreduction of carbon dioxide to carbon monoxide on bimetallic layered conjugated metal-organic frameworks. *Nat. Commun.* **2020**, 11, 1409. DOI
90. Yi, J. D.; Si, D. H.; Xie, R.; et al. Conductive two-dimensional phthalocyanine-based metal-organic framework nanosheets for efficient electroreduction of CO₂. *Angew. Chem. Int. Ed.* **2021**, 60, 17108-14. DOI
91. Zhang, M.; Si, D.; Yi, J.; Yin, Q.; Huang, Y.; Cao, R. Conductive phthalocyanine-based metal-organic framework as a highly efficient electrocatalyst for carbon dioxide reduction reaction. *Sci. China. Chem.* **2021**, 64, 1332-9. DOI
92. Kim, Y.; Park, S.; Shin, S.; et al. Time-resolved observation of C-C coupling intermediates on Cu electrodes for selective

- electrochemical CO₂ reduction. *Energy. Environ. Sci.* **2020**, *13*, 4301-11. DOI
93. Qiu, X. F.; Zhu, H. L.; Huang, J. R.; Liao, P. Q.; Chen, X. M. Highly selective CO₂ electroreduction to C₂H₄ using a metal-organic framework with dual active sites. *J. Am. Chem. Soc.* **2021**, *143*, 7242-6. DOI PubMed
94. Liu, J.; Yang, D.; Zhou, Y.; et al. Tricycloquinazoline-based 2D conductive metal-organic frameworks as promising electrocatalysts for CO₂ reduction. *Angew. Chem. Int. Ed.* **2021**, *60*, 14473-9. DOI
95. Liu, Y.; Li, S.; Dai, L.; et al. The synthesis of hexaazatrinaphthylene-based 2D conjugated copper metal-organic framework for highly selective and stable electroreduction of CO₂ to methane. *Angew. Chem. Int. Ed.* **2021**, *60*, 16409-15. DOI
96. Chen, S.; Li, W. H.; Jiang, W.; et al. MOF encapsulating N-heterocyclic carbene-ligated copper single-atom site catalyst towards efficient methane electrosynthesis. *Angew. Chem. Int. Ed.* **2022**, *61*, e202114450. DOI
97. Zhang, Y.; Dong, L. Z.; Li, S.; et al. Coordination environment dependent selectivity of single-site-Cu enriched crystalline porous catalysts in CO₂ reduction to CH₄. *Nat. Commun.* **2021**, *12*, 6390. DOI PubMed PMC
98. Zheng, W.; Yang, X.; Li, Z.; et al. Designs of tandem catalysts and cascade catalytic systems for CO₂ upgrading. *Angew. Chem. Int. Ed.* **2023**, *62*, e202307283. DOI
99. Mo, Q.; Li, S.; Chen, C.; Song, H.; Gao, Q.; Zhang, L. Engineering dual sites into the confined nanospace of the porphyrinic metal-organic framework for tandem transformation of CO₂ to ethylene. *ACS. Sustain. Chem. Eng.* **2024**, *12*, 6093-101. DOI
100. Du, H.; Fu, J.; Liu, L.; et al. Recent progress in electrochemical reduction of carbon monoxide toward multi-carbon products. *Mater. Today.* **2022**, *59*, 182-99. DOI
101. Cho, J. H.; Lee, C.; Hong, S. H.; et al. Transition metal ion doping on ZIF-8 enhances the electrochemical CO₂ reduction reaction. *Adv. Mater.* **2023**, *35*, e2208224. DOI
102. Chen, T.; Huang, B.; Day, S.; et al. Differential adsorption of l- and d-lysine on achiral MFI zeolites as determined by synchrotron X-ray powder diffraction and thermogravimetric analysis. *Angew. Chem. Int. Ed.* **2020**, *59*, 1093-7. DOI
103. Xue, Q.; Xie, Y.; Wu, S.; et al. A rational study on the geometric and electronic properties of single-atom catalysts for enhanced catalytic performance. *Nanoscale* **2020**, *12*, 23206-12. DOI
104. Liu, K.; Bigdeli, F.; Panjehpour, A.; et al. Metal organic framework composites for reduction of CO₂. *Coord. Chem. Rev.* **2023**, *493*, 215257. DOI
105. Zhao, Y.; Zheng, L.; Jiang, D.; et al. Nanoengineering metal-organic framework-based materials for use in electrochemical CO₂ reduction reactions. *Small* **2021**, *17*, e2006590. DOI
106. Yoon, Y.; Hall, A. S.; Surendranath, Y. Tuning of silver catalyst mesostructure promotes selective carbon dioxide conversion into fuels. *Angew. Chem. Int. Ed.* **2016**, *55*, 15282-6. DOI PubMed
107. Nam, D. H.; De, L. P.; Rosas-Hernández, A.; et al. Molecular enhancement of heterogeneous CO₂ reduction. *Nat. Mater.* **2020**, *19*, 266-76. DOI
108. Mukhopadhyay, S.; Shimoni, R.; Liberman, I.; Ifraimov, R.; Rozenberg, I.; Hod, I. Assembly of a metal-organic framework (MOF) membrane on a solid electrocatalyst: introducing molecular-level control over heterogeneous CO₂ reduction. *Angew. Chem. Int. Ed.* **2021**, *60*, 13423-9. DOI PubMed PMC
109. Mukhopadhyay, S.; Naeem, M. S.; Shiva, S. G.; et al. Local CO₂ reservoir layer promotes rapid and selective electrochemical CO₂ reduction. *Nat. Commun.* **2024**, *15*, 3397. DOI PubMed PMC
110. Guntern, Y. T.; Pankhurst, J. R.; Vávra, J.; et al. Nanocrystal/metal-organic framework hybrids as electrocatalytic platforms for CO₂ conversion. *Angew. Chem. Int. Ed.* **2019**, *58*, 12632-9. DOI
111. Kung, C.; Audu, C. O.; Peters, A. W.; Noh, H.; Farha, O. K.; Hupp, J. T. Copper nanoparticles installed in metal-organic framework thin films are electrocatalytically competent for CO₂ reduction. *ACS. Energy. Lett.* **2017**, *2*, 2394-401. DOI
112. Sun, B.; Hu, H.; Liu, H.; et al. Highly-exposed copper and ZIF-8 interface enables synthesis of hydrocarbons by electrocatalytic reduction of CO₂. *J. Colloid. Interface. Sci.* **2024**, *661*, 831-9. DOI
113. Takaoka, Y.; Song, J. T.; Takagaki, A.; Watanabe, M.; Ishihara, T. Bi/Uio-66-derived electrocatalysts for high CO₂-to-formate conversion rate. *Appl. Catal. B. Environ.* **2023**, *326*, 122400. DOI
114. Lu, X.; Zhu, C.; Wu, Z.; Xuan, J.; Francisco, J. S.; Wang, H. In situ observation of the pH gradient near the gas diffusion electrode of CO₂ reduction in alkaline electrolyte. *J. Am. Chem. Soc.* **2020**, *142*, 15438-44. DOI
115. Aparna, R. K.; Surendran, V.; Roy, D.; Pathak, B.; Shaijumon, M. M.; Mandal, S. Silver nanoparticle-decorated defective Zr-based metal-organic frameworks for efficient electrocatalytic carbon dioxide reduction with ultrahigh mass activity. *ACS. Appl. Energy. Mater.* **2023**, *6*, 4072-8. DOI
116. Cheng, Q.; Huang, M.; Xiao, L.; et al. Unraveling the influence of oxygen vacancy concentration on electrocatalytic CO₂ reduction to formate over indium oxide catalysts. *ACS. Catal.* **2023**, *13*, 4021-9. DOI
117. Pourebrahimi, S.; Pirooz, M.; Ahmadi, S.; Kazemeini, M.; Vafajoo, L. Nanoengineering of metal-based electrocatalysts for carbon dioxide (CO₂) reduction: a critical review. *Mater. Today. Phys.* **2023**, *38*, 101250. DOI
118. Liu, H.; Wang, H.; Song, Q.; et al. Assembling metal organic layer composites for high-performance electrocatalytic CO₂ reduction to formate. *Angew. Chem. Int. Ed.* **2022**, *61*, e202117058. DOI PubMed PMC
119. Wang, L.; Li, X.; Hao, L.; Hong, S.; Robertson, A. W.; Sun, Z. Integration of ultrafine CuO nanoparticles with two-dimensional MOFs for enhanced electrochemical CO₂ reduction to ethylene. *Chin. J. Catal.* **2022**, *43*, 1049-57. DOI
120. Tan, X.; Yu, C.; Zhao, C.; et al. Restructuring of Cu₂O to Cu₂O@Cu-metal-organic frameworks for selective electrochemical reduction of CO₂. *ACS. Appl. Mater. Interfaces.* **2019**, *11*, 9904-10. DOI

121. Sun, M.; Xu, X.; Min, S.; He, J.; Li, K.; Kang, L. Controllable preparation of Cu₂O/Cu-CuTCPP MOF heterojunction for enhanced electrocatalytic CO₂ reduction to C₂H₄. *Appl. Surf. Sci.* **2024**, *659*, 159937. DOI
122. Wang, P.; Yang, H.; Tang, C.; et al. Boosting electrocatalytic CO₂-to-ethanol production via asymmetric C-C coupling. *Nat. Commun.* **2022**, *13*, 3754. DOI PubMed PMC
123. Zhang, Y.; Chen, Y.; Wang, X.; Feng, Y.; Zhang, H.; Zhang, G. Self-polarization triggered multiple polar units toward electrochemical reduction of CO₂ to ethanol with high selectivity. *Angew. Chem. Int. Ed.* **2023**, *62*, e202302241. DOI
124. Xin, Z.; Wang, Y.; Chen, Y.; Li, W.; Dong, L.; Lan, Y. Metalloocene implanted metalloporphyrin organic framework for highly selective CO₂ electroreduction. *Nano. Energy.* **2020**, *67*, 104233. DOI
125. Xin, Z.; Liu, J.; Wang, X.; et al. Implanting polypyrrole in metal-porphyrin MOFs: enhanced electrocatalytic performance for CO₂ RR. *ACS. Appl. Mater. Interfaces.* **2021**, *13*, 54959-66. DOI
126. Dou, S.; Song, J.; Xi, S.; et al. Boosting electrochemical CO₂ reduction on metal-organic frameworks via ligand doping. *Angew. Chem. Int. Ed.* **2019**, *58*, 4041-5. DOI
127. Zheng, Y.; Li, S.; Huang, N.; Li, X.; Xu, Q. Recent advances in metal-organic framework-derived materials for electrocatalytic and photocatalytic CO₂ reduction. *Coordin. Chem. Rev.* **2024**, *510*, 215858. DOI
128. Zheng, Y.; Cheng, P.; Xu, J.; et al. MOF-derived nitrogen-doped nanoporous carbon for electroreduction of CO₂ to CO: the calcining temperature effect and the mechanism. *Nanoscale* **2019**, *11*, 4911-7. DOI
129. Payra, S.; Ray, S.; Sharma, R.; Tarafder, K.; Mohanty, P.; Roy, S. Photo- and electrocatalytic reduction of CO₂ over metal-organic frameworks and their derived oxides: a correlation of the reaction mechanism with the electronic structure. *Inorg. Chem.* **2022**, *61*, 2476-89. DOI PubMed
130. Wu, J. X.; Zhu, X. R.; Liang, T.; et al. Sn(101) derived from metal-organic frameworks for efficient electrocatalytic reduction of CO₂. *Inorg. Chem.* **2021**, *60*, 9653-9. DOI
131. Zhang, W.; Li, H.; Feng, D.; et al. MOF-derived 1D/3D N-doped porous carbon for spatially confined electrochemical CO₂ reduction to adjustable syngas. *Carbon. Energy.* **2024**, *6*, e461. DOI
132. Guo, Y.; Yang, H.; Zhou, X.; et al. Electrocatalytic reduction of CO₂ to CO with 100% faradaic efficiency by using pyrolyzed zeolitic imidazolate frameworks supported on carbon nanotube networks. *J. Mater. Chem. A.* **2017**, *5*, 24867-73. DOI
133. Ren, Q.; Wang, H.; Lu, X. F.; Tong, Y. X.; Li, G. R. Recent progress on MOF-derived heteroatom-doped carbon-based electrocatalysts for oxygen reduction reaction. *Adv. Sci.* **2018**, *5*, 1700515. DOI PubMed PMC
134. Kuang, M.; Guan, A.; Gu, Z.; Han, P.; Qian, L.; Zheng, G. Enhanced N-doping in mesoporous carbon for efficient electrocatalytic CO₂ conversion. *Nano. Res.* **2019**, *12*, 2324-9. DOI
135. Ye, L.; Ying, Y.; Sun, D.; et al. Highly efficient porous carbon electrocatalyst with controllable N-species content for selective CO₂ reduction. *Angew. Chem. Int. Ed.* **2020**, *59*, 3244-51. DOI
136. Wang, R.; Sun, X.; Ould-Chikh, S.; et al. Metal-organic-framework-mediated nitrogen-doped carbon for CO₂ electrochemical reduction. *ACS. Appl. Mater. Interfaces.* **2018**, *10*, 14751-8. DOI
137. Frank, S.; Svensson, G. E.; Bojesen, E. D.; et al. Exploring the influence of atomic level structure, porosity, and stability of bismuth(iii) coordination polymers on electrocatalytic CO₂ reduction. *J. Mater. Chem. A.* **2021**, *9*, 26298-310. DOI
138. Liu, J.; Peng, L.; Zhou, Y.; et al. Metal-organic-frameworks-derived Cu/Cu₂O catalyst with ultrahigh current density for continuous-flow CO₂ electroreduction. *ACS. Sustain. Chem. Eng.* **2019**, *7*, 15739-46. DOI
139. Guo, W.; Sun, X.; Chen, C.; et al. Metal-organic framework-derived indium-copper bimetallic oxide catalysts for selective aqueous electroreduction of CO₂. *Green. Chem.* **2019**, *21*, 503-8. DOI
140. Payra, S.; Roy, S. From Trash to treasure: probing cycloaddition and photocatalytic reduction of CO₂ over cerium-based metal-organic frameworks. *J. Phys. Chem. C.* **2021**, *125*, 8497-507. DOI
141. Smolders, S.; Jacobsen, J.; Stock, N.; De, V. D. Selective catalytic reduction of NO by cerium-based metal-organic frameworks. *Catal. Sci. Technol.* **2020**, *10*, 337-41. DOI
142. Han, Y.; Liu, M.; Li, K.; et al. In situ synthesis of titanium doped hybrid metal-organic framework UiO-66 with enhanced adsorption capacity for organic dyes. *Inorg. Chem. Front.* **2017**, *4*, 1870-80. DOI
143. Yang, D.; Zhu, Q.; Sun, X.; et al. Nanoporous Cu/Ni oxide composites: efficient catalysts for electrochemical reduction of CO₂ in aqueous electrolytes. *Green. Chem.* **2018**, *20*, 3705-10. DOI
144. Kempasiddaiah, M.; Samanta, R.; Panigrahy, S.; Trivedi, R. K.; Chakraborty, B.; Barman, S. Electrochemical reconstruction of a 1D Cu(PyDC)(H₂O) MOF into in situ formed Cu-Cu₂O heterostructures on carbon cloth as an efficient electrocatalyst for CO₂ conversion. *Nanoscale* **2024**, *16*, 10458-73. DOI
145. Zhang, Y.; Sun, T.; Zhang, P.; Liu, K.; Li, F.; Xu, L. Synthesizing MOF-derived NiNC catalyst via surfactant modified strategy for efficient electrocatalytic CO₂ to CO. *J. Colloid. Interface. Sci.* **2023**, *631*, 96-101. DOI
146. Zhang, X.; Fu, J.; Liu, Y.; Zhou, X.; Qiao, J. Bismuth anchored on MWCNTs with controlled ultrafine nanosize enables high-efficient electrochemical reduction of carbon dioxide to formate fuel. *ACS. Sustain. Chem. Eng.* **2020**, *8*, 4871-6. DOI
147. Vasileff, A.; Zheng, Y.; Qiao, S. Z. Carbon solving carbon's problems: recent progress of nanostructured carbon-based catalysts for the electrochemical reduction of CO₂. *Adv. Energy. Mater.* **2017**, *7*, 1700759. DOI
148. Gong, Q.; Ding, P.; Xu, M.; et al. Structural defects on converted bismuth oxide nanotubes enable highly active electrocatalysis of carbon dioxide reduction. *Nat. Commun.* **2019**, *10*, 2807. DOI PubMed PMC
149. Jia, M.; Choi, C.; Wu, T. S.; et al. Carbon-supported Ni nanoparticles for efficient CO₂ electroreduction. *Chem. Sci.* **2018**, *9*, 8775-80.

[DOI PubMed PMC](#)

150. Huang, H.; Shen, K.; Chen, F.; Li, Y. Metal-organic frameworks as a good platform for the fabrication of single-atom catalysts. *ACS Catal.* **2020**, *10*, 6579-86. [DOI](#)
151. Wang, H.; Wu, X.; Liu, G.; Wu, S.; Xu, R. Bimetallic MOF derived nickel nanoclusters supported by nitrogen-doped carbon for efficient electrocatalytic CO₂ reduction. *Nano. Res.* **2023**, *16*, 4546-53. [DOI](#)
152. Chang, B.; Min, Z.; Liu, N.; et al. Electrocatalytic CO₂ reduction to syngas. *Green. Energy. Environ.* **2024**, *9*, 1085-100. [DOI](#)
153. Ringe, S. The importance of a charge transfer descriptor for screening potential CO₂ reduction electrocatalysts. *Nat. Commun.* **2023**, *14*, 2598. [DOI PubMed PMC](#)
154. Song, C.; Wang, X.; Song, G.; et al. Electrocatalytic reduction of CO₂ by Co-Cu metastable alloy nanoparticles derived from MOFs. *J. Alloys. Compd.* **2024**, *994*, 174693. [DOI](#)
155. Fan, J.; Zhao, X.; Mao, X.; et al. Large-area vertically aligned bismuthene nanosheet arrays from galvanic replacement reaction for efficient electrochemical CO₂ conversion. *Adv. Mater.* **2021**, *33*, e2100910. [DOI](#)
156. Liu, S. Q.; Shahini, E.; Gao, M. R.; et al. Bi₂O₃ nanosheets grown on carbon nanofiber with inherent hydrophobicity for high-performance CO₂ electroreduction in a wide potential window. *ACS. Nano.* **2021**, *15*, 17757-68. [DOI](#)
157. Ma, S.; Wu, K.; Fan, S.; et al. Electrocatalytic CO₂ reduction enhanced by Sb doping in MOF-derived carbon-supported Bi-based materials. *Sep. Purif. Technol.* **2024**, *339*, 126520. [DOI](#)
158. Wang, Y.; Sui, P.; Xu, C.; et al. Optimizing Bi active sites by Ce doping for boosting formate production in a wide potential window. *Inorg. Chem. Front.* **2024**, *11*, 926-35. [DOI](#)
159. Zhao, K.; Liu, Y.; Quan, X.; Chen, S.; Yu, H. CO₂ electroreduction at low overpotential on oxide-derived Cu/carbons fabricated from metal organic framework. *ACS. Appl. Mater. Interfaces.* **2017**, *9*, 5302-11. [DOI](#)
160. Yang, H.; Yu, X.; Shao, J.; et al. *In situ* encapsulated and well dispersed Co₃O₄ nanoparticles as efficient and stable electrocatalysts for high-performance CO₂ reduction. *J. Mater. Chem. A.* **2020**, *8*, 15675-80. [DOI](#)
161. Deng, P.; Yang, F.; Wang, Z.; et al. Metal-organic framework-derived carbon nanorods encapsulating bismuth oxides for rapid and selective CO₂ electroreduction to formate. *Angew. Chem. Int. Ed.* **2020**, *59*, 10807-13. [DOI](#)
162. Chen, Y.; Zhang, J.; Yang, L.; Wang, X.; Wu, Q.; Hu, Z. Recent advances in non-precious metal-nitrogen-carbon single-site catalysts for CO₂ electroreduction reaction to CO. *Electrochem. Energy. Rev.* **2022**, *5*, 156. [DOI](#)
163. Ma, S.; Han, W.; Han, W.; Dong, F.; Tang, Z. Recent advances and future perspectives in MOF-derived single-atom catalysts and their application: a review. *J. Mater. Chem. A.* **2023**, *11*, 3315-63. [DOI](#)
164. Wang, S.; Yuan, X.; Zhou, S.; et al. Single-atomic-Ni electrocatalyst derived from phthalocyanine-modified MOF for conveying CO₂ intelligent utilization. *Energy. Mater.* **2024**, *4*, 400032. [DOI](#)
165. Chen, X.; Ma, D.; Chen, B.; et al. Metal-organic framework-derived mesoporous carbon nanoframes embedded with atomically dispersed Fe-N active sites for efficient bifunctional oxygen and carbon dioxide electroreduction. *Appl. Catal. B. Environ.* **2020**, *267*, 118720. [DOI](#)
166. Ye, Y.; Cai, F.; Li, H.; et al. Surface functionalization of ZIF-8 with ammonium ferric citrate toward high exposure of Fe-N active sites for efficient oxygen and carbon dioxide electroreduction. *Nano. Energy.* **2017**, *38*, 281-9. [DOI](#)
167. Qin, X.; Zhu, S.; Xiao, F.; Zhang, L.; Shao, M. Active sites on heterogeneous single-iron-atom electrocatalysts in CO₂ reduction reaction. *ACS. Energy. Lett.* **2019**, *4*, 1778-83. [DOI](#)
168. Yan, C.; Li, H.; Ye, Y.; et al. Coordinatively unsaturated nickel-nitrogen sites towards selective and high-rate CO₂ electroreduction. *Energy. Environ. Sci.* **2018**, *11*, 1204-10. [DOI](#)
169. Chung, H. T.; Cullen, D. A.; Higgins, D.; et al. Direct atomic-level insight into the active sites of a high-performance PGM-free ORR catalyst. *Science* **2017**, *357*, 479-84. [DOI](#)
170. Liu, K.; Wu, G.; Wang, G. Role of local carbon structure surrounding FeN₄ sites in boosting the catalytic activity for oxygen reduction. *J. Phys. Chem. C.* **2017**, *121*, 11319-24. [DOI](#)
171. Pan, F.; Zhang, H.; Liu, Z.; et al. Atomic-level active sites of efficient imidazolate framework-derived nickel catalysts for CO₂ reduction. *J. Mater. Chem. A.* **2019**, *7*, 26231-7. [DOI](#)
172. Jiao, L.; Yang, W.; Wan, G.; et al. Single-atom electrocatalysts from multivariate metal-organic frameworks for highly selective reduction of CO₂ at low pressures. *Angew. Chem. Int. Ed.* **2020**, *59*, 20589-95. [DOI](#)
173. Li, J.; Pršlja, P.; Shinagawa, T.; et al. Volcano trend in electrocatalytic CO₂ reduction activity over atomically dispersed metal sites on nitrogen-doped carbon. *ACS. Catal.* **2019**, *9*, 10426-39. [DOI](#)
174. Lee, S. M.; Cheon, W. S.; Lee, M. G.; Jang, H. W. Coordination environment in single-atom catalysts for high-performance electrocatalytic CO₂ reduction. *Small. Struct.* **2023**, *4*, 2200236. [DOI](#)
175. Wang, H.; Tong, Y.; Chen, P. Microenvironment regulation strategies of single-atom catalysts for advanced electrocatalytic CO₂ reduction to CO. *Nano. Energy.* **2023**, *118*, 108967. [DOI](#)
176. Zhang, Y.; Jiao, L.; Yang, W.; Xie, C.; Jiang, H. L. Rational fabrication of low-coordinate single-atom Ni electrocatalysts by MOFs for highly selective CO₂ reduction. *Angew. Chem. Int. Ed.* **2021**, *60*, 7607-11. [DOI](#)
177. Gong, Y. N.; Jiao, L.; Qian, Y.; et al. Regulating the coordination environment of MOF-templated single-atom nickel electrocatalysts for boosting CO₂ reduction. *Angew. Chem. Int. Ed.* **2020**, *59*, 2705-9. [DOI](#)
178. Wang, X.; Chen, Z.; Zhao, X.; et al. Regulation of coordination number over single Co sites: triggering the efficient electroreduction of CO₂. *Angew. Chem. Int. Ed.* **2018**, *57*, 1944-8. [DOI](#)

179. Jia, C.; Tan, X.; Zhao, Y.; et al. Sulfur-dopant-promoted electroreduction of CO₂ over coordinatively unsaturated Ni-N₂ moieties. *Angew. Chem. Int. Ed.* **2021**, *60*, 23342-8. DOI
180. Zhao, D.; Yu, K.; Song, P.; et al. Atomic-level engineering Fe₁N₂O₂ interfacial structure derived from oxygen-abundant metal-organic frameworks to promote electrochemical CO₂ reduction. *Energy. Environ. Sci.* **2022**, *15*, 3795-804. DOI
181. Wei, S.; Jiang, X.; He, C.; et al. Construction of single-atom copper sites with low coordination number for efficient CO₂ electroreduction to CH₄. *J. Mater. Chem. A.* **2022**, *10*, 6187-92. DOI
182. Guan, A.; Chen, Z.; Quan, Y.; et al. Boosting CO₂ electroreduction to CH₄ via tuning neighboring single-copper sites. *ACS. Energy. Lett.* **2020**, *5*, 1044-53. DOI
183. Jiao, L.; Zhu, J.; Zhang, Y.; et al. Non-bonding interaction of neighboring Fe and Ni single-atom pairs on MOF-derived N-doped carbon for enhanced CO₂ electroreduction. *J. Am. Chem. Soc.* **2021**, *143*, 19417-24. DOI
184. Zhong, D. C.; Gong, Y. N.; Zhang, C.; Lu, T. B. Dinuclear metal synergistic catalysis for energy conversion. *Chem. Soc. Rev.* **2023**, *52*, 3170-214. DOI PubMed
185. Pei, J.; Zhang, G.; Liao, J.; et al. Low-coordinated Co-Mn diatomic sites derived from metal-organic framework nanorods promote electrocatalytic CO₂ reduction. *J. Mater. Chem. A.* **2024**, *12*, 13694-702. DOI
186. Jin, Z.; Yang, M.; Dong, Y.; et al. Atomic dispersed hetero-pairs for enhanced electrocatalytic CO₂ reduction. *Nanomicro. Lett.* **2023**, *16*, 4. DOI PubMed PMC
187. Wang, Y.; Sun, R.; Chen, Y.; et al. Highly crystalline covalent triazine frameworks modified separator for lithium metal batteries. *Energy. Mater.* **2024**, *4*, 400056. DOI
188. Chen, X.; Geng, K.; Liu, R.; et al. Covalent organic frameworks: chemical approaches to designer structures and built-in functions. *Angew. Chem. Int. Ed.* **2020**, *59*, 5050-91. DOI
189. Ali, S. A.; Sadiq, I.; Ahmad, T. Superlative porous organic polymers for photochemical and electrochemical CO₂ reduction applications: from synthesis to functionality. *Langmuir* **2024**, *40*, 10414-32. DOI PubMed
190. Zhu, X.; Tian, C.; Wu, H.; et al. Pyrolyzed triazine-based nanoporous frameworks enable electrochemical CO₂ reduction in water. *ACS. Appl. Mater. Interfaces.* **2018**, *10*, 43588-94. DOI
191. Li, X.; Zhao, X.; Liu, Y.; Hatton, T. A.; Liu, Y. Redox-tunable Lewis bases for electrochemical carbon dioxide capture. *Nat. Energy.* **2022**, *7*, 1065-75. DOI
192. Xiao, Y.; Lu, J.; Chen, K.; Cao, Y.; Gong, C.; Ke, F. S. Linkage engineering in covalent organic frameworks for metal-free electrocatalytic C₂H₄ production from CO₂. *Angew. Chem. Int. Ed.* **2024**, *63*, e202404738. DOI
193. Liu, M.; Yang, S.; Yang, X.; et al. Post-synthetic modification of covalent organic frameworks for CO₂ electroreduction. *Nat. Commun.* **2023**, *14*, 3800. DOI PubMed PMC
194. Dubed, B. G. C.; Franco, F.; Liu, C.; et al. Toward the understanding of the structure-activity correlation in single-site Mn covalent organic frameworks for electrocatalytic CO₂ reduction. *ACS. Appl. Energy. Mater.* **2024**, *7*, 1348-57. DOI
195. Zhang, L.; Li, X. X.; Lang, Z. L.; et al. Enhanced cuprophilic interactions in crystalline catalysts facilitate the highly selective electroreduction of CO₂ to CH₄. *J. Am. Chem. Soc.* **2021**, *143*, 3808-16. DOI
196. Sakamoto, N.; Nishimura, Y. F.; Nonaka, T.; et al. Self-assembled cuprous coordination polymer as a catalyst for CO₂ electrochemical reduction into C₂ products. *ACS. Catal.* **2020**, *10*, 10412-9. DOI
197. Sakamoto, N.; Sekizawa, K.; Sato, S.; et al. Electrochemical CO₂ reduction improved by tuning the Cu-Cu distance in halogen-bridged dinuclear cuprous coordination polymers. *J. Catal.* **2021**, *404*, 12-7. DOI
198. Song, Y.; Zhang, J.; Zhu, Z.; et al. Zwitterionic ultrathin covalent organic polymers for high-performance electrocatalytic carbon dioxide reduction. *Appl. Catal. B. Environ.* **2021**, *284*, 119750. DOI
199. Arisnabarreta, N.; Hao, Y.; Jin, E.; et al. Single-layered imine-linked porphyrin-based two-dimensional covalent organic frameworks targeting CO₂ reduction. *Adv. Energy. Mater.* **2024**, *14*, 2304371. DOI
200. Zhang, M.; Liao, J. P.; Li, R. H.; et al. Green synthesis of bifunctional phthalocyanine-porphyrin cofcs in water for efficient electrocatalytic CO₂ reduction coupled with methanol oxidation. *Natl. Sci. Rev.* **2023**, *10*, nwad226. DOI PubMed PMC
201. Wei, S.; Zou, H.; Rong, W.; Zhang, F.; Ji, Y.; Duan, L. Conjugated nickel phthalocyanine polymer selectively catalyzes CO₂-to-CO conversion in a wide operating potential window. *Appl. Catal. B. Environ.* **2021**, *284*, 119739. DOI
202. Xie, T.; Chen, S.; Yue, Y.; Sheng, T.; Huang, N.; Xiong, Y. Biomimetic phthalocyanine-based covalent organic frameworks with tunable pendant groups for electrocatalytic CO₂ reduction. *Angew. Chem. Int. Ed.* **2024**, *63*, e202411188. DOI
203. Kong, X.; Liu, B.; Tong, Z.; et al. Charge-switchable ligand ameliorated cobalt polyphthalocyanine polymers for high-current-density electrocatalytic CO₂ reduction. *SmartMat* **2024**, *5*, e1262. DOI
204. Lu, C.; Yang, J.; Wei, S.; et al. Atomic Ni anchored covalent triazine framework as high efficient electrocatalyst for carbon dioxide conversion. *Adv. Funct. Mater.* **2019**, *29*, 1806884. DOI
205. Wang, T.; Guo, L.; Pei, H.; et al. Electron-rich pincer ligand-coupled cobalt porphyrin polymer with single-atom sites for efficient (photo)electrocatalytic CO₂ reduction at ultralow overpotential. *Small* **2021**, *17*, e2102957. DOI
206. Johnson, E. M.; Haiges, R.; Marinescu, S. C. Covalent-organic frameworks composed of rhenium bipyridine and metal porphyrins: designing heterobimetallic frameworks with two distinct metal sites. *ACS. Appl. Mater. Interfaces.* **2018**, *10*, 37919-27. DOI PubMed
207. Zhang, X.; Yuan, Y.; Li, H.; et al. Viologen linker as a strong electron-transfer mediator in the covalent organic framework to enhance electrocatalytic CO₂ reduction. *Mater. Chem. Front.* **2023**, *7*, 2661-70. DOI

208. Li, J.; Tan, Y.; Lin, J.; et al. Coupling electrocatalytic redox-active sites in a three-dimensional bimetalloporphyrin-based covalent organic framework for enhancing carbon dioxide reduction and oxygen evolution. *J. Mater. Chem. A*. **2024**, *12*, 9478-85. DOI
209. Endo, K.; Raza, A.; Yao, L.; et al. Downsizing porphyrin covalent organic framework particles using protected precursors for electrocatalytic CO₂ reduction. *Adv. Mater.* **2024**, *36*, e2313197. DOI
210. Yue, Y.; Cai, P.; Xu, K.; et al. Stable bimetallic polyphthalocyanine covalent organic frameworks as superior electrocatalysts. *J. Am. Chem. Soc.* **2021**, *143*, 18052-60. DOI
211. Qiu, X. F.; Huang, J. R.; Yu, C.; et al. A stable and conductive covalent organic framework with isolated active sites for highly selective electroreduction of carbon dioxide to acetate. *Angew. Chem. Int. Ed.* **2022**, *61*, e202206470. DOI
212. Zhang, M. D.; Huang, J. R.; Shi, W.; Liao, P. Q.; Chen, X. M. Self-accelerating effect in a covalent-organic framework with imidazole groups boosts electroreduction of CO₂ to CO. *Angew. Chem. Int. Ed.* **2023**, *62*, e202308195. DOI
213. Wu, Q. J.; Si, D. H.; Wu, Q.; Dong, Y. L.; Cao, R.; Huang, Y. B. Boosting electroreduction of CO₂ over cationic covalent organic frameworks: hydrogen bonding effects of halogen ions. *Angew. Chem. Int. Ed.* **2023**, *62*, e202215687. DOI PubMed
214. Liu, M.; Cui, C. X.; Yang, S.; et al. Elaborate modulating binding strength of intermediates via three-component covalent organic frameworks for CO₂ reduction reaction. *Angew. Chem. Int. Ed.* **2024**, *63*, e202401750. DOI
215. Wang, T.; Xu, L.; Chen, Z.; et al. Central site regulation of cobalt porphyrin conjugated polymer to give highly active and selective CO₂ reduction to CO in aqueous solution. *Appl. Catal. B. Environ.* **2021**, *291*, 120128. DOI
216. Lu, Y.; Zhang, J.; Wei, W.; Ma, D. D.; Wu, X. T.; Zhu, Q. L. Efficient carbon dioxide electroreduction over ultrathin covalent organic framework nanolayers with isolated cobalt porphyrin units. *ACS. Appl. Mater. Interfaces*. **2020**, *12*, 37986-92. DOI
217. Wang, Y.; Zhang, X.; Lei, H.; et al. Tuning electronic structures of covalent co porphyrin polymers for electrocatalytic CO₂ reduction in aqueous solutions. *CCS. Chem.* **2022**, *4*, 2959-67. DOI
218. Wang, R.; Wang, X.; Weng, W.; et al. Proton/electron donors enhancing electrocatalytic activity of supported conjugated microporous polymers for CO₂ reduction. *Angew. Chem. Int. Ed.* **2022**, *61*, e202115503. DOI
219. Wang, T.; Wang, J.; Lu, C.; et al. Single-atom anchored curved carbon surface for efficient CO₂ electro-reduction with nearly 100% co selectivity and industrially-relevant current density. *Adv. Mater.* **2023**, *35*, e2205553. DOI
220. Ao, K.; Zhao, P.; Zhang, Q.; et al. Activating the Ni-containing carbon nanotube by covalent triazine frameworks to form atomically dispersed Ni sites with curvature effect for electrocatalytic CO₂ reduction. *Small. Struct.* **2024**, *5*, 2300500. DOI
221. Trindell, J. A.; Clausmeyer, J.; Crooks, R. M. Size stability and H₂/CO selectivity for Au nanoparticles during electrocatalytic CO₂ reduction. *J. Am. Chem. Soc.* **2017**, *139*, 16161-7. DOI
222. Zhang, L.; Wei, Z.; Thanneeru, S.; et al. A polymer solution to prevent nanoclustering and improve the selectivity of metal nanoparticles for electrocatalytic CO₂ reduction. *Angew. Chem. Int. Ed.* **2019**, *58*, 15834-40. DOI
223. Zheng, Y.; Vasileff, A.; Zhou, X.; Jiao, Y.; Jaroniec, M.; Qiao, S. Z. Understanding the roadmap for electrochemical reduction of CO₂ to multi-carbon oxygenates and hydrocarbons on copper-based catalysts. *J. Am. Chem. Soc.* **2019**, *141*, 7646-59. DOI
224. Popović, S.; Smiljanić, M.; Jovanović, P.; Vavra, J.; Buonsanti, R.; Hodnik, N. Stability and degradation mechanisms of copper-based catalysts for electrochemical CO₂ reduction. *Angew. Chem. Int. Ed.* **2020**, *59*, 14736-46. DOI PubMed
225. Zheng, M.; Wang, P.; Zhi, X.; et al. Electrocatalytic CO₂-to-C₂₊ with ampere-level current on heteroatom-engineered copper via tuning *CO intermediate coverage. *J. Am. Chem. Soc.* **2022**, *144*, 14936-44. DOI
226. Liu, Z.; Lv, X.; Kong, S.; et al. Interfacial water tuning by intermolecular spacing for stable CO₂ electroreduction to C₂₊ products. *Angew. Chem. Int. Ed.* **2023**, *62*, e202309319. DOI
227. Zhu, Z.; Zhu, Y.; Ren, Z.; et al. Covalent organic framework ionomer steering the CO₂ electroreduction pathway on Cu at industrial-grade current density. *J. Am. Chem. Soc.* **2024**, *146*, 1572-9. DOI
228. Meng, D. L.; Zhang, M. D.; Si, D. H.; et al. Highly selective tandem electroreduction of CO₂ to ethylene over atomically isolated nickel-nitrogen site/copper nanoparticle catalysts. *Angew. Chem. Int. Ed.* **2021**, *60*, 25485-92. DOI
229. Zhou, L.; Tian, Q.; Shang, X.; et al. Heterostructure construction of covalent organic frameworks/Ti₃C₂-MXene for high-efficiency electrocatalytic CO₂ reduction. *Green. Chem.* **2024**, *26*, 1454-61. DOI
230. Popov, D. A.; Luna, J. M.; Orchanian, N. M.; Haiges, R.; Downes, C. A.; Marinescu, S. C. A 2,2'-bipyridine-containing covalent organic framework bearing rhenium(i) tricarbonyl moieties for CO₂ reduction. *Dalton. Trans.* **2018**, *47*, 17450-60. DOI PubMed
231. Tang, J.; Zhu, C.; Jiang, T.; et al. Anion exchange-induced single-molecule dispersion of cobalt porphyrins in a cationic porous organic polymer for enhanced electrochemical CO₂ reduction via secondary-coordination sphere interactions. *J. Mater. Chem. A*. **2020**, *8*, 18677-86. DOI
232. Wu, Q. J.; Si, D. H.; Ye, S.; Dong, Y. L.; Cao, R.; Huang, Y. B. Photocoupled electroreduction of CO₂ over photosensitizer-decorated covalent organic frameworks. *J. Am. Chem. Soc.* **2023**, *145*, 19856-65. DOI
233. Yang, Y. L.; Wang, Y. R.; Dong, L. Z.; et al. A honeycomb-like porous crystalline hetero-electrocatalyst for efficient electrocatalytic CO₂ reduction. *Adv. Mater.* **2022**, *34*, e2206706. DOI
234. Liu, G.; Li, X.; Liu, M.; et al. Dimensional engineering of covalent organic frameworks derived carbons for electrocatalytic carbon dioxide reduction. *SusMat* **2023**, *3*, 834-42. DOI
235. Lin, L.; Li, H.; Wang, Y.; et al. Temperature-dependent CO₂ electroreduction over Fe-N-C and Ni-N-C single-atom catalysts. *Angew. Chem. Int. Ed.* **2021**, *133*, 26786-90. DOI
236. Liu, M.; Liu, S.; Xu, Q.; et al. Dual atomic catalysts from COF-derived carbon for CO₂ RR by suppressing HER through synergistic effects. *Carbon. Energy*. **2023**, *5*, e300. DOI